

**LIFE EVALUATION OF A CLOSED-LOOP OSCILLATING  
HEAT-PIPE WITH CHECK VALVE (CLOHP/CV)**

**SATITPONG SANGIAMSUK**

**A dissertation submitted in partial fulfillment of the requirements for  
the degree of Doctor of Philosophy in Mechanical Engineering  
at Maharakham University**

**December 2013**

**All rights reserved by Maharakham University**



**LIFE EVALUATION OF A CLOSED-LOOP OSCILLATING  
HEAT-PIPE WITH CHECK VALVE (CLOHP/CV)**

**SATITPONG SANGIAMSUK**

**A dissertation submitted in partial fulfillment of the requirements for  
the degree of Doctor of Philosophy in Mechanical Engineering  
at Maharakham University**

**December 2013**

**All rights reserved by Maharakham University**





The examining committee has unanimously approved this dissertation, submitted by Satitpong Sangiamsuk, as a partial fulfillment of the requirements for the Doctor of Philosophy degree in Mechanical engineering, Maharakham University.

Examining Committee

..... *T. Teerapat* ..... Chairman  
(Teerapat Chompookham, D.Eng.) (Faculty graduate committee)

..... *S. Rittidech* ..... Committee  
(Assoc. Prof. Sampan Rittidech, D.Eng.) (Advisor)

..... *Bopit Bubphachot* ..... Committee  
(Asst. Prof. Bopit Bubphachot, Ph.D.) (Co-advisor)

..... *Osamu Watanabe* ..... Committee  
(Prof. Osamu Watanabe, D.Eng.) (Co-advisor)

..... *Thanya P.* ..... Committee  
(Thanya Parametthanuwat, Ph.D.) (External expert)

Maharakham University has granted approval to accept this dissertation as a partial fulfillment of the requirements for the Doctor of Philosophy degree in Mechanical engineering

..... *S. Rittidech* .....  
(Assoc. Prof. Sampan Rittidech, D.Eng.)  
Dean of the Faculty of Engineering

..... *T. Mekkapan-opas* .....  
(Assoc. Prof. Thiensak Mekkapan-opas)  
Acting Dean of the Faculty of

Graduate Studies  
*December 25, 2013*



## ACKNOWLEDGEMENTS

This dissertation was granted financial support by the Thailand Research Fund that awarded me a scholarship through the Royal Golden Jubilee Ph.D. Program (RGJ-Grant No. PHD/0002/2553).

The dissertation would not have been accomplished without help from several people. First of all, I would like to thank Association professor Dr. Sampan Rittidech, who is the chairperson of my advisory committee, for inspiration, knowledge, experience, research perspective and valuable suggestions that caused this study to be completed. I would like to thank Assistant professor Dr. Bopit Bubphachot and Professor Dr. Osamu Watanabe for being my advisory committee and providing me suggestions. I would like to thank Dr. Thanya Parametthanuwat for being my external examining committee and granting suggestions to me.

I am very thankful to all the students at the Heat Pipe and Thermal Tools Design Research Unit (HTDR), Mechanical Engineering, Department of Engineering Mechanics, Faculty of Engineering, Mahasarakham University, Thailand who are both my friends and colleagues, for all their help.

I would also like to thank to all the students at the Watanabe's laboratory, Solid Mechanics and Material Science, Department of Engineering Mechanics and Energy, Faculty of Systems and Information Engineering, University of Tsukuba, Japan.

I was very fortunate to have many friends both within and outside the Faculty of Engineering during my doctoral life. I thank them all for their being very supportive. I also thank many people who help me, but I cannot present each of their names here. Finally, I would like to express my deepest gratefulness to Mr. Taweewat, Mrs. Supannaporn and Ms. Siriphen Sangiamsuk and also Ms. Pornpimon Tungjai, for valuable love, care, help, willpower and support in my whole life.

Satitpong Sangiamsuk





<b>TITLE</b>	Life Evaluation of a Closed-Loop Oscillating Heat-Pipe with Check Valve (CLOHP/CV)		
<b>CANDIDATE</b>	Mr. Satitpong Sangiamsuk		
<b>DEGREE</b>	Doctor of Philosophy (Mechanical Engineering)		
<b>ADVISOR</b>	Assoc. Prof. Dr. Sampan Rittidech, Ph.D. Asst. Prof. Dr. Bopit Bubphachot, Ph.D. Prof. Dr. Osamu Watanabe, Ph.D.		
<b>UNIVERSITY</b>	Maharakham University	<b>YEAR</b>	2013

### ABSTRACT

The thesis aimed to study and experimentally investigate the methodology that is presented, which can be divided into three parts. The first is a quantitative experiment in order to determine the thermal performance and internal pressure of a closed-loop oscillating heat-pipe with check valve (CLOHP/CV) at a normal operating state. The second is to determine the internal corrosion of the compound as well as the physical and chemical analysis of the CLOHP/CV. The last is to study the fatigue failure of the copper tube, to be applied to the CLOHP/CV, in order to improve the engineering of the heat pipe design.

The first part shows the internal pressure and thermal performance as characteristic parameters of the CLOHP/CV under normal operating conditions. The test CLOHP/CV was made of a copper capillary tube with various inner diameters, an angle of inclination and working temperature were varied in the experiments. The working fluids used were distilled water, ethanol and R123, with a filling ratio of 50% respect to total volume at internal tube; the number of meandering turns was 40 and the number of check valves was two. The length of the evaporator, adiabatic and condenser sections were equal. The evaporator section was heated via electric strip heaters. The heat was removed from the condenser section via a forced convective flow of ambient air blown through the sections. The adiabatic section was well insulated with foam insulation. The thermal performance of the CLOHP/CV was evaluated by calculating the rate of heat transferred from the condenser to the ambient air temperature. It was found that the thermal performance of the CLOHP/CV improved when increasing the



working temperature, an angle of inclination and the inner diameter. The best performance of the entire test CLOHP/CVs occurred for the case of R123 as the working fluid, 2.03 mm inner diameter, 90° inclination angle and a working temperature of 200 °C, where the maximum internal pressure was 7.53 MPa and the minimum thermal resistance was 0.048°C/W.

The second part shows the basic information and understanding of the corrosion behavior of the CLOHP/CV using distilled water and ethanol as the working fluids over a range of relevant operation conditions when the working temperature was 200 °C. The CLOHP/CV had an inner diameter of 2.03 mm. The run times of the experiments were 500, 1000 and 3000 hours. The investigation included scanning electron microscopy (SEM) and flame atomic absorption spectroscopy (Flame-AAS). These were used to test and observe the inner surfaces of the CLOHP/CV and check the copper solution in the working fluids. The elemental content was obtained from the inner surface using Energy Dispersive X-ray spectrometry (EDX). The results showed that after the 3000 hours of test, corrosion of the CLOHP/CV could be clearly identified. The concentrations and corrosion rates of the inner copper tube were employed to analyze the data. It was found that the concentrations of copper particles and corrosion rates were inversely proportional to time. Moreover, the concentration of the copper particles in the ethanol, used as the working fluid, after the 3000 hours duration of test, which resulted in the greatest corrosive concentration was 18.57228 ppm or 0.408590 mg; while, with water as the working fluid, the corrosive concentration was 0.097095 ppm or 0.002136 mg, in which their relationship was a logarithmic function. From this result the internal corrosion rates of the CLOHP/CV using distilled water and ethanol can be divided into two parts: the first was when the time of testing was 500 to 1000 hours and there were greater the corrosion rates. The second one was when the time of testing was 1000 to 3000 hours and there was a lower corrosion rate. From these, it was possible to develop relative equations of the corrosion rates when the duration time of testing in the equations show the relationship for the polynomial function between the corrosion rates and duration time in an experiment where the working temperature was 200 °C. Using ethanol as the working fluid rather than water caused greater corrosion rates after 3000 hours that were about  $9.09 \times 10^{-9}$  and  $1.74 \times 10^{-6}$  mm/y respectively, by using the following equation:



$$Cr_w = -1.2290 \times 10^{-14}(t^2) + 4.4241 \times 10^{-11}(t) - 1.3018 \times 10^{-8}$$

$$Cr_E = -8.7107 \times 10^{-13}(t^2) + 2.0812 \times 10^{-9}(t) + 3.3359 \times 10^{-6}$$

The final part shows the investigations of the effect of the fatigue failure of the copper tube use to fabricate the CLOHP/CV. The method could predict the fatigue life for a copper tube used in a CLOHP/CV. The fatigue test was carried out using specimens made from copper tube (C1220) at room temperature (15 °C), 200 °C and 300 °C. The sinusoidal waveform had tensile and compressive peak stress loading at 200 MPa, which had been predicted. The geometry of the specimen type changed in the same manner as during the fatigue test by varying the number or differences in the hourglass shaped specimen. The fatigue test was carried out using three types of specimen, labeled as uniform type, one-wave type and two-wave type specimens. It was found that the effect was a direct extension of the specimen and the hourglass shaped can be said to be the number of cycles to failure ( $N_f$ ) of the two-wave type specimen. The hourglass shaped specimen was rather sensitive to the fatigue motion during testing and it was found that when the temperature was 300 °C there was the greatest impact.



## CONTENTS

	<b>Page</b>
Acknowledgement	i
Abstract	ii
List of Tables	vii
List of Figures	viii
Chapter 1 Introduction	1
1.1 Background	1
1.2 Objective of the study	3
1.3 Scopes of the study for pressure testing	3
1.4 Scopes of the study for internal corrosion	4
1.5 Scopes of the study for fatigue testing	4
1.6 Profits from the study	5
Chapter 2 Theory and Literature Review	6
2.1 Heat pipe	6
2.2 Oscillating heat pipe	8
2.3 Check valve	10
2.4 Corrosion	13
2.5 Fatigue	25
2.6 Life test	31
2.7 Literature review	33
Chapter 3 Experimental Setup and Procedure	39
3.1 Instruments and equipments	39
3.2 Experimental setup and procedure	46
Chapter 4 Results and Discussion	61
4.1 Operation behavior of CLOHP/CV	61
4.2 Results of internal pressure	64
4.3 Results of copper corrosion	78
4.4 Results of fatigue on copper tube	92



	<b>Page</b>
Chapter 5 Conclusion and Suggestion	102
5.1 Conclusions	102
5.2 Suggestions	104
References	105
Appendices	112
Appendix A Calculation	113
Appendix B Data analysis	118
Appendix C Experimental Set	131
Appendix D Physical Properties of Working Fluids	161
Appendix E Nomenclature	169
Biography	172



**List of Tables**

		<b>Page</b>	
Table	2.1	Partial electromotive force (emf) series	14
Table	3.1	Chemical composition (wt%) of copper tube (C1220)	56
Table	3.2	Physical and mechanical properties	56
Table	4.1	All elements analyzed for the copper tube surface by EDX	82
Table	4.2	Concentration value of copper particles	87
Table	4.3	Summary of fatigue tests	93



## List of Figures

		<b>Page</b>
Figure 2.1	The structure of conventional heat pipe and thermosyphon	7
Figure 2.2	Type of oscillating heat-pipe: (a) Close-end oscillating heat-pipe (CEOHP), (b) Close-loop oscillating heat-pipe (CLOHP) Type of oscillating heat-pipe: (c) Close-loop oscillating heat-pipe with check valves (CLOHP/CV)	10
Figure 2.3	Structure of check-valve	11
Figure 2.4	Uniform corrosion	17
Figure 2.5	Pitting corrosion	17
Figure 2.6	Crevice corrosion	18
Figure 2.7	Filiform corrosion	18
Figure 2.8	Intergranular corrosion	19
Figure 2.9	Exfoliation corrosion	19
Figure 2.10	Galvanic corrosion	20
Figure 2.11	Fatigue corrosion	21
Figure 2.12	Hydrogen embrittlement corrosion	21
Figure 2.13	Stress corrosion	22
Figure 2.14	Erosion corrosion	23
Figure 2.15	Fretting corrosion	23
Figure 2.16	Dealloying	24
Figure 2.17	Schematic of the corrosion reaction	25
Figure 2.18	Schematic illustrating cyclic loading parameters	26
Figure 2.19	Strain estimated by Neuber's law and SRL method	28
Figure 2.20	Typical S-N Curves	30
Figure 2.21	Slug flow	34
Figure 2.22	Copper-water heat pipe of Murakami	36
Figure 3.1	Pitot tube	39
Figure 3.2	Data logger	40
Figure 3.3	Temperature controller	40
Figure 3.4	Electric plate heaters	41



	<b>Page</b>
Figure 3.5 Thermocouples	41
Figure 3.6 Working fluid filling set	42
Figure 3.7 The position of check-valves on oscillating heat pipe	42
Figure 3.8 The CLOHP/CV	43
Figure 3.9 Scanning electron microscopy (SEM)	44
Figure 3.10 Flame atomic absorption spectroscopy (Flame-AAS)	45
Figure 3.11 Shimadzu servo-hydraulic test machine	45
Figure 3.12 The CLOHP/CV for testing	46
Figure 3.13 Filling working fluid	47
Figure 3.14 Experimental setup for internal pressure testing	48
Figure 3.15 Experimental procedure	49
Figure 3.16 Experimental setup for internal corrosion testing	52
Figure 3.17 Photographs of the actual copper tubes (a): cross-sectional view copper tube for experimental (b): inner surface of the copper tube before testing	53
Figure 3.18 Geometry of specimens: Screw-model specimen: (a) uniform type and (b) one-wave type	54
Geometry of specimens: Flange-model specimen: (a) uniform type, (b) two-wave type and (c) one-wave type	55
Figure 3.19 Photographs of specimens (screw-type)	55
Figure 3.20 Experimental setup of fatigue testing	57
Figure 3.21 The CCD video camera	58
Figure 3.22 Assumed load wave for fatigue test	59
Figure 3.23 Stress amplitude controllers of screw type in fatigue test	59
Stress amplitude controllers of flange type in fatigue test	60
Figure 3.24 Extension meter	60
Figure 4.1 Relationship between heat transfer rate and inclination angles of the CLOHP/CV	61
Figure 4.2 Adiabatic temperature in adjacent tube of the CLOHP/CV	63
Figure 4.3 Relationship between inclination angles and internal pressure	65
Figure 4.4 Effect of working temperature difference on the internal pressure	66





	<b>Page</b>
Figure 4.5 Relationship between inclination angles and thermal resistance	67
Figure 4.6 Effect of working temperature difference on the thermal resistance	67
Figure 4.7 Relationship between evaporator lengths and internal pressure	68
Figure 4.8 Relationship between evaporator lengths and thermal resistance	69
Figure 4.9 Relationship between inner diameters and internal pressure	70
Figure 4.10 Relationship between inner diameters and thermal resistance	71
Figure 4.11 Relationship between working temperatures and internal pressure	73
Figure 4.12 Relationship between working temperature and thermal resistance	74
Figure 4.13 Comparison the heat transfer rate	77
Figure 4.14 Comparison the thermal resistance	78
Figure 4.15 Photographs of the actual copper tubes: (a) cross-sectional view copper tube for experimental, (b) inner surface of the copper tube before testing and (c) inner surface of the copper tube after testing	79
Figure 4.16 SEM micrographs for CLOHP/CV: before testing	80
Figure 4.16-1 SEM micrographs for the CLOHP/CV at 500 hours: (a) distilled water as the working fluid and (b) ethanol as the working fluid	80
Figure 4.16-2 SEM micrographs for the CLOHP/CV at 1000 hours: (c) distilled water as the working fluid and (d) ethanol as the working fluid	81
Figure 4.16-3 SEM micrographs for the CLOHP/CV at 3000 hours: (e) distilled water as the working fluid and (f) ethanol as the working fluid	82
Figure 4.17 EDX for CLOHP/CV: (a) before testing	83
Figure 4.17-1 EDX for CLOHP/CV at 500 hours: (b) distilled water as the working fluid	83
Figure 4.17-2 EDX for CLOHP/CV at 500 hours: (c) ethanol as the working fluid	84
Figure 4.17-3 EDX for CLOHP/CV at 1000 hours: (d) distilled water as the working fluid	84



	<b>Page</b>
Figure 4.17-4 EDX for CLOHP/CV at 1000 hours: (e) ethanol as the working fluid	85
Figure 4.17-5 EDX for CLOHP/CV at 3000 hour: (f) water as the working fluid	85
Figure 4.17-6 EDX for CLOHP/CV at 3000 hour: (g) ethanol as the working fluid	86
Figure 4.18 The calibration curve of copper solution	86
Figure 4.19 Relationship between concentrations of Cu and time with distilled water as working fluid	88
Figure 4.20 Relationship between concentrations of Cu and time with ethanol as working fluid	88
Figure 4.21 Relationship between corrosion rates and time with distilled water as working fluid	90
Figure 4.22 Relationship between corrosion rates and time with ethanol as working fluid	91
Figure 4.23 S-N curves for DHP and C1220 copper in fatigue test (screw-model)	95
Figure 4.24 Photographs of the before and after in fatigue test (One-Wave type, 200 °C)	95
Figure 4.25 Photographs of (a) One-wave type 300 °C and (b) Uniform-type 200 °C in fatigue test	96
Figure 4.26 S-N curves for DHP and C1220 copper in fatigue test (flange-model)	97
Figure 4.27 Fracture surfaces of the specimens (Flange-model)	101



## CHAPTER 1

### INTRODUCTION

#### 1.1 Background

Nowadays, equipment design in engineering must ensure that the equipment in question will not become damaged during use. Time dependant maintenance must also be factored into the design. Producing reliable equipment that can become standardized and fixing the time for proper maintenance will require individuals that are knowledgeable about the materials that are going to be used in the design of such equipment. These individuals must study the theory and perform testing simultaneously. Therefore, the study can be mainly divided into two parts. The first is corrosion tests on heat pipes that are commonly regarded as being primarily concerned with the identification of any incompatibilities, which may occur between the working fluid and the inner wall material [34]. The ultimate corrosion test, however, would be in the form of a long-term performance test under conditions appropriate to those in which the particular application will be used [17, 44]. The number of factors considered when examining corrosion tests on a particular working fluid/wall combination is very extensive and would require a large number of heat pipes to be fully comprehensive [4, 14, 36].

Thus, copper corrosion in aqueous solutions has been found to involve electron or charge-transfer between equation (1.1) copper dissolution and equations (1.2), (1.3) dissolved oxygen reduction reactions, which may be separated into partial or half-cell electrochemical reactions [18],



and



Representing equivalent reduction reactions in equation (1.2) acid and equation (1.3) neutral or alkaline solutions, respectively. The second is an educational text that provides guidance in this regard that is called “Mechanical Behavior of



Materials". It discusses the damage to materials that may occur in many different ways. The damages discussed are the format, such as elastic and plastic deformation as well as the damage to tough and brittle materials including damage due to fatigue testing processes and the environment. The main component in the text's analysis is plastic deformation. Plastic deformation is permanent deformation; there is also damage that can occur from fatigue. The type of damage relates to the material being used and the avoidance of such damage is determined by performing various tests on the proposed material. As the material has been made in a load cycle, it will be damaged under a stress load at a lower yield that varies in the fatigue tests. Sometimes we have to simulate a test frequency other than that of actual usage because of limited time for testing. This can be done if the environment does not affect the frequency of the fatigue damage. In some cases, the temperature being higher than room temperature or a gaseous environment will affect the frequency of the fatigue damage. A test piece will be damaged because of two elements: fatigue damage that is based on cycle dependent processing and the environment that is a time dependent process as well.

The pulsating heat-pipe (PHP) or the oscillating heat-pipe (OHP) is one type of heat transfer device that it is a relatively new member in the heat pipes family [35]. In the 1990s, Akachi invented a new type of heat-pipe that was made of a capillary tube [1] and it could be divided into 3 groups: (a) closed-end oscillating heat-pipe (CEOHP), a capillary tube that is bent into meandering turns and closed at both ends; (b) closed-loop oscillating heat-pipe (CLOHP), a capillary tube is connected at both ends to form a close-loop; and (c) closed-loop oscillating heat-pipe with check valves (CLOHP/CV), in which both ends of the capillary tube are connected to form a closed-loop. The CLOHP/CV is installed with check valves in the center of the heat pipe so the check valves can control the flow of the working fluid direction within the pipe and ensure that flow is in the same direction [30]. Each loop has one or more check valves. The CLOHP/CV is a new type of heat transfer device. It gives a high performance and several advantages. The CLOHP/CV is a very effective heat transfer device. Heat is transported from an evaporator to the condenser by the oscillation of a working fluid moving in an axial direction inside the tube. In this type of system, the inner diameter of the pipe is important. It must be small enough because under operation conditions liquid slugs and vapor plugs can be formed. The study has been performed on the operational



behavior, including various experimental studies [7, 26, 42]. However, the CLOHP/CV can be considered to be a standard cooling device that exhibits high performance in heat transfer. It works well in a wide variety of applications, such as cooling a CPU in a set of computers by constructing a heat exchanger, etc. However, when damage occurs to the heat pipe its causes can be complex and requires time-consuming maintenance, so it is imperative to study internal surface corrosion and fatigue in the early design phases of a system to determine the real operating life and projected maintenance requirements before damage occurs.

Therefore, this research aimed to study the parameters that affect a CLOHP/CV.

## **1.2 Objectives of the study**

1.2.1 To study the inner diameter of the tubes, inclination angle, evaporator length, working fluids and working temperatures and determine if they affected the internal pressure and the thermal performance of the CLOHP/CV under normal operating conditions.

1.2.2 To study the internal corrosion of the CLOHP/CV under normal operating conditions.

1.2.3. To study the fatigue of the copper tube and to apply this to a CLOHP/CV under normal operating conditions.

1.2.4. To construct an equation for the corrosion rate of the CLOHP/CV under normal operating conditions.

## **1.3 Scope of the study for pressure testing**

### **1.3.1 Independent Variables**

1.3.1.1 Copper tube inner diameters: 1.77 and 2.03 mm

1.3.1.2 Inclination angle: 90°, 80°, 60°, 40° and 20°

1.3.1.3 Lengths of evaporator section: 50, 100 and 150 mm

1.3.1.4 Working fluids: water, ethanol and R123

1.3.1.5 Working temperature in evaporator section: 100, 150 and 200 °C



### 1.3.2 Dependent variables

1.3.2.1 Internal pressure of the CLOHP/CV

1.3.2.2 Thermal performance of the CLOHP/CV

### 1.3.3 Control variables

1.3.3.1 Number of meandering turns: 40

1.3.3.2 Number of check valves: 2

1.3.3.3 Filling ratio 50% of total volume

1.3.3.4 Air velocity of condenser section: 0.6 m/s

## 1.4 Scope of the study for internal corrosion

### 1.4.1 Independent Variables

1.4.1.1 Working fluids: water and ethanol

1.4.1.2 Duration of testing: 500, 1000 and 3000 hours

### 1.4.2 Dependent variables

1.4.2.1 Internal corrosion of the CLOHP/CV

1.4.2.2 Capability predicting long term of CLOHP/CV

### 1.4.3 Control variables

1.4.3.1 Copper tube inner diameter: 2.03 mm

1.4.3.2 Length of evaporator section: 50 mm

1.4.3.3 Number of meandering turns: 40

1.4.3.4 Number of check valves: 2

1.4.3.5 Working temperature in evaporator section: 200 °C

1.4.3.6 Filling ratio 50% of total volume

1.4.3.7 Air velocity of condenser section: 0.6 m/s

## 1.5 Scope of the study for fatigue testing

### 1.5.1 Independent Variables

1.5.1.1 Copper tube: 2 types (screw and flange types)

1.5.1.2 Copper model: 3 models (one, two and uniform wave)

1.5.1.3 Temperature: 200 and 300 °C



### 1.5.2 Dependent variables

1.5.2.1 Fatigue of the copper tube

1.5.2.2 Number of cycles to failure

1.5.2.3 Life evaluation of the copper tube

### 1.5.3 Control variables

1.5.3.1 Stress controller: 200 MPa

## 1.6 Profits from the study

1.6.1 To determine the inner diameter of the tubes, inclination angle, evaporator length, working fluids and working temperatures that affected the internal pressure and thermal performance of the CLOHP/CV under normal operating conditions.

1.6.2 To determine the internal corrosion of the CLOHP/CV under normal operating conditions.

1.6.3 To determine the fatigue of the copper tube and to apply this to a CLOHP/CV under normal operating conditions.

1.6.4 To obtain an equation for the corrosion rate of a CLOHP/CV under normal operating conditions.



## CHAPTER 2

### Theory and Literature Review

#### 2.1 Heat pipe

##### 2.1.1 Structure and Principle Operation

The heat pipe was firstly invented in 1831 by L. P. Perkins. He patented the heat pipe as the “Single-phase Perkins Tube”. Later in 1892, L.P.Perkins and W.E. Buck developed and patented the two-phase heat pipe. Since then, the heat pipe has been continuously developed and applied in engineering work. At present, heat pipe technology has developed a lot of usability. As a result, there are several types of heat pipe such as Rotating Heat Pipe, Loop Heat Pipe and Gravitational Assisted Two-Phase Closed Thermosyphon, etc. However, various types of the heat pipe have been developed from the basics of two types of heat pipe. The first one, the conventional heat pipe, is a heat pipe with a wick structure inside. The other one, thermosyphon, is a heat pipe without a wick structure and gravity is used to circulate the working fluids inside the tube. The components of the conventional heat pipe and thermosyphon are as follows;

##### 2.1.1.1 Container

It contains the working fluids and wick structure. Generally, it is constructed from high thermal conductivity materials. It has enough strength to resist the vapor pressure of the working fluids inside the tube and any chemical reactions that should take place among these materials, the working fluids and surrounding. Normally, the heat pipe can be divided into three parts. First, the evaporator section receives the heat from the heat source. The middle part is the adiabatic section. The last is the condenser section, which removes the heat from the evaporator section to the heat sink.

##### 2.1.1.2 Working fluid

It is the medium transferring the heat from the high temperature to the low temperature reservoir. When the working fluids in the evaporator section receive heat from the heat source, they will evaporate and become a vapor before moving to the condenser section. When the vapor contacts on the cool surface of the condenser, the





latent heat of the vapor will be transferred to the inner surface of the condenser. Then, the working fluid will condense into a liquid and flow back to the evaporator section.

### 2.1.1.3 Wick structure

Its function is to transport the condensate working fluids from the condenser section back to the evaporator section with capillary force. This principle means a conventional heat pipe is able to transfer heat at all orientations. The heat pipe can be operated in a horizontal position or top heat mode. A heat pipe without the wick structure is called a thermosyphon. As it does not have a wick structure, the condensate working fluids are returned back to the evaporator by gravity. Thus, a thermosyphon can be only operated in a vertical position or near vertical position in the bottom heat mode. It is unable to operate in either horizontal orientation or top heat mode. The structure of a conventional heat pipe and thermosyphon are shown in Figure 2.1.

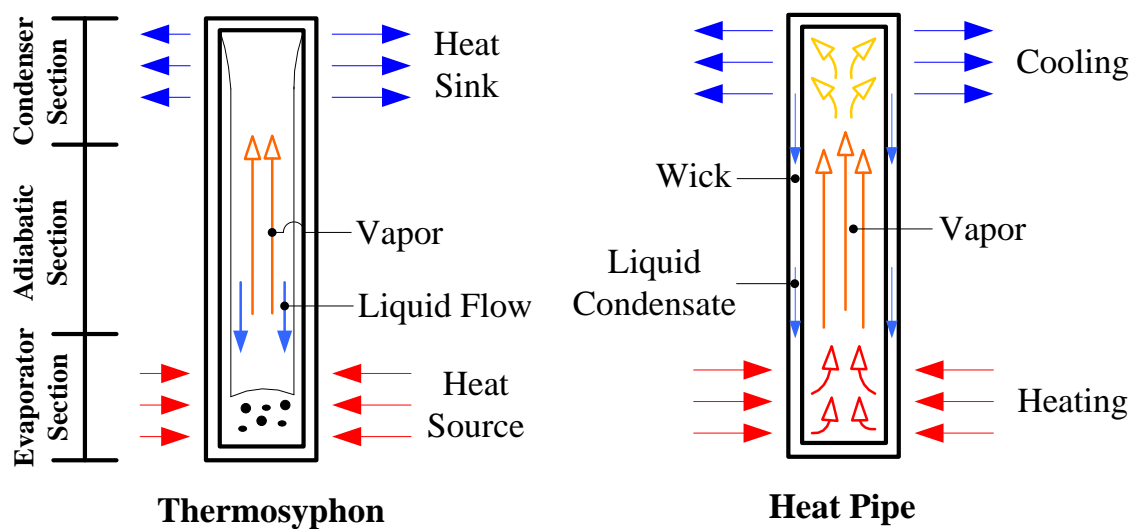


Figure 2.1 Structure of conventional heat pipe and thermosyphon [12]



## 2.2 Oscillating heat pipe

In this the heat pipe is reduced in size and this produces a problem. This problem is associated with the conventional heat pipe and it occurs when the pipe diameter becomes small, reaching the capillary scale. At this scale, the meniscus effect will take place from the surface tension of the working fluid and this forms liquid slugs alternating with vapor bubbles throughout the entire length of the heat pipe [28]. Thus, the heat pipe cannot transport the heat. Moreover, it is important to examine other limitations such as, the capillary limit, which occurs when the wick structure can not return enough liquid to the evaporator section. The entrainment limit, which is due to the counter-flow effect between the liquid and vapor, also needs to be examined.

Taking advantage of the alternating formation of liquid and vapor, new inventions and developments have been made. One new idea is to connect a bundle of parallel capillary tubes into a single undulating tube, without an internal capillary structure. When the first end of the bundle of turns of the undulating capillary pipe is subjected to high temperature, the working fluid oscillates axially in the capillary tube to carry heat to the end with a lower temperature [11].

The basic heat transfer mechanism in a pulsating heat pipe is the oscillating movement of the fluid plus the phase change phenomena. This mechanism occurs when the inner diameter of the tube is sufficiently small, according to the working fluid type. The driving force of a pulsating heat pipe is the pressure force generated by evaporation at the higher temperature end, as in a conventional heat pipe [13, 16]. However, unlike the conventional heat pipe, no steady state pressure equilibrium can be achieved. The evaporation at the higher temperature end increases the vapor pressure, which causes the bubbles in the evaporator section to grow. This pushes the liquid column toward the lower temperature end. The condensation at this end will further enhance the pressure difference between the two ends. Due to the interconnection of the tube, the motion of the liquid slugs and vapor bubbles in one section of the tube towards the condenser also leads to the motion of slugs and bubbles in the next tube section towards the higher temperature end in the next section [41, 43]. This mechanism occurs due to the restoring force. The inter-play between the driving force and the restoring force leads to an oscillation of the liquid slugs and vapor bubbles in the axial direction. The frequency



and amplitude of the oscillation are expected to be dependent on the heat transferred and the filling ratio of the working fluid [8]. The oscillating heat pipe is a relatively new type of heat pipe and an improvement over a thermosyphon. It is commonly referred to as an oscillating heat pipe (OHP) or pulsating heat pipe. The oscillation of slugs and plugs in the OHP are self-sustained through the evaporation of liquid slugs and the condensation of vapor plugs. Therefore, the heat from the high temperature section can be transported to another section at a lower temperature. The advantages of the OHP include simplicity of construction, only one tube, no capillary structure, high thermal performance, ability to operate in any position and operational flexibility.

OHPs can be divided into three types: closed-end oscillating heat pipe, closed-loop oscillating heat pipe and closed-loop oscillating heat pipe with check valves.

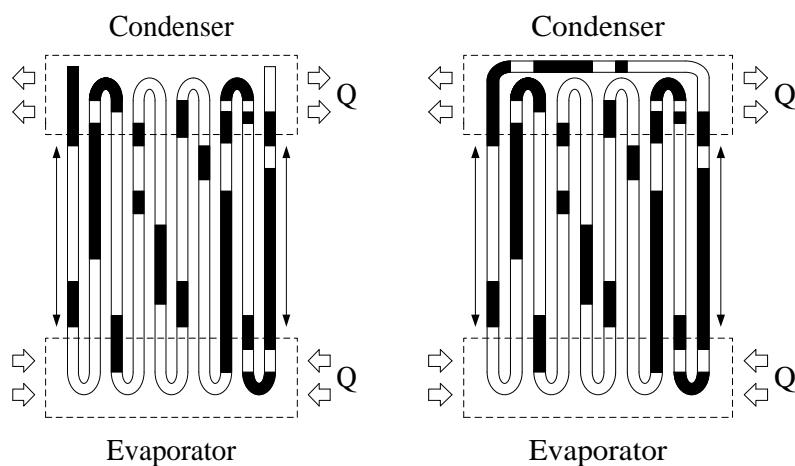
2.2.1 A closed-end oscillating heat pipe (CEOHP) is presented in Figure 2.2(a). It is made from a meandering capillary tube that is closed at both ends. In this case, heat transfer occurs by oscillation, which is driven by fluctuating pressure, perturbation pressure and fast wave.

2.2.2 A closed-loop oscillating heat pipe (CLOHP) is shown in Figure 2.2(b). It consists of a meandering capillary tube forming a closed loop. Heat transfer occurs by oscillation of the working fluid in the direction of the pipe's longitudinal axis superimposed on bulk circulation in either direction.

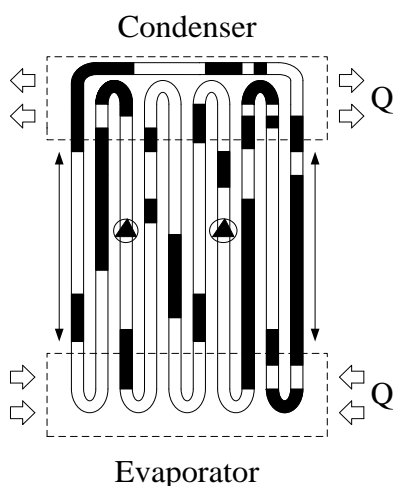
2.2.3 A closed-loop oscillating heat pipe with check valves (CLOHP/CV) is illustrated in Figure 2.2(c). It is made from a meandering capillary tube. The ends of the tube are welded together to form a closed-loop and check valves are inserted at different points along the capillary tube.

The CLOHP/CV gives the best type of heat transfer from the evaporator section to the condenser section. Moreover, the heat transfer rate of the CLOHP/CV is better than that of the CLOHP and the CEOHP [25]. Therefore, the CLOHP/CV was selected for use in this study.





(a) Closed-end oscillating heat-pipe (CEOHP) (b) Closed-loop oscillating heat-pipe (CLOHP)



(c) Closed-loop oscillating heat-pipe with check valves (CLOHP/CV)

Figure 2.2 Types of oscillating heat-pipe: (a) Closed-end oscillating heat-pipe (CEOHP), (b) Closed-loop oscillating heat-pipe (CLOHP) and (c) Closed-loop oscillating heat-pipe with check valves (CLOHP/CV) [25]

### 2.3 Check valve

It consists of four sections: a ball, case, conical valve seat and ball stopper, as shown in Figure 2.3. The advantage of a check valve is that it permits liquid slugs to flow in only one direction. The ball is used to control the flow direction; it is inserted in the middle of the component. The conical valve seat and ball stopper are covered by a case; they can stop the ball and prevent a reversal of the liquid slug or vapor plug.



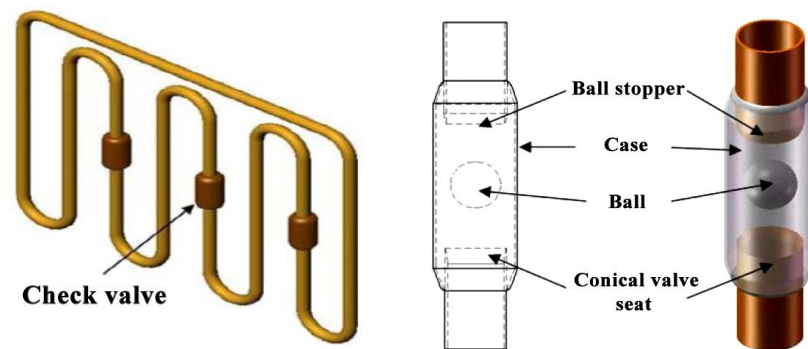


Figure 2.3 Structure of check-valve [31]

The OHP is a new type of heat pipe technology. Therefore, it is necessary to understand the principle of operation, which is explained by Akachi et al. [2]. The fundamental mechanism of the oscillating heat pipe's heat transfer results from the working fluid oscillating that incorporates the phase change of the working fluids. The operation can be done if there is a coexistence of liquid plugs and vapor bubbles throughout the length of the tube. This condition can be established by vacuuming a

tube that has an inner diameter less than  $2\sqrt{\frac{\sigma}{\rho_l g}}$  (Maezawa et al. [20]) and partially

filling the tube with working fluid. When the oscillating heat pipe is operated, there is evaporation on the side that contacts the high temperature reservoir resulting in higher vapor pressure and vapor bubble size. The change in size of the bubble causes the driving force, pushing the liquid slug to the condenser, which has the lower temperature. In addition, the condensation at the condenser will cause the increase in the pressure difference between both sides. It should be noted that the oscillating heat pipe is made from a single tube; therefore, the movement of the liquid slug and vapor bubble in a particular turn will cause the other turns to move as well. That is when the liquid is pushed by the vapor into the condenser section, the liquid and vapor in the next turn will also be pushed into the evaporator section. The liquid and vapor that are pushed back into the evaporator will have higher pressure resulting in restoring force. The cooperation between the driving and restoring forces generates the oscillating flow along the tube axis [32]. Although there are many studies about the principle of



operation of an OHP, there are still many questions, especially for the heat transfer characteristic. This question concerned a number of reports that have studied the oscillating heat pipe's heat transfer characteristic and these will be discussed later.

The thermal performance of the CLOHP/CV at normal operation means the investigation of parameters that have an effect on heat transfer for the oscillating heat pipe at a particular operating point where the heat transfer rate is lower than that at the performance limits. These parameters are the geometry of the tube (i.e., inner diameter, evaporator length and number of turns or total lengths), heat transfer rate, types of working fluids and inclination angles of the oscillating heat pipe. The thermal performance of the CLOHP/CV was evaluated by calculating the heat transfer rate to the ambient air at the condenser part and applying the heat transfer rate for a heating process [29], which is shown as equation (2.1),

$$Q = \dot{m}C_p(T_{out} - T_{in}) \quad (2.1)$$

The error of the calculation by equation (2.2) was found as [5],

$$dQ = \left[ \left( \frac{\partial Q}{\partial \dot{m}} d\dot{m} \right)^2 + \left( \frac{\partial Q}{\partial T_{out}} dT_{out} \right)^2 + \left( \frac{\partial Q}{\partial T_{in}} dT_{in} \right)^2 \right]^{1/2} \quad (2.2)$$

where  $Q$  is the heat transfer rate of the CLOHP/CV,  $C_p$  is the specific heat capacity of dry air and  $T_{out}$  and  $T_{in}$  are the temperature of dry air at the outlet and the inlet of the condenser section.  $\dot{m}$  is the mass flow rate of dry air that can be calculated by the following equation (2.3):

$$\dot{m} = \rho v A \quad (2.3)$$

where  $\rho$  is the dry air density,  $v$  is the dry air velocity and  $A$  is the cross sectional air flowing area. In this experiment, the CLOHP/CV thermal resistance ( $R$ ) would be equal to the temperature difference between the condenser section and evaporator section and the heat transfer rate that can be calculated by equation (2.4):



$$R = \frac{T_e - T_c}{Q} \quad (2.4)$$

where  $T_e$  and  $T_c$  are the wall temperatures of the evaporator section and condenser section, respectively.

The conduction heat transfer rate of copper capillary tubes can be evaluated by equation (2.5):

$$Q_{cond} = \frac{kAN(T_{evap} - T_{cond})}{L} \quad (2.5)$$

where  $Q_{cond}$  is the conduction heat transfer rate of the copper tube,  $k$  is the heat conduction of copper,  $A$  is the cross section area of the tube,  $N$  is the number of tubes,  $L$  is the summation of the evaporator, adiabatic and condenser lengths,  $T_{evap}$  is the temperature at the evaporator section and  $T_{cond}$  is the temperature at condenser section, compared with the heat pipe as a working fluid.

## 2.4 Corrosion

Corrosion involves the deterioration of a material as it reacts with its environment. Corrosion is the primary means by which metals deteriorate. Corrosion literally consumes the material reducing its load carrying capability and causing stress concentrations. Corrosion is often a major part of maintenance costs and corrosion prevention is vital in many designs. Corrosion is not expressed in terms of a design property value like other properties but rather in more qualitative terms such as a material is immune, resistant, susceptible, or very susceptible to corrosion.

The corrosion process is usually electrochemical in nature, having the essential features of a battery. Corrosion is a natural process that commonly occurs because unstable materials, such as refined metals, want to return to a more stable compound. For example, some metals, such as gold and silver, can be found in the earth in their natural, metallic state and they have little tendency to corrode. Iron is a moderately active metal and corrodes readily in the presence of water. The natural state of iron is



iron oxide and the most common iron ore is Hematite, with a chemical composition of  $\text{Fe}_2\text{O}_3$ . Rust, the most common corrosion product of iron, also has a chemical composition of  $\text{Fe}_2\text{O}_3$ .

The difficulty in terms of energy required to extract metals from their ores is directly related to the ensuing tendency to corrode and release this energy. The electromotive force series (Table 2.1) is a ranking of metals with respect to their inherent reactivity. The most noble metal is at the top and has the highest positive electrochemical potential. The most active metal is at the bottom and has the most negative electrochemical potential.

Table 2.1 Partial electromotive force (emf) series [10]

Partial Electromotive Force Series	
Standard Potential	Electrode Reaction (at 25°C), V-SHE
$\text{Au}^{3+} + 3\text{e}^- \rightarrow \text{Au}$	1.498
$\text{Pd}^{2+} + 2\text{e}^- \rightarrow \text{Pd}$	0.987
$\text{Hg}^{2+} + 2\text{e}^- \rightarrow \text{Hg}$	0.854
$\text{Ag}^+ + \text{e}^- \rightarrow \text{Ag}$	0.799
$\text{Cu}^+ + \text{e}^- \rightarrow \text{Cu}$	0.521
$\text{Cu}^{2+} + 2\text{e}^- \rightarrow \text{Cu}$	0.337
$2\text{H}^+ + 2\text{e}^- \rightarrow \text{H}_2$	0.000
$\text{Pb}^{2+} + 2\text{e}^- \rightarrow \text{Pb}$	-0.126
$\text{Sn}^{2+} + 2\text{e}^- \rightarrow \text{Sn}$	-0.136
$\text{Ni}^{2+} + 2\text{e}^- \rightarrow \text{Ni}$	-0.250
$\text{Co}^{2+} + 2\text{e}^- \rightarrow \text{Co}$	-0.277
$\text{Cd}^{2+} + 2\text{e}^- \rightarrow \text{Cd}$	-0.403
$\text{Fe}^{2+} + 2\text{e}^- \rightarrow \text{Fe}$	-0.440
$\text{Cr}^{3+} + 3\text{e}^- \rightarrow \text{Cr}$	-0.744
$\text{Cr}^{2+} + 2\text{e}^- \rightarrow \text{Cr}$	-0.910
$\text{Zn}^{2+} + 2\text{e}^- \rightarrow \text{Zn}$	-0.763
$\text{Mn}^{2+} + 2\text{e}^- \rightarrow \text{Mn}$	-1.180
$\text{Ti}^{2+} + 2\text{e}^- \rightarrow \text{Ti}$	-1.630
$\text{Al}^{3+} + 3\text{e}^- \rightarrow \text{Al}$	-1.662
$\text{Be}^{2+} + 2\text{e}^- \rightarrow \text{Be}$	-1.850
$\text{Mg}^{2+} + 2\text{e}^- \rightarrow \text{Mg}$	-2.363
$\text{Li}^+ + \text{e}^- \rightarrow \text{Li}$	-3.050





Corrosion involves two chemical processes, oxidation and reduction. Oxidation is the process of stripping electrons from an atom and reduction occurs when an electron is added to an atom. The oxidation process takes place at an area known as the anode. At the anode, positively charged atoms leave the solid surface and enter into an electrolyte as ions. The ions leave their corresponding negative charge in the form of electrons in the metal; they travel to the location of the cathode through a conductive path. At the cathode, the corresponding reduction reaction takes place and consumes the free electrons. The electrical balance of the circuit is restored at the cathode when the electrons react with neutralizing positive ions, such as hydrogen ions, in the electrolyte. From this description, it can be seen that there are four essential components that are needed for a corrosion reaction to proceed. These components are an anode, a cathode, an electrolyte with oxidizing species and some direct electrical connection between the anode and cathode. Although atmospheric air is the most common environmental electrolyte, natural waters, such as seawater or rain, as well as man-made solutions, are the environments most frequently associated with corrosion problems.

A typical situation might involve a piece of metal that has anodic and cathodic regions on the same surface. If the surface becomes wet, corrosion may take place through ionic exchange in the surface water layer between the anode and cathode. Electron exchange will take place through the bulk metal. Corrosion will proceed at the anodic site according to a reaction such as [10].



where M is a metal atom. The resulting metal cations ( $M^+$ ) are available at the metal surface to become corrosion products, such as oxides and hydroxides, etc. The liberated electrons travel through the bulk metal (or another low resistance electrical connection) to the cathode, where they are consumed by cathodic reactions such as:



The basic principles of corrosion that were just covered, generally apply to all corrosion situations except certain types of high temperature corrosion. However, the



process of corrosion can be very straightforward, but is often very complex due to a variety of variables that can contribute to the process. A few of these variables are the composition of the material acting in the corrosion cell, the heat treatment and stress state of the materials, the composition of the electrolyte, the distance between the anode and the cathode, temperature, protective oxides and coating, etc.

Corrosion is the gradual destruction of material, usually metals, by chemical reactions with its environment. In the most common use of the word, this means electrochemical oxidation of metals in reaction with an oxidant such as oxygen. Rusting, the formation of iron oxides is a well-known example of electrochemical corrosion. This type of damage typically produces oxide(s) or salt(s) of the original metal. Corrosion can also occur in materials other than metals, such as ceramics or polymers, although in this context, the term degradation is more common. Corrosion degrades the useful properties of materials and structures including strength, appearance and permeability to liquids and gases. Many structural alloys corrode merely from exposure to moisture in the air, but the process can be strongly affected by exposure to certain substances. Corrosion can be concentrated locally to form a pit or crack, or it can extend across a wide area more or less uniformly corroding the surface. As corrosion is a diffusion-controlled process, it occurs on exposed surfaces. As a result, methods to reduce the activity of the exposed surface, such as passivation and chromate conversion, can increase a material's corrosion resistance. However, some corrosion mechanisms are less visible and less predictable.

Corrosion is commonly classified based on the appearance of the corroded material. The classifications used vary slightly from reference to reference but there are generally considered to be eight different forms of corrosion. There forms are:

2.4.1 Uniform or general corrosion that is distributed more or less uniformly over a surface. The surface effect produced by most direct chemical attacks (e.g. as by an acid) is a uniform etching of the metal.



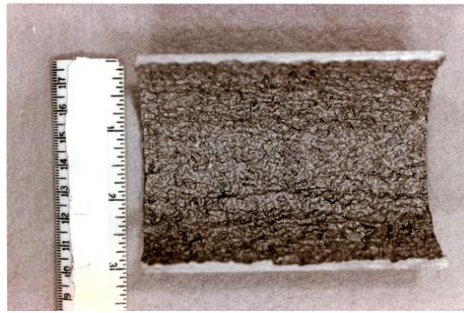


Figure 2.4 Uniform corrosion

(<http://octane.nmt.edu/WaterQuality/corrosion/uniform.aspx>) [45]

2.4.2 Localized corrosion that is confined to small area. Localized corrosion often occurs due to a concentrated cell. A concentrated cell is an electrolytic cell in which the electromotive force is caused by a concentration of some components in the electrolyte. This difference leads to the formation of distinct anode and cathode regions.

2.4.2.1 Pitting corrosion that is confined to small areas and takes the form of cavities on a surface. Pitting corrosion is localized corrosion that occurs as microscopic defects on a metal surface. The pits are often found underneath surface deposits caused by corrosion product accumulation.



Figure 2.5 Pitting corrosion

(<http://www.rmutphysics.com/charud/pdf-learning/2/material/2Corrosion.pdf>) [46]

2.4.2.2 Crevice corrosion occurring at locations where easy access to the bulk environment is prevented, such as the mating surfaces of two components. Crevice or contact corrosion is the corrosion produced at the region of contact of metals with



metals or metals with nonmetals. It may occur at washers, under barnacles, at sand grains, under applied protective films and at pockets formed by threaded joints.



Figure 2.6 Crevice corrosion

(<http://coxengineering.sharepoint.com/Pages/Crevice.aspx>) [47]

2.4.2.3 Filiform corrosion that occurs under some coatings in the form of randomly distributed threadlike filaments. This type of corrosion occurs on painted or plated surfaces when moisture permeates the coating. Long branching filaments of corrosion product extend out from the original corrosion pit and cause degradation of the protective coating.



Figure 2.7 Filiform corrosion

(<http://corrosion.ksc.nasa.gov/filicor.htm>) [48a]

2.4.3 Intergranular preferential corrosion at or along the grain boundaries of a metal or alloy. Intergranular corrosion is an attack on or adjacent to the grain boundaries of a metal or alloy. A highly magnified cross section of most commercial alloys will show their granular structure. This structure consists of the quantities of



individual grains and each of these tiny grains has a clearly defined boundary that chemically differs from the metal within the grain center. Heat treatment of stainless steels and aluminum alloys accentuates this problem.

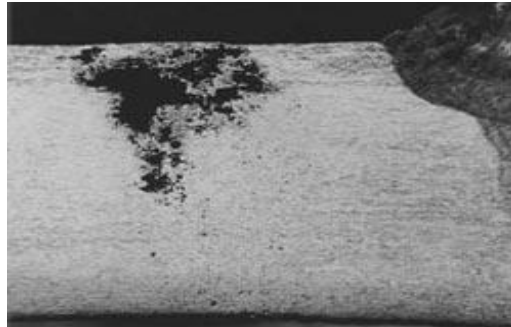


Figure 2.8 Intergranular corrosion  
(<http://corrosion.ksc.nasa.gov/intercor.htm>) [48b]

2.4.3.1 Exfoliation is a specific form of corrosion that travels along grain boundaries parallel to the surface of the part causing lifting and flaking at the surface. The corrosion products expand between the uncorroded layers of metal to produce a look that resembles the pages of a book. Exfoliation corrosion is associated with sheet, plate and extruded products and usually initiates at unpainted or unsealed edges or holes of susceptible metals.



Figure 2.9 Exfoliation corrosion  
(<http://corrosion.ksc.nasa.gov/intercor.htm>) [48b]

2.4.4 Galvanic corrosion is associated primarily with the electrical coupling of materials with significantly different electrochemical potentials. Galvanic corrosion is an electrochemical action of two dissimilar metals in the presence of an electrolyte and an electron conductive path. It occurs when dissimilar metals are in contact, for example, when aluminum alloys or magnesium alloys are in contact with steel (carbon steel or stainless steel), galvanic corrosion can occur and accelerate the corrosion of the aluminum or magnesium. This can be seen in Figure 2.10 where the aluminum helicopter blade has corroded near where it was in contact with steel.



Figure 2.10 Galvanic corrosion

(<http://siamkaewkumsai.blogspot.com/2010/05/galvanic-corrosion.html>) [49]

2.4.5 Environmental cracking is the brittle fracture of a normally ductile material that occurs partially due to the corrosive effect of an environment.

2.4.5.1 Corrosion fatigue is fatigue cracking that is characterized by uncharacteristically short initiation time and/or growth rate due to damage from corrosion or buildup of corrosion products. Corrosion fatigue is a special case of stress corrosion caused by the combined effects of cyclic stress and corrosion. No metal is immune from some reduction of its resistance to cyclic stressing if the metal is in a corrosive environment. Damage from corrosion fatigue is greater than the sum of the damage from both cyclic stresses and corrosion. Control of corrosion fatigue can be accomplished by either lowering the cyclic stresses or by corrosion control.



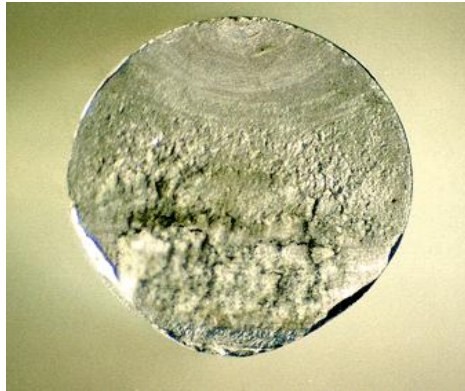


Figure 2.11 Fatigue corrosion

(<http://www.rmutphysics.com/charud/pdf-learning/2/material/2Corrosion.pdf>) [46]

2.4.5.2 High temperature hydrogen attack is the loss of strength and ductility of steel due to a high temperature reaction of absorbed hydrogen with carbides. The result of the reaction is decarburization and internal fissuring.

2.4.5.3 Hydrogen embrittlement is the loss of ductility of a metal resulting from absorption of hydrogen. Hydrogen embrittlement is a problem with high-strength steels, titanium and some other metals. Control is by eliminating hydrogen from the environment or by the use of resistant alloys.



Figure 2.12 Hydrogen embrittlement corrosion

([www.hydrogen-generators.ws/hydrogen-embrittlement.htm](http://www.hydrogen-generators.ws/hydrogen-embrittlement.htm)) [50]





2.4.5.4 Liquid metal cracking is cracking caused by contact with a liquid metal.

2.4.5.5 Stress corrosion is cracking of a metal due to the combined action of corrosion and a residual or applied tensile stress. Stress corrosion cracking (SCC) is caused by the simultaneous effects of tensile stress and a specific corrosive environment. Stresses may be due to the applied loads, residual stresses from the manufacturing process, or a combination of both.

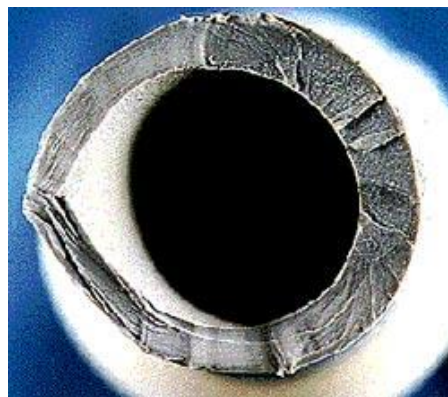


Figure 2.13 Stress corrosion

(<http://corrosion.ksc.nasa.gov/stresscor.htm>) [48c]

2.4.6 Erosion corrosion is a corrosion reaction that has been accelerated by the relative movement of a corrosive fluid and a metal surface. Erosion corrosion is the result of a combination of an aggressive chemical environment and high fluid-surface velocities. This can be the result of fast fluid flow past a stationary object, such as in the case of the oil-field check valve shown in Figure 2.14, or it can result from the quick motion of an object in a stationary fluid, such as happens when a ship's propeller churns the ocean.







Figure 2.14 Erosion corrosion

(<http://corrosion.ksc.nasa.gov/eroscor.htm>) [48d]

2.4.7 Fretting corrosion is damage at the interface of two contacting surfaces under load but capable of some relative motion. The damage is accelerated by movement at the interface that mechanically abrades the surface and exposes fresh material to corrosive attack. Figure 2.15 shows fretting corrosion of a fence post and wires that swing in the wind and wear against the post. Both the fence post and the connecting wires are experiencing fretting corrosion.



Figure 2.15 Fretting corrosion

(<http://corrosion.ksc.nasa.gov/fretcor.htm>) [48e]



2.4.8 Dealloying is the selective corrosion of one or more components of a solid solution alloy. Dealloying is a rare form of corrosion found in copper alloys, gray cast iron and some other alloys. Dealloying occurs when the alloy loses the active component of the metal and retains the more corrosion resistant component in a porous "sponge" on the metal surface.

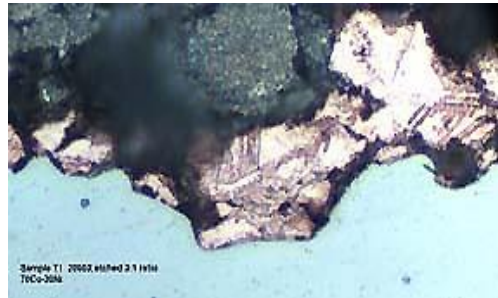


Figure 2.16 Dealloying

(<http://corrosion.ksc.nasa.gov/dealloying.htm>) [48f]

2.4.8.1 Dezincification is corrosion resulting in the selective removal of zinc from copper-zinc alloys.

Thus, the copper corrosion in aqueous solutions has been found to involve electron or charge-transfer between equation (2.8) copper dissolution and equations (2.9), (2.10) dissolved oxygen reduction reactions, which may be separated into partial or half-cell electrochemical reactions [18],



and



Representing the equivalent reduction reactions in equation (2.9) acid and equation (2.10) neutral or alkaline solutions, respectively, as show in Figure 2.17.



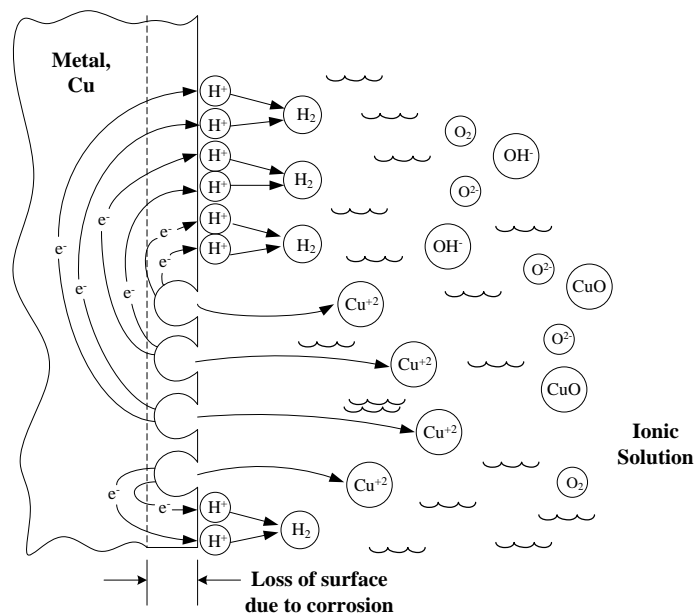


Figure 2.17 Schematic of the corrosion reaction

## 2.5 Fatigue

Most engineering failures are mainly due to fatigue, in which the components are subjected to fluctuating or cyclic loading such as suspended bridges, rails, or airplane wings. Though the fluctuating load is normally less than the yield strength of the materials, it results in fracture behavior that is more severe than that achieved from static loading. Fatigue failures are therefore unpredictable and provide high-risk situations, if the operators are not aware of material behavior when subjected to fatigue loading.

Fatigue failures can be easily observed from the unique characteristics of the fracture surfaces, revealed as a beach mark pattern. Fatigue failures are also driven by severe environments. For example, corrosion fatigue is a combined situation of fatigue loading in a corrosive environment. Fatigue is the condition whereby a material cracks or fails as a result of repeated (cyclic) stresses applied below the ultimate strength of the material. Fatigue failures generally involve three stages:

2.5.1 Crack initiation

2.5.2 Crack propagation

2.5.3 Fast fracture



Fatigue failures often occur quite suddenly with catastrophic (disastrous) results, and although most insidious for metals, polymers and ceramics (except for glass) are also susceptible to sudden fatigue failures. Fatigue causes brittle like failures even in normally ductile materials with little gross plastic deformation occurring prior to fracture. The process occurs through the initiation and propagation of cracks and ordinarily, the fracture surface is close to perpendicular to the direction of maximum tensile stress.

Applied stresses may be axial (tension-compression), flexural (bending), or torsional (twisting) in nature. In general, there are three possible fluctuating stress-time modes possible. The simplest is completely reversed constant amplitude, where the alternating stress varies from a maximum tensile stress to a minimum compressive stress of equal magnitude. The second type, termed repeated constant amplitude, occurs when the maxima and minima are asymmetrical relative to the zero stress level. Lastly, the stress level may vary randomly in amplitude and frequency, which is merely termed random cycling. The following parameters are utilized to identify fluctuating stress cycles:

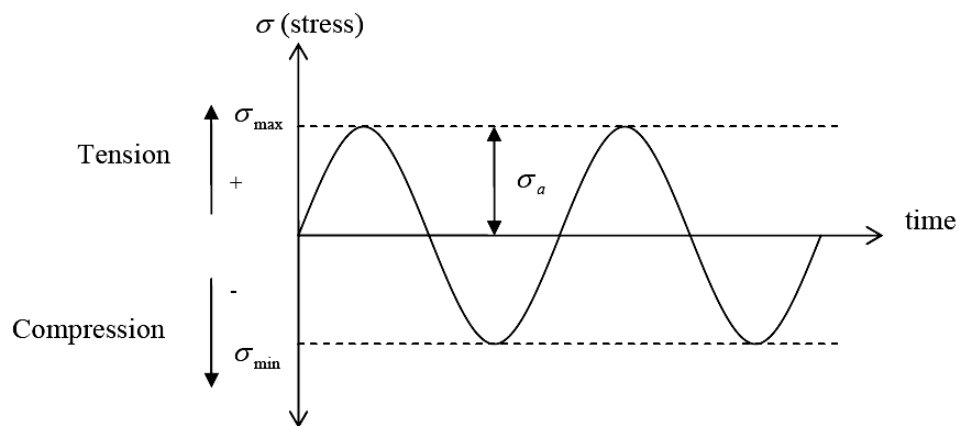


Figure 2.18 Schematic illustrating cyclic loading parameters

$$\text{Mean Stress } (\sigma_m): \quad \sigma_m = \frac{\text{Maximum Stress } (\sigma_{\max}) + \text{Minimum Stress } (\sigma_{\min})}{2} \quad (2.11)$$

$$\text{Stress Amplitude } (\sigma_a): \quad \sigma_a = \frac{\text{Maximum Stress } (\sigma_{\max}) - \text{Minimum Stress } (\sigma_{\min})}{2} \quad (2.12)$$

$$\text{Stress Range } (\sigma_r): \quad \sigma_r = \sigma_{\max} - \sigma_{\min} \quad (2.13)$$



$$\text{Stress Ratio (R): } R = \frac{\sigma_{\min}}{\sigma_{\max}} \quad (2.14)$$

$$\text{Amplitude ratio (A): } A = \frac{\sigma_a}{\sigma_m} \quad (2.15)$$

Tensile stresses are normally considered positive and compressive stresses are considered negative.

The fatigue life cycles ( $N_f$ ) of a component is defined by the total number of stress cycles required to cause failure. Fatigue life can be separated into three stages where:

$$N_f = N_i + N_p \quad (2.16)$$

Crack initiation cycles ( $N_i$ ) required before initiating a crack. Generally results from dislocation pile-ups and/or imperfections such as surface scratches and voids, etc.

Crack growth cycles ( $N_p$ ) required before growth of the crack in a stable manner to a critical size. Generally controlled by stress level; since most common materials contain flaws, the prediction of crack growth is the most studied aspect of fatigue.

Rapid fracture is a very rapid critical crack growth that occurs when the crack length reaches a critical value. Since rapid fracture occurs quickly, there is no rapid fracture term in the fatigue life expression.

Determination of Stress and Strain: Stress or strain concentration is taken into account by employing simplified methods, such as Neuber's law. Neuber's rule indicates that once the elastic stress and strain are obtained as  $(\sigma^e, \varepsilon^e)$  then the stress and strain  $(\sigma, \varepsilon)$  in the inelastic region changes so as to keep the products of the stress and strain constant in the inelastic region, namely [38],

$$\sigma \varepsilon = \sigma^e \varepsilon^e = K_t^2 \sigma_n \varepsilon_n = \text{const. (Neuber's law)} \quad (2.17)$$



The local stress amplitude and strain amplitude in the high stress region are obtained as the intersection point between Neuber hyperbola and the cyclic material stress-strain relation for fatigue strength evaluation.

As a simplified method to predict the inelastic behavior, stress redistribution locus (abbreviated as SRL) is a method that has been recently proposed and investigated in conjunction with the evaluation scheme of creep-fatigue strength. The SRL approach is based on stress redistribution locus as in Figure 2.19. This locus is unique for similar structures; therefore, this locus is used for concentrated strain estimation. The SRL approach can be expressed in a similar form to Neuber's rule; therefore, the SRL equation becomes Equation (2.18) using the reduction coefficient  $\kappa$  as:

$$\sigma \left( \frac{\sigma}{E} + \kappa \varepsilon_p \right) = \sigma \varepsilon = \sigma^e \varepsilon^e = K_t^2 \sigma_n \varepsilon_n = \text{const.} \quad (2.18)$$

The stress and strain can be calculated as the intersection point of the SRL curve and stress-strain curve as shown in Figure 2.19 and predicts the smaller strain compared to Neuber's rule.

Both Neuber's curve and SRL express stress redistribution and strain concentration. The local stress and strain can be located on a cyclic stress-strain curve. Therefore, the concentrated strains can be estimated by the intersection point of Neuber's rule or SRL cyclic stress-strain curve (in Figure 2.19, stress-strain relation).

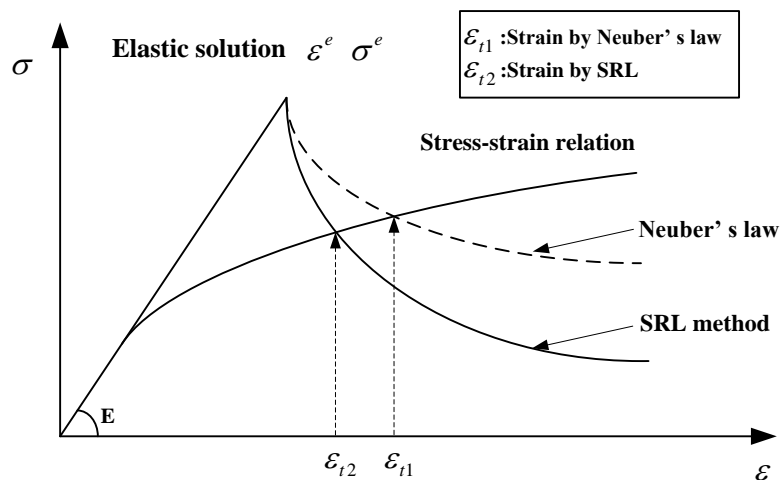


Figure 2.19 Strain estimated by Neuber's law and SRL method [37]



### S-N Fatigue Properties

There are two general types of fatigue tests conducted. One test focuses on the nominal stress required to cause a fatigue failure in a certain number of cycles. This test results in data presented as a plot of stress (S) against the number of cycles to failure (N), which is known as an S-N curve. A log scale is almost always used for N. The data is obtained by cycling smooth or notched specimens until failure. The usual procedure is to test the first specimen at a high peak stress where failure is expected in a fairly short number of cycles. The test stress is decreased for each succeeding specimen until one or two specimens do not fail in the specified numbers of cycles, which is usually at least  $10^7$  cycles. The highest stress at which a run out (non-failure) occurs is taken as the fatigue threshold. Not all materials have a fatigue threshold (most nonferrous metallic alloys do not) and for these materials the test is usually terminated after about  $10^8$  or  $5 \times 10^8$  cycles. Since the amplitude of the cyclic loading has a major effect on the fatigue performance, the S-N relationship is determined for one specific loading amplitude. The amplitude is expressed as the R ratio value, which is the minimum peak stress divided by the maximum peak stress. ( $R = \sigma_{\min} / \sigma_{\max}$ ). It is most common to test at an R ratio of 0.1, but families of curves, with each curve at a different R ratio, are often developed. A variation to the cyclic stress controlled fatigue test is the cyclic strain controlled test. In this test, the strain amplitude is held constant during cycling. Strain controlled cyclic loading is more representative of the loading found in thermal cycling, where a component expands and contracts in response to fluctuations in the operating temperature. It should be noted that there are several shortcomings of S-N fatigue data. First, the conditions of the test specimens do not always represent actual service conditions. For example, components with surface conditions, such as pitting from corrosion, which differs from the condition of the test specimens will have significantly different fatigue performances. Furthermore, there is often a considerable amount of scatter in fatigue data even when carefully machined standard specimens out of the same lot of material are used. Since there is considerable scatter in the data, a reduction factor is often applied to the S-N curves to provide conservative values for the design of components.

**Stress-Life Diagram (S-N Diagram):** The basis of the stress-life method is the S-N diagram, shown schematically for two materials in Figure 2.20. The S-N



diagram plots nominal stress amplitude  $S$  versus cycles to failure  $N$ . There are numerous testing procedures to generate the required data for a proper S-N diagram. S-N test data is usually displayed on a log-log plot, with the actual S-N line representing the mean of data from several tests.

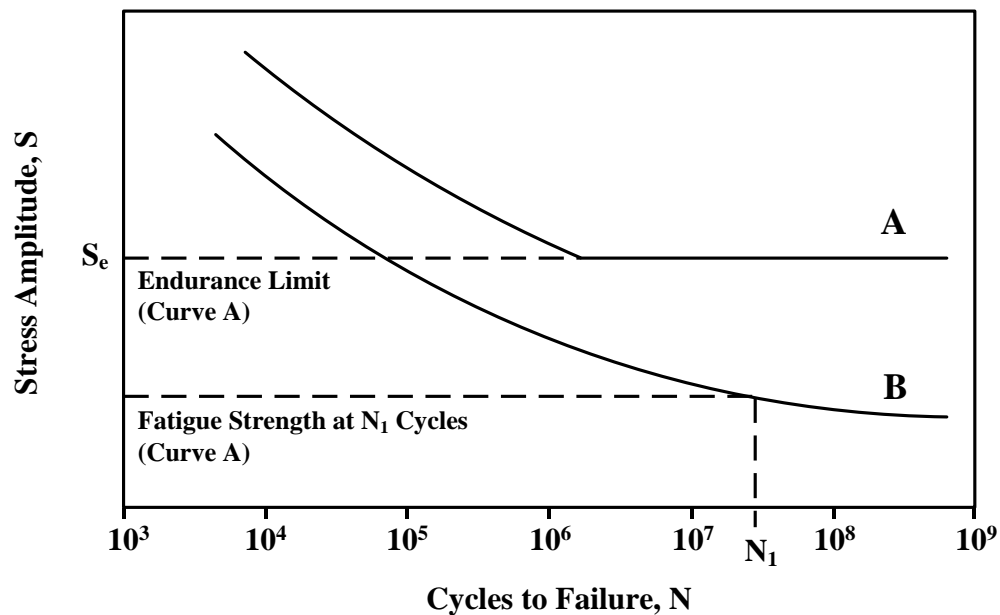


Figure 2.20 Typical S-N Curves  
(<http://www.keytometals.com>) [51]

**Endurance Limit:** Certain materials have a fatigue limit or endurance limit that represents a stress level below which the material does not fail and can be cycled infinitely. If the applied stress level is below the endurance limit of the material, the structure is said to have an infinite life. This is characteristic of steel and titanium in benign environmental conditions. A typical S-N curve corresponding to this type of material is shown as Curve A in Figure 2.20. Many non-ferrous metals and alloys, such as aluminum, magnesium and copper alloys, do not exhibit well-defined endurance limits. These materials instead display a continuously decreasing S-N response, similar to Curve B in Figure 2.20. In such cases, a fatigue strength  $S_f$  for a given number of cycles must be specified. An effective endurance limit for these materials is sometimes defined as the stress that causes failure at  $1 \times 10^8$  or  $5 \times 10^8$  loading cycles.





The concept of an endurance limit is used in infinite-life or safe stress designs. It is due to interstitial elements (such as carbon or nitrogen in iron) that pin dislocations, thus preventing the slip mechanism that leads to the formation of micro-cracks. Care must be taken when using an endurance limit in design applications because it can disappear due to:

1. Periodic overloads (unpin dislocations)
2. Corrosive environments (due to fatigue corrosion interaction)
3. High temperatures (mobilize dislocations)

The endurance limit is not a true property of a material, since other significant influences such as surface finish cannot be entirely eliminated. However, test values obtained from polished specimens provide a baseline to which other factors can be applied. Influences that can affect the endurance limit include:

1. Surface finish
2. Temperature
3. Stress concentration
4. Notch sensitivity
5. Size
6. Environment
7. Reliability

## **2.6 Life test**

Doing a life test and getting performance measurements of the heat pipes are the most important factors in the study. In space craft use, for example, the heat pipe should be suitable for an operation of 7 to 10 years in space after 5 years of ground storage and testing during the space craft development [12]. It is especially stated that evidence of long term compatibility of the pipe and working fluids must be available before a spacecraft “qualification” can be granted.

The life test of a heat pipe is an important test because the life of the operation is the question that many manufacturers need to know the answer to. They determined the factors that must be considered when the life test was proposed. The working fluid should have properties such as: good purity, stable at operating temperature, high latent



heat and compatible with container. While, the container should have properties such as: high strength, homogenous, inert with environment and compatible with working fluid. Both the working fluid and container must be compatible. If the two are incompatible, a non-condensable gas (NCG) can be generated that would significantly reduce the heat pipe performance. So, in the life test program the compatibility of the working fluid and container should be considered first.

Life tests on heat pipes are commonly regarded as being primarily concerned with the identification of any incompatibilities that may occur between the working fluid and the wall material. The ultimate life test, however, would be in the form of long term performance under conditions approximate to those in the particular application.

The number of factors to be considered when examining for life tests on a particular working fluid/wall combination is very extensive and would require a large number of heat pipes to be fully comprehensive.

Several of these may be discounted because of existing available data on particular aspects, but one important point that must be emphasized is the fact that quality control and assembly techniques inevitably vary from one laboratory to another, and these differences can be manifested in differing compatibility data and performance.

There are many factors to be taken into account when setting up the full life test program and the relative merits of alternative techniques available are discussed.

The working fluid: the selection of working fluid must take into account the following factors, which can all be experimentally investigated:

1. Purity: the working fluid must be free of dissolved gasses and other liquids. It is important to ensure that the handling of the working fluid following purification does not expose it to contaminants.

2. Temperature: some working fluids are sensitive to operating temperature. If such behavior is suspected, the safe temperature band must be identified.

3. Heat flux: high heat flux can create vigorous boiling actions, which can lead to erosion.

4. Compatibility with wall: the working fluid must not react with the wall. This can also be a function of temperature and heat flux, the tendency for reactions to occur generally increases with increasing temperature or flux.



The heat pipe wall: in addition to the interface with the heat pipe working fluid, as discussed above, the wall and associated components, such as the end caps, have their own particular requirements with regard to life. The successful operation of heat pipes must take them into account.

1. Quality assurance: the selection of the material should be based on the purity, or at least the known alloy or specification of the material used.

2. Vibration or acceleration: the structure must be able to withstand any likely vibration or acceleration. Any qualification procedures designed to ensure that the unit meets these specifications should be regarded as an integral part of any life test program.

3. External environment: the external environment could affect the case material properties, or cause degradation of an outer surface. This should also be the subject of a life test investigation if any deterioration is suspected.

4. Interface corrosion: it is possible that some corrosion could occur at metallic interfaces, particularly where dissimilar metals are used that come in contact with a working fluid.

Life test procedure: there are many ways of carrying out the life tests, all having the same aim, which is to demonstrate that the heat pipe can be expected to last for its designed life with an excellent degree of certainty.

The most difficult part of any life test program is the interpretation of the results and the extrapolation of these results to predict long term performance. The main disadvantage of carrying out life tests on one particular combination of materials, either in accelerated tests or at the design load, is the fact that if any reaction does occur, insufficient data is probably available to enable one to explain the main cause of the degradation.

## 2.7 Literature review

Maezawa et al. [20] studied the working principle of an OHP. It was able to transfer heat by the fluctuant phenomena of the working fluid. The source of this fluctuation may be due to the process of bubbles forming caused by nucleate boiling: growing, breaking in the evaporator and collapsing in the condenser. The fluctuation



character in the meandering capillary tube was very complex and was affected by the heat transfer rate, filling ratio of working fluid, operating mode, tube diameter and the number of meandering turns. The internal flow pattern of the slug and vapor bubbles was also studied, as shown in Figure 2.21.

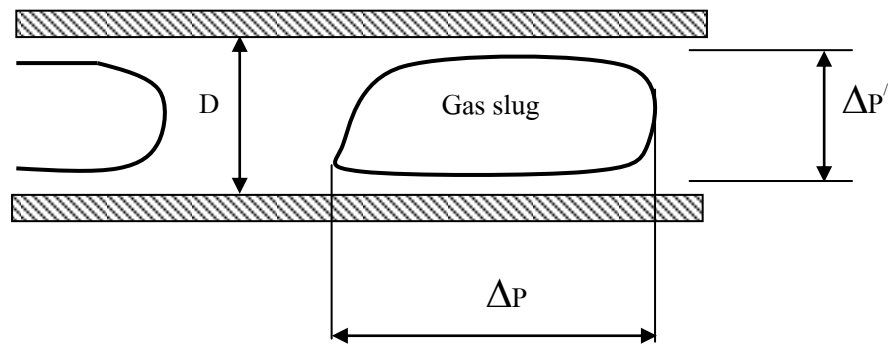


Figure 2.21 Slug flow [20]

Figure 2.21 shows the radial pressure difference ( $\Delta P'$ ) and axis pressure difference ( $\Delta P$ ) of the OHP. For the condition of  $\Delta P > \Delta P'$ , the slug exists inside the tube. The maximum inner diameter of the capillary tube can be defined in equation (2.19):

$$d_{\max} < 2\sqrt{\frac{\sigma}{\rho_1 g}} \quad (2.19)$$

Miyazaki et al. [21] studied a CLOHP/CV made from a copper capillary tube with three check valves and an inner diameter of 2 mm. The channel passes alternatively between the heating section and the cooling section 14 times and the channel ends were connected in a loop. The heat pipe has short heat transfer sections of 50 mm and a long adiabatic section of 500 mm. The working fluid was R-134a and the charging quantity ratio was approximately 0.5. It was found that when the channel ends were connected in a loop and the loop was equipped with check valves, a single directional flow was caused by summing the amplitudes of the oscillatory flow. This allows the effective flow into the heat transfer sections to be maintained even when the amplitudes of oscillatory flow were small. It was seen that the heat pipe without check



valves only works in bottom heat mode and does not work in the horizontal mode. In contrast, the heat pipe with check valves works not only in horizontal mode but also top heat mode.

Rittidech et al. [37] studied the heat-transfer characteristics of a CLOHP/CV. The CLOHP/CV was made from a copper tube with inner diameters of 1.77 and 2.03 mm. The evaporator, adiabatic and condenser lengths were equal to 50, 100 and 150 mm. The selected working fluids were water, ethanol and R123, with a filling ratio of 50% of total volume. The number of turns was 40. The experimental results showed that the heat-flux increases with an increase of  $R_{cv}$  and decrease with an increased aspect ratio. A correlation for predicting the heat-transfer rate of the heat-pipe in the vertical position was established as equation (2.20).

$$Ku_{90} = 0.0004 \left[ Bo^{2.2} Fr^{1.42} Ja^{1.2} Pr^{1.02} \left[ \frac{\rho v}{\rho l} \right]^{0.98} R_{cv}^{1.4} We^{0.8} \left[ \frac{L_e}{D_i} \right]^{0.5} \right]^{0.138} \quad (2.20)$$

Yang et al. [40] studied the operational limitations of closed loop pulsating heat pipes (CLPHPs), which consist of a total of 40 copper tubes with 1 mm and 2 mm inner diameters (ID). R123 was employed as the working fluid with filling ratios of 30%, 50% and 70%. Three operational orientations were investigated, viz. vertical bottom heated, horizontal heated and vertical top heated orientations. The effects of inner diameter, operational orientation, filling ratio and heat input flux on thermal performance and performance limitation were investigated. The results show that for the CLPHP with 2 mmID tubes the best performance existed in the vertical orientation with heating at the bottom, while for the CLPHP with 1 mmID tubes, orientation played almost no role. A filling ratio of 50% was optimum for both CLPHPs to obtain best performances in all orientations. The CLPHPs were operated until a performance limit characterized by serious evaporator overheating (dry-out) occurred. Rather high heat loads could be accommodated. Dry-out heat fluxes in the vertical bottom heat mode were about 1242 W/cm<sup>2</sup> (1 mmID) and 430 W/cm<sup>2</sup> (2 mmID) for axial heat transport and about 32 W/cm<sup>2</sup> (1 mmID) and 24 W/cm<sup>2</sup> (2 mmID) for radial heat input.



Baker [3] studied the accelerated life test of a stainless-water heat pipe to find the result of NCG-generation. He found that the NCG was hydrogen. The cause of the hydrogen generation was the oxidizing reaction of water with some element in the stainless pipe. Moreover, he concluded that the Arrhenius model could also predict NCG-generation. The Arrhenius model is applicable to the activation process, including corrosion, oxidation, creep and diffusion. Where the Arrhenius plot is valid, when plotting the log of the response parameter on a graph against the reciprocal of absolute temperature it can be seen as a straight line.

Murakami et al. [23] studied the life test of copper-water heat pipes as shown in Figure 2.22 to find out the NCG generation characteristics. They found that the components of the container affected NCG generation. The NCG of this system was carbon dioxide gas ( $\text{CO}_2$ ). The temperature difference in the condenser section was  $5^\circ\text{C}$  during a period of 20 years at a  $60^\circ\text{C}$  operating temperature.

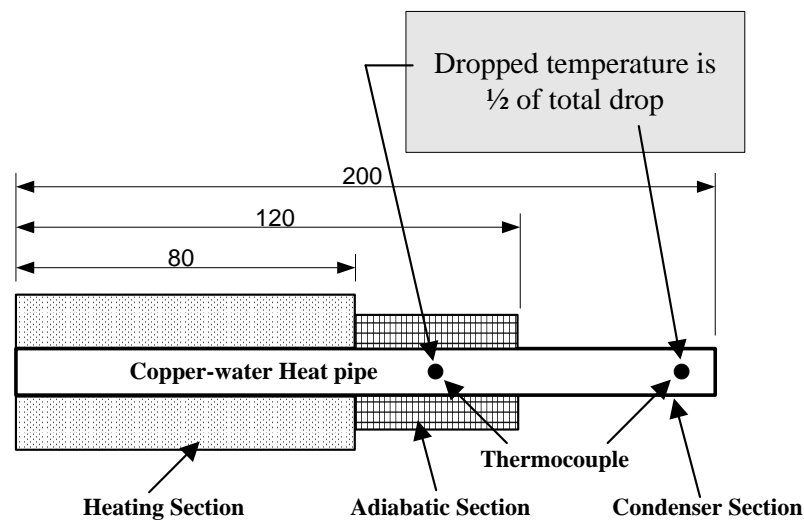
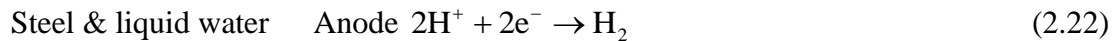
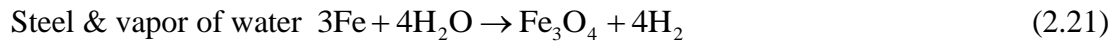


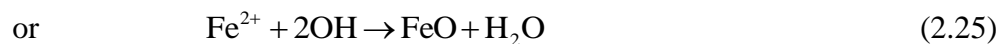
Figure 2.22 Copper-water heat pipe of Murakami [23]

Kai et al. [15] studied the life test of a carbon steel-water heat pipe in order to find out the NCG-generation in such a system. The chemical reaction of the steel-water pipe can be expressed as:

Step 1: Gas generation process:



Step 2: Fouling generation process



They found that the temperature difference in the condenser section increased with operating temperature. Moreover, the accumulation of the NCG only occurred at 60-70 days and the maximum generation rate of the NCG occurred during 10-30 days of the testing. The cause of the generation was the incompatibility between the working fluid and container.

Charoensawan et al. [9] studied the methods for preventing corrosion inside a thermosyphon. By using the results of Novotna et al. [24], they found that the method using the combination of internal protection and external protection is the best method to prevent corrosion. The internal protection is protection from the inhibitor, which was added into the working fluid. The external protection is the protection from the magnetite, which covered the internal surface of the pipe. By using the Arrhenius model, they predicted the rate of corrosion and NCG-generation as a function of operating temperature and duration of testing.

Kuźnicka [17] studied the shell and tube heat exchanger failed before 5 years of operation. The failure was caused by pits on the tube outside surface developing until its perforation. Inside the Cu-DHP tubes in soft temper a cooling agent circulated to cool down industrial water at the shell side from 16 to 4 °C. The cooled water was hard, rich in chloride ions with relatively low sulphate ions concentration and pH ranging from 4 to 7. The leaking tubes were subject to standard metallographic examination, hardness measurement, scanning electron microscopy and X-ray energy dispersion analysis. It was found that the tube damage was caused by erosion–corrosion induced by two factors: disturbed flow of water containing suspended solid particles and



chemical composition of water rich in chlorides that resulted in loss of stability of protective cuprous oxide layer.

Watanabe and Koike [37] studied a creep-fatigue life evaluation method for perforated plates at an elevated temperature. The accurate evaluation scheme for creep-fatigue strength is one of the continuing main issues for elevated temperature design; particularly, the three-dimensional structure having stress concentration is becoming more important. The present paper investigates fatigue strength and creep-fatigue strength of a perforated plate having stress concentration as an example. The specimens were made of type 304 SUS stainless steel and the temperature was kept to 550 °C. Whole cycles of the experiment record were analyzed, and the characteristics of the structure having stress concentration were discussed. The present paper employs stress redistribution locus (abbreviated as SRL) in evaluation of plastic behavior in cyclic fatigue process as well as stress relaxation in creep process, and the feasibility is discussed in conjunction with the comparison to experimental results.

Watanabe et al. [39] studied the stress and strain locus of a perforated plate in inelastic deformation (strain-controlled loading case). Plastic strain of structures having stress concentration is estimated by using the simplified method or the finite element elastic solutions. As the simplified methods used in codes and standards, it is possible to cite Neuber's formula and elastic follow-up procedure. In addition, the stress redistribution locus (abbreviated as SRL) method, recently proposed as another simplified method, will be cited. In the present paper, inelastic finite element analysis of a perforated plate, whose stress concentration is about 2.2~2.5, is carried out, and the stress and strain locus in the inelastic range by the detailed finite element solutions is investigated to compare accuracy of the simplified methods. As strain controlled loading conditions, monotonic loading, cyclic loading and cyclic loading having hold time in tension are assumed. The inelastic strain significantly affects the life evaluation of fatigue and creep-fatigue and the stress and strain locus is discussed from the detailed inelastic finite element solutions.





## CHAPTER 3

### Experimental Setup and Procedure

The basic principles and theories were proposed in chapter 2. In this chapter, the research methodology will be presented and it can be divided into three parts. The first one is the quantitative experiment in order to determine the thermal performance and the internal pressure of the CLOHP/CV under a normal operating state only. The second one is to determine the internal corrosion of the compound through physical and chemical analysis of the CLOHP/CV. The last is studying the fatigues on the copper tube and applying to the CLOHP/CV in order to improve the engineering heat pipe design. For greater understanding of the three parts of the experiment methodology, it will be described in more detail.

#### 3.1 Instruments and equipments

##### Humidity and anemometer measurement

Humidity and anemometer measurements were taken using pitot tube probe types. A Testo 445 with  $\pm 0.05$  % accuracy as show in Figure 3.1 was used.



Figure 3.1 Pitot tube



### Data logger

It was used to measure the temperature at any point and record the data. The data logger was a Yokogawa DX200 with  $\pm 0.1$  °C accuracy, 20 channel input and -200 to 1100 °C measurement temperature-range, as shown in Figure 3.2.



Figure 3.2 Data logger

### Temperature controller

The temperature controller was used to control the temperature of the evaporator section by automatically turning on and off the circuit with a  $\pm 0.2$  °C accuracy and operating range from 0 to 400 °C, as show in Figure 3.3.



Figure 3.3 Temperature controller



### Electric plate heaters

The evaporator sections of the CLOHP/CV were heated by electric plate heaters (2×1500 Watt). The heaters were placed on the outer surface of the tube walls and connected to the AC power input source and temperature controller, as shown in Figure 3.4.

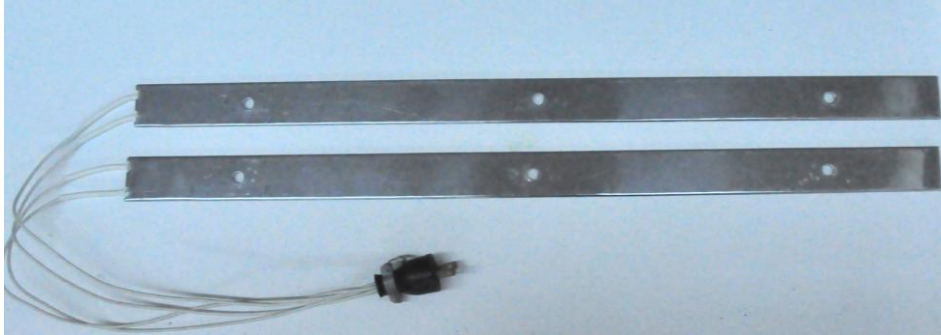


Figure 3.4 Electric plate heaters

### Thermocouples

The thermocouples used in the experimental were type K (OMEGA with  $\pm 0.1$  °C accuracy); the range of operating temperatures was between -100 and 1300 °C, as shown in Figure 3.5.



Figure 3.5 Thermocouples



### Working fluid filling set

This consisted of four valves; a burette or pipette was connected to valve A for filling the working fluid, valve B was connected to a vacuum pump, valve C was connect to the heat pipe or tube and valve D was connected to a pressure gauge for measuring the pressure in the tube as shown in Figure 3.6.

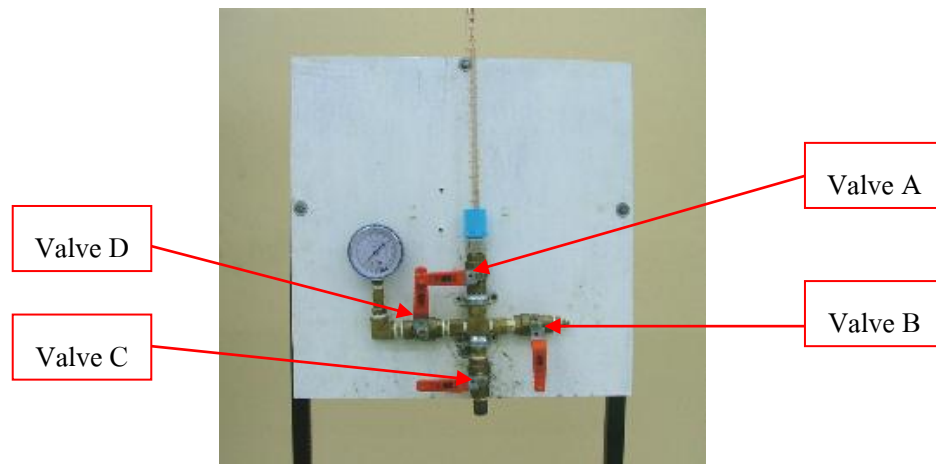


Figure 3.6 Working fluid filling set

### Oscillating heat pipe with check-valves (CLOHP/CV)

The CLOHP/CV was made from copper capillary tube. In this study, it was formed from three sections (evaporator, adiabatic and condenser section) and two check-valves as shown in Figures 3.7 and 3.8.

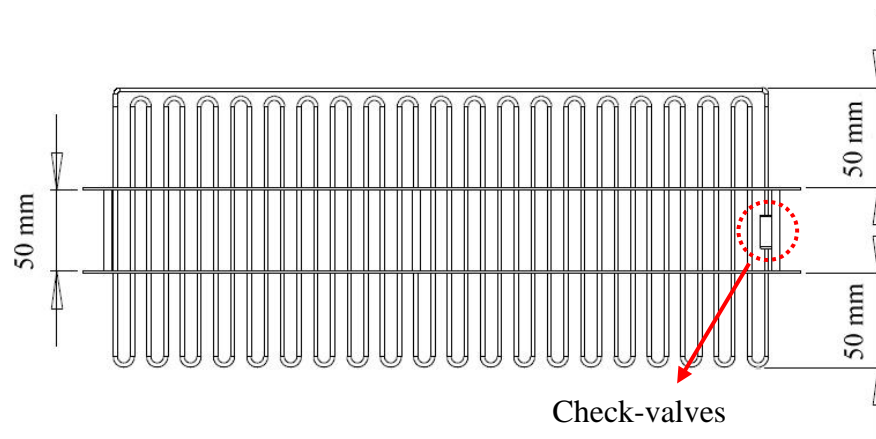


Figure 3.7 Position of check-valves on oscillating heat pipe

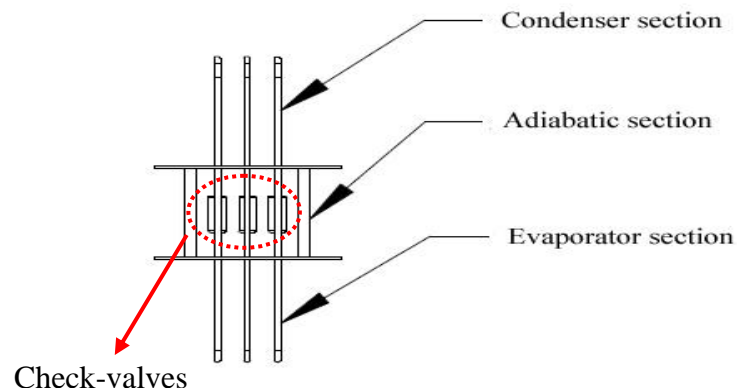


Figure 3.7 Position of check-valves on oscillating heat pipe (Continue)

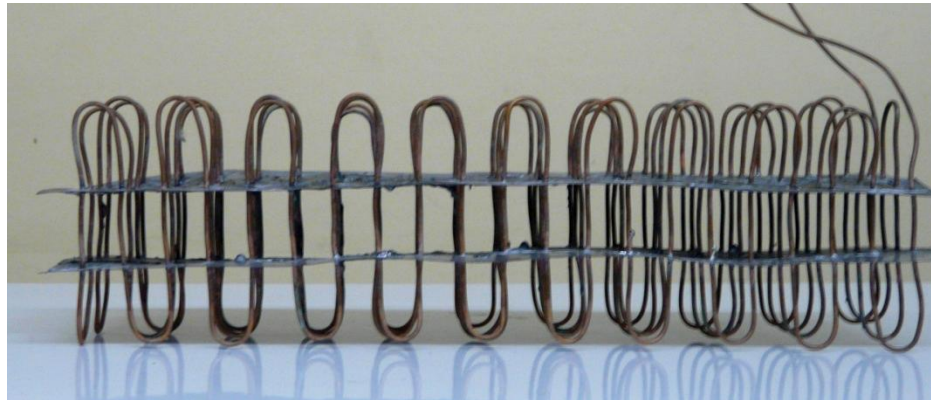


Figure 3.8 The CLOHP/CV

### Scanning electron microscope (SEM)

The scanning electron microscope (SEM) used was a model JEOL, JSM-6400. A SEM uses electrons to illuminate a sample, instead of visible light used in an optical microscope. Since the wavelength of electrons is much smaller than that of visible light, the SEM is capable of imaging at a much higher magnification than light microscopes. The high image resolution of a scanning electron microscopy allows users to focus on features of the sample in a range of millimeters down to a few nanometers. SEM is equipment for the characterization and observation of solid samples using images obtained with secondary and backscattered electrons (photography and Z-contrast). It has an RX energy dispersive spectrometer that enables the semi-quantitative chemical analysis of samples as shown in Figure 3.9.





Figure 3.9 Scanning electron microscopy (SEM)

#### Energy dispersive X-ray spectrometry (EDX)

The technique for detecting metals in solution in samples is defined. The EDX spectrometry (EDX, INCA Insight OXFORD Instruments) makes use of the X-ray spectrum emitted by a solid sample bombarded with a focused beam of electrons to obtain a localized chemical analysis. All elements from atomic number 4 (Be) to 92 (U) can be detected in principle, though not all instruments are equipped for 'light' elements ( $Z < 10$ ). Qualitative analysis involves the identification of the lines in the spectrum and is fairly straightforward owing to the simplicity of X-ray spectra. Quantitative analysis (determination of the concentrations of the elements present) entails measuring line intensities for each element in the sample and for the same elements in calibration standards of known composition.

#### Flame atomic absorption spectroscopy (Flame-AAS)

The Flame-AAS used was a model Shimadzu, AA-680. The technique for detecting metals solution in samples. The technique is based on the fact that ground state metals absorb light at specific wavelengths. Metal ions in a solution are converted to an atomic state by means of a flame. Light of an appropriate wavelength is supplied and the amount of light absorbed can be measured against standard curve valves as shown in Figure 3.10.







Figure 3.10 Flame atomic absorption spectroscopy (Flame-AAS)

#### Shimadzu servo-hydraulic test machine

A Shimadzu servo-hydraulic test machine and a control device were the equipment used for the fatigue test. An electric furnace is incorporated in the testing machine for elevated temperatures as shown in Figure 3.11.



Figure 3.11 Shimadzu servo-hydraulic test machine



## 3.2 Experimental setup and procedure

3.2.1 Experimental setup and procedure for testing and determining internal pressure of the CLOHP/CV

3.2.1.1 CLOHP/CVs with evaporator section lengths of 50, 100 and 150 mm were set up in evaporator and condenser jackets and the thermocouples were attached to the surface of the tube for measuring the temperature, four thermocouples were used to measure the vapor plug and liquid slug temperature inside in adjacent tube, as shown in Figure 3.12. After that, it was covered with a black foam insulator (Aero flex) to prevent heat loss during the experimental process.



Figure 3.12 The CLOHP/CV for testing

3.2.1.2 The experimental set was vacuumed with a vacuum pump; the working fluid was filled into the CLOHP/CV with a 50% total volume fill of the CLOHP/CV, as shown in Figure 3.13.





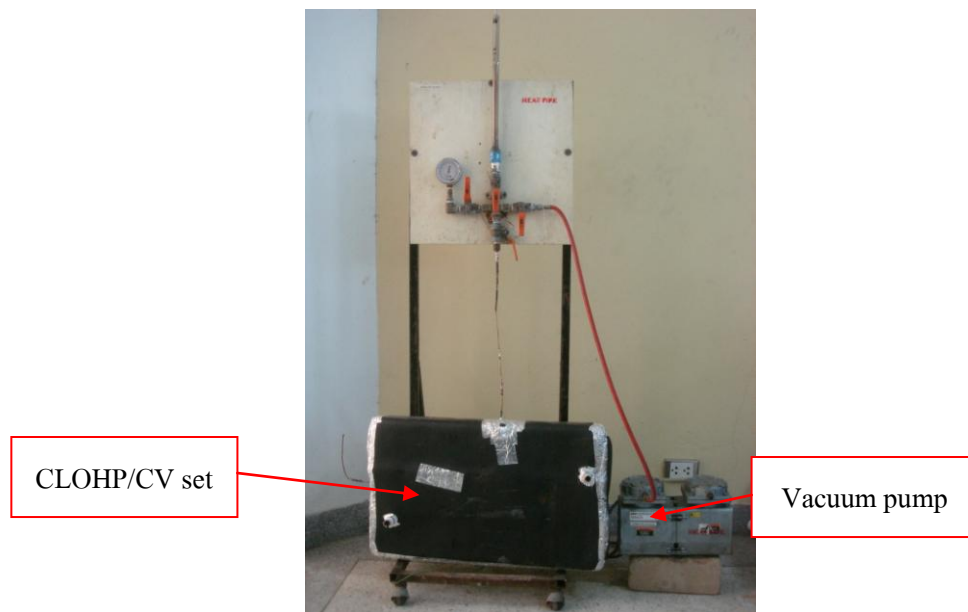


Figure 3.13 Filling working fluid

3.2.1.3 Experimental setup with test rig. The system consisted of a test CLOHP/CV, a heater power supply with temperature controller, a cooling air fan with a motor speed controller, a temperature recorder and a personal computer. The CLOHP/CV was made of a copper capillary tube. The evaporator, adiabatic and condenser sections were adjusted to be an equal length. The evaporator section was heated by electric plate heaters; the heaters were placed on the outer surface of the tube walls and were connected to the AC power supply with the temperature controller (Linking PID LT400 series with  $\pm 2$  °C accuracy). The evaporator temperature was varied using the temperature controller. The heat was removed from the condenser section by forced convective heat transfer to ambient air that was blown through the section. The airflow velocity was controlled by an AC motor controller at 0.6 m/s and the temperature of the air conditioner was kept at 25 °C. The adiabatic section was insulated well using foam insulation (Aero flex). Thermocouples (OMEGA type K with an uncertainty of 0.58 °C) were used to measure the temperature of the evaporator, adiabatic and condenser sections of the CLOHP/CV. The ambient air temperature was measured at the inlet and outlet of the airflow duct. A transient record of the internal pressure was measured and was then converted to an average pressure. All the temperature data was recorded by the data logger (Yokogawa DX200 with  $\pm 0.1$  °C



accuracy) and then transferred to a PC every hour. The air velocity was monitored with the humidity and anemometer measurement equipment (A testo 445 with  $\pm 0.05\%$  accuracy) of a pitot tube probe type. First, the CLOHP/CV was evacuated by a high performance vacuum pump (Makashi, 50 l/min) and then filled with the required amount of working fluid. The test CLOHP/CV was set into a test rig that could be tilted to a vertical orientation. The evaporator temperature was set to the desired value through controlling the AC electric power supplied to the strip heaters. Simultaneously, ambient air at a 25 °C temperature was blown at 0.6 m/s velocity through the condenser section. After a quasi steady state was reached, all temperatures were recorded. Then the experimental parameters were varied according to the required conditions. As shown in Figures 3.14 and 3.15.



Figure 3.14 Experimental setup for internal pressure testing



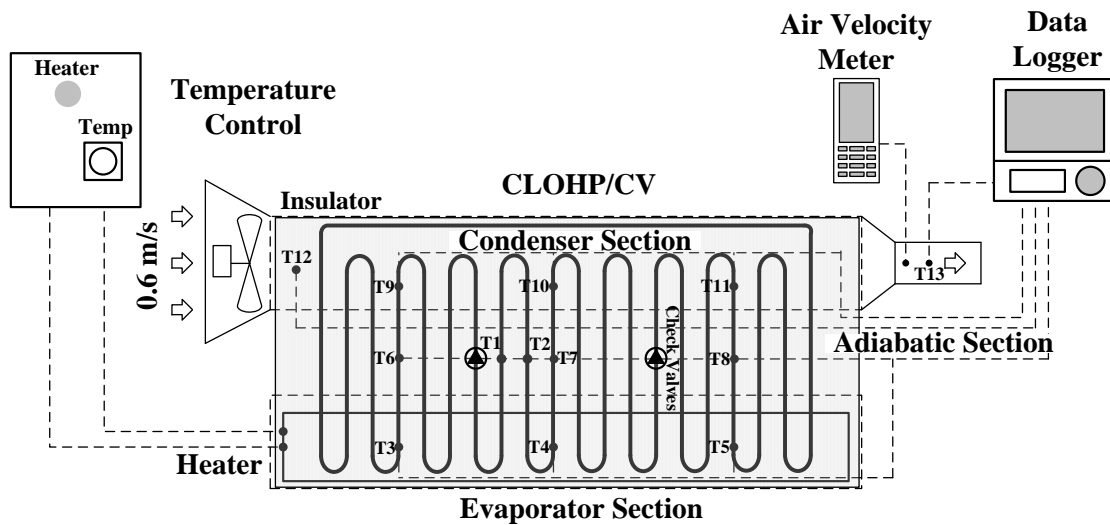


Figure 3.15 Experimental procedure

3.2.1.4 When the experimental system reached a steady state, the temperatures at all points were recorded and the air flow rate was measured. The heat transfer rate was calculated by the calorific method [29], as following equation (3.1):

$$Q = \dot{m}C_p(T_{out} - T_{in}) \quad (3.1)$$

where  $\dot{m}$  is the mass flow rate of dry air (kg/s).

$C_p$  is the specific thermal capacity of the cooling medium (kJ/kg.°C).

$T_{out} - T_{in}$  is the temperature difference between the inlet and outlet dry air at the condenser section (°C).

The heat transfer rate calculated in equation (3.1) was required to know the flow rate of the dry air and temperature difference between the inlet and outlet at the condenser section as recorded by the data logger. In this experiment, the CLOHP/CV thermal resistance  $R$  was defined as the temperature difference between the condenser section and the evaporator section divided by the heat transfer rate, as in the following equation (3.2):



$$R = \frac{T_e - T_c}{Q} \quad (3.2)$$

where  $T_e$  and  $T_c$  are the wall temperatures of the evaporator section and the condenser section, respectively. It could be seen that each of the measuring equipments also had an error in the measurement. Thus, an error in the calculated heat transfer rate occurred. The error of the calculated heat transfer rate could be calculated by equation (3.3) [5].

$$dQ = \left[ \left( \frac{\partial Q}{\partial \dot{m}} d\dot{m} \right)^2 + \left( \frac{\partial Q}{\partial C_p} dC_p \right)^2 + \left( \frac{\partial Q}{\partial T_{out}} dT_{out} \right)^2 + \left( \frac{\partial Q}{\partial T_{in}} dT_{in} \right)^2 \right]^{1/2} \quad (3.3)$$

As  $C_p$  was constant, resulting in  $\left( \frac{\partial Q}{\partial C_p} dC_p \right)^2$  equals zero. Equation (3.3) was reduced to equation (3.4)

$$dQ = \left[ \left( \frac{\partial Q}{\partial \dot{m}} d\dot{m} \right)^2 + \left( \frac{\partial Q}{\partial T_{out}} dT_{out} \right)^2 + \left( \frac{\partial Q}{\partial T_{in}} dT_{in} \right)^2 \right]^{1/2} \quad (3.4)$$

where  $dQ$  is the error of the measuring equipment.

$\partial \dot{m}$  is the sensitivity value from the flow rate measurement.

$\partial T_{out}$  and  $\partial T_{in}$  are the sensitivity values from the temperature measurement.

3.2.1.5 The experiment was repeated three times to produce experimental results, which was considered as the end of experiment one inclination angle.

3.2.1.6 The inclination angle was adjusted to decrease the degree until it reached the 20 degree heat mode, which was considered as the end of one experimental set. After that, the working fluid, evaporator length and inner diameter were varied following the experimental conditions.

3.2.1.7 The experimental results were analyzed following the experimental conditions. The methods used to analyze the experimental results were as follows.



3.2.1.7.1 The temperature results from the evaporator section were analyzed to find out how much the temperature caused the operating state and what the heat transfer rate and internal pressure were.

3.2.1.7.2 The inclination angle results were analyzed to find out how inclination angle affected the heat flux state and which inclination angle gave the highest heat transfer and internal pressure.

3.2.1.7.3 The evaporator length results were analyzed to find out which length, short or long, gave a greater heat transfer rate and internal pressure.

3.2.1.7.4 The inner diameter results were analyzed to find out which diameter, small or large, gave a greater heat transfer rate and internal pressure.

3.2.1.7.5 The working fluid property results were analyzed (latent heat).

3.22. Experimental setup and procedure for internal corrosion of the CLOHP/CV

3.2.2.1 The CLOHP/CV with an evaporator section length of 50 mm was set in the evaporator and condenser jackets and the thermocouples were attached to the surface of the tube for measuring the temperature and recording by the data logger (Yokogawa DX200 with  $\pm 0.1$  °C accuracy) and then transferred to a PC every 4 hours. The duration of the testing was 500, 1000 and 3000 hours (based on normal operating times of the CLOHP/CV) and the temperature at the evaporator section was 200 °C. Ambient air at a 25 °C temperature was blown at a 0.6 m/s velocity through the condenser section, as shown in Figure 3.16. After that, it was covered by a black foam insulator (Aero flex) to prevent heat loss during the experimental process.





Figure 3.16 Experimental setup for internal corrosion testing

### 3.2.2.2 Analysis of copper tubes

#### 3.2.2.2.1 Photography analysis of inner surface

Six types of copper tubes used in the CLOHP/CV set were sectioned to observe the inner surfaces. Six different specimens with tube corrosion were examined by a visual inspection and scanning electron microscopy (SEM), model JEOL, JSM-6400 and select from the evaporator section in the analysis [33].

#### 3.2.2.2.2 Chemical analysis of working fluid

A technique for detecting metals in solution samples was used that is based on the fact that ground state metals absorb light at specific wavelengths. Metal ions in a solution are converted to an atomic state by means of a flame. Light of an appropriate wavelength is supplied and the amount of light absorbed can be measured against a standard curve. In this study, the concentration of copper particles in the working fluid was determined by flame atomic absorption spectroscopy (Flame-AAS), model Shimadzu, AA-680.

#### 3.2.2.3 Materials and preparation

Under a steady temperature condition in the furnace, the CLOHP/CV set was operated for about 3000 hours. The CLOHP/CV was then taken out. After a careful





cleaning procedure, metallographical specimens were prepared by cutting from selected positions on the CLOHP/CV. The CLOHP/CV specimens were used to examine the corrosion and oxidation on the inner surface. The SEM with Flame-AAS analyzer was also employed to further identify the corrosion mechanism and the composition of the corrosion products. Specimens were of cylindrical pure copper tubing (>99.97%) with an inner diameter and thickness of 2.03 and 1.27 mm, respectively. The working fluids inside the CLOHP/CV were distilled water and ethanol. Specimens with dimensions 10.0 mm × 3.3 mm were mechanically cut from sheets of 1.0 mm thickness as show in Figure 3.17. Chemical composition as determined by emission spectroscopy with spark excitation was (wt%): (As remainder), Ag 0.001, P 0.024, Fe < 0.001, Ni < 0.001, Pb < 0.001, Sb < 0.001, Zn 0.001, Bi < 0.0005, As < 0.001 and S 0.001.

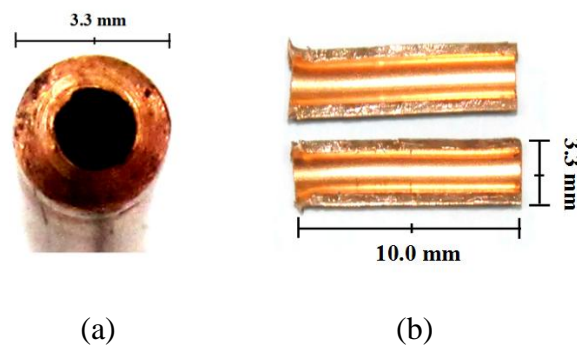


Figure 3.17 Photographs of the actual copper tubes: (a) cross-sectional view copper tube for experiment and (b) inner surface of the copper tube before testing

### 3.2.3 Experimental setup of Fatigue testing

3.2.3.1 Preparation of specimens: The fatigue test was carried out by using two models of specimens; labeled as screw-model and flange-model specimens, both of which were made out of copper tube (C1220) as shown in Figure 3.18 that shows the geometry of the specimens: (a) screw-model specimen, (b) flange-model specimen. The surface of the specimens was polished mechanically by #1000 and #2000 fine sand papers. The chemical compositions of the tested copper tube (C1220) are listed in (Table 3.1); while, the physical and mechanical properties of the testing specimens (this section refers to the deoxidized high phosphorus copper and C1220) are shown in



(Table 3.2). Comparing the fatigue specimen with the cylindrical gage section with an hourglass shaped specimen, the resistance for buckling during the push-pull fatigue testing at high strain amplitude is rather high for the latter. Screw and flange-models were used for the handling and specimen clamping. The configuration of the test area of the specimen was determined to be proportional to the hourglass fatigue specimen with circular cross section in ASTM. To minimize the effort for the design and the development of the equipment, the material was used in the form of a tube that had a tubular geometry with an outer diameter of 12 mm and an inner diameter of 6 mm at the gage section. The bar was cut to the specimen length, total length of 70 mm and an end width of 12 mm was chosen to be the same as those for our tensile specimens in the current experiments and it has a different hourglass section of the test specimen. The configuration of the specimen is shown in Figure 3.18. This is one of the reasons for the choice of the hourglass type configuration. On the other hand, there are some difficulties in estimating the axial strain range from the results of the diametric strain on the hourglass specimens. For this reason, the choice of a specimen configuration with a cylindrical gage section has been recommended by several researchers.

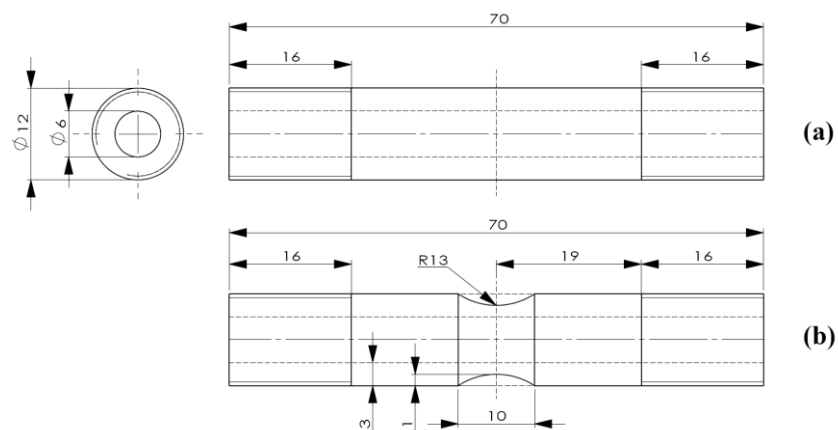


Figure 3.18 Geometry of specimens: Screw-model specimen: (a) uniform type and (b) one-wave type





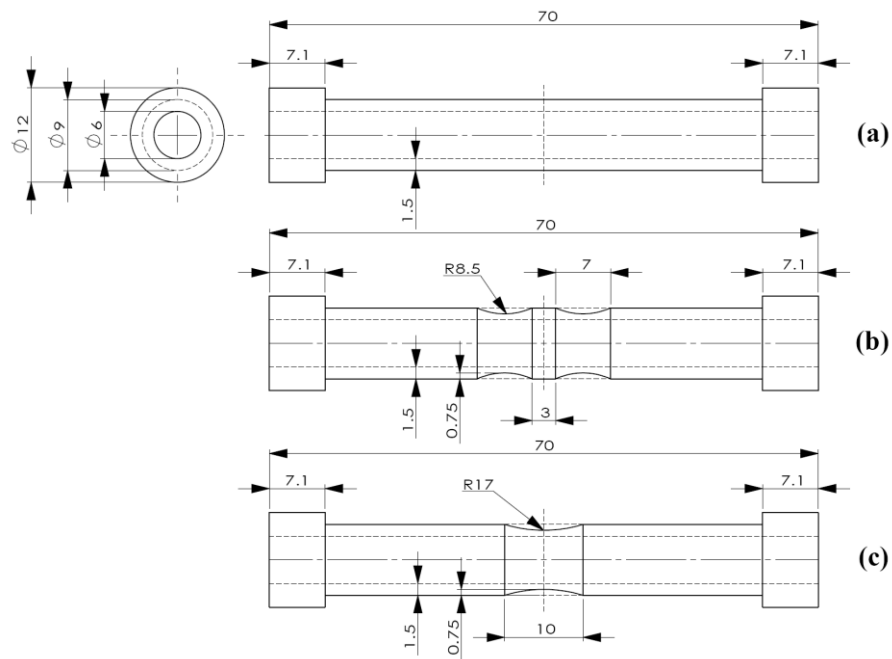


Figure 3.18 Geometry of specimens: Flange-model specimen: (a) uniform type, (b) two-wave type and (c) one-wave type (Continued)



Figure 3.19 Photographs of specimens (screw-type)

Table 3.1 Chemical composition (wt %) of copper tube (C1220)

Type	Cu	Pb	Zn	Bi	Cd	Hg	O	P	S	Se	Te
Copper-C1220	99.99	0.001	0.0001	0.001	0.0001	0.0001	0.001	0.0003	0.0018	0.001	0.001

Table 3.2 Physical and mechanical properties

Characteristics		Deoxidized high phosphorus copper (DHP)	Copper tube (C1220)
Physical properties	Melting point (°C)	1083	1083
	Thermal conductivity at RT (W/(m.K))	339	339
	Electrical conductivity (%IACS)	85	85
Mechanical properties	Tensile strength (MPa)	230-255	260-290
	Elongation (%)	48-54	20-40
	0.2% proof stress (MPa)	50-70	280

3.2.3.2 The experimental setup was as shown in Figure 3.20 for the fatigue test carried out using a Shimadzu servo-hydraulic test machine under stress control and a control device [38]: the frequency used in the test was 10 Hz and the sampling rate was 200. An electric furnace was controlled by the program, which is incorporated in the testing machine, for setting the conditions of the test temperature. The operating temperatures, which were taken to be constant, were room temperature (15 °C), 200 and 300 °C and the temperature increase rate was 100 °C/hour. The displacement was measured between two points having this gage length and the applied load was



measured by the load cell. The data output and input were converted through the AD and DA board from the test machine to the personal computer. A CCD video camera with a zoom lens was focused on the electric furnace for monitoring crack initiation and propagation as shown in Figure 3.21. The laborious procedures associated with optical detection of cracks have been reduced by using the automated system of CCD video camera. The present CCD video camera recorded photographs of the surface of the specimen every 10 minutes with a resolution of  $1280 \times 1024$  pixels.

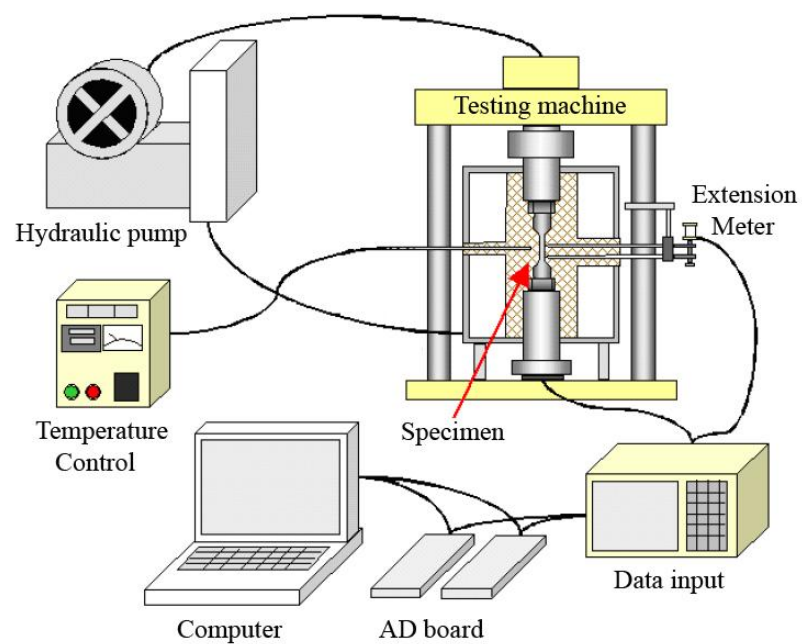


Figure 3.20 Experimental setup of fatigue testing



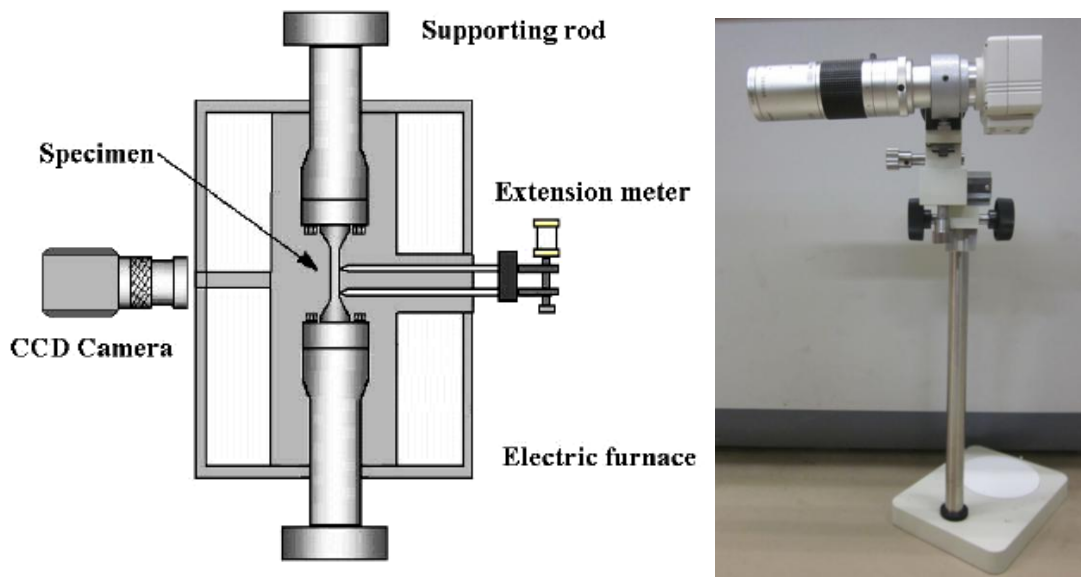


Figure 3.21 CCD video camera

3.2.3.3 Experimental data: The fatigue loading applied to the specimen was tension-compression. The load was obtained from the load cell of the machine that was converted to stress of the specimen, which was obtained from the net area of the specimens at the center. The obtained strain and stress were regarded as nominal strain and stress, respectively. The obtained axial load was controlled for the fatigue test and the controlled load changed as an alternating cyclic waveform as shown in Figure 3.22. The assumed nominal stress amplitude from peak to peak was 200 MPa for all test specimens. A Shimadzu servo-hydraulic controlled testing machine with 17 kN and 7 kN load cell was used (screw and flange models, respectively) as shown in Figure 3.23, from which the calculation of the applied load for the fatigue test from the shape of specimen of the copper tube with a fully-reversed stress cycle with a sinusoidal form was calculated. For this kind of stress cycle, the maximum and minimum stresses are of equal magnitude but opposite signs. Usually, tensile stress is considered to be positive and compressive stress negative. Tests were performed with a sinusoidal waveform at zero mean strain for all specimens. Tests were terminated when the specimen was ruptured. The failure cycle number  $N_f$  was defined by the number when the tensile load  $L_{peak}$  decreased and reached 75% of the maximum peak load  $L_{max}$ . Under this condition, the testing machine stopped.



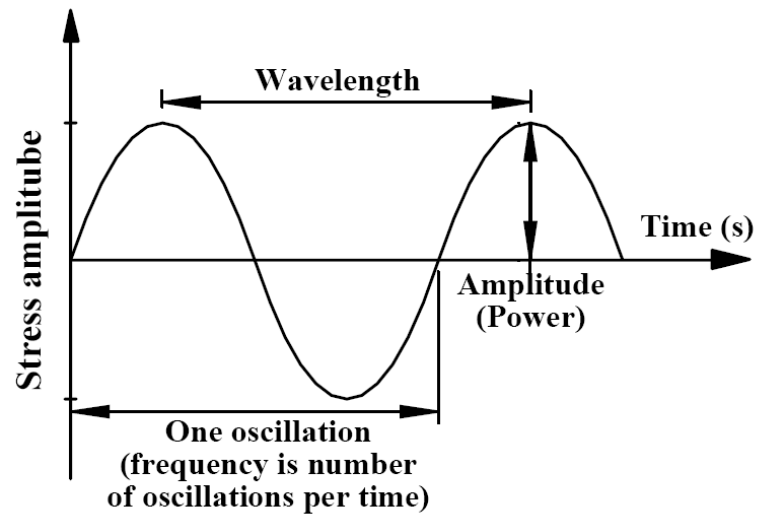


Figure 3.22 Assumed load wave for fatigue test

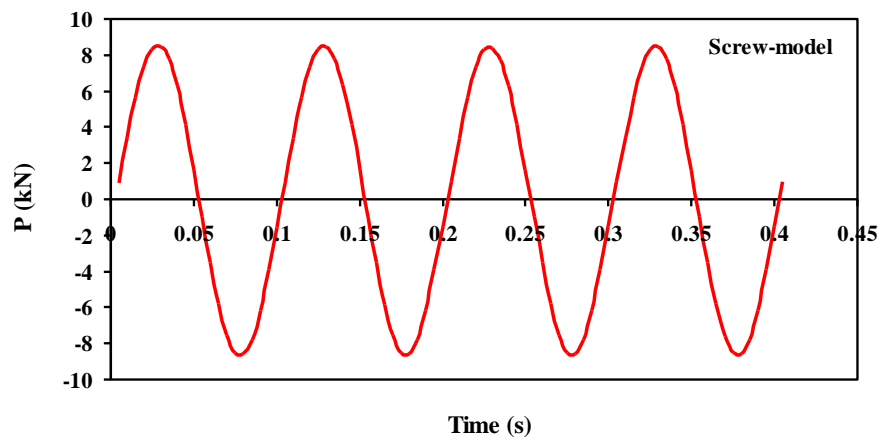


Figure 3.23 Stress amplitude controllers of screw type in fatigue test



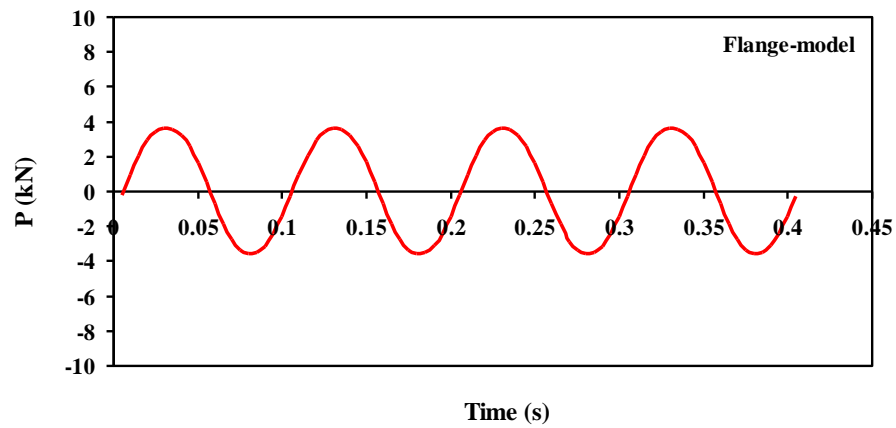


Figure 3.23 Stress amplitude controllers of flange type in fatigue test (Continue)

The strain of the specimen was converted from the displacement for the gauge length of the extension meter and the obtained strain was regarded as the nominal strain, as shown in Figure 3.24.



Figure 3.24 Extension meter

## CHAPTER 4

### Results and Discussion

#### 4.1 Operation behavior of CLOHP/CV

After calculating the heat transfer rate,  $Q$ , of the CLOHP/CV, a comparison was made between the data from normal CLOHP/CV operation and that without heat pipe operation. After calculating the heat transfer rate of the CLOHP/CV ( $Q$ ), the data was compared with the measurement error of  $Q$  ( $dQ$ ) and the axial heat conduction through the copper tube wall ( $Q_{cond}$ ). If  $dQ$  is less than 5% and  $Q$  is more than  $Q_{cond}$ . It was found that the heat conduction through the pipe walls of the heat pipe was rather small as shown in Figure 4.1. The heat transfer rate of the CLOHP/CV was not higher than five times that of the heat conduction rate of the copper tube wall by calculating the rate of heat transferred to the ambient air at the condenser part and thus the CLOHP/CV actually worked as a heat transport device. Figure 4.1 shows the heat transfer rate of the CLOHP/CV using R123 as the working fluid. The maximum heat transfer rate was achieved at a working temperature of 200 °C and an inclination angle of 90°. The influence of the inner diameter, working fluid, working temperature and inclination angle on the performance will be presented later.

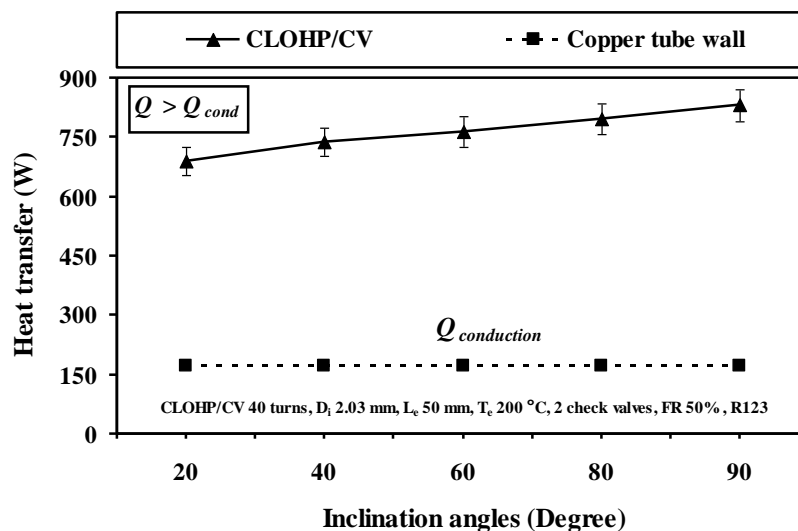


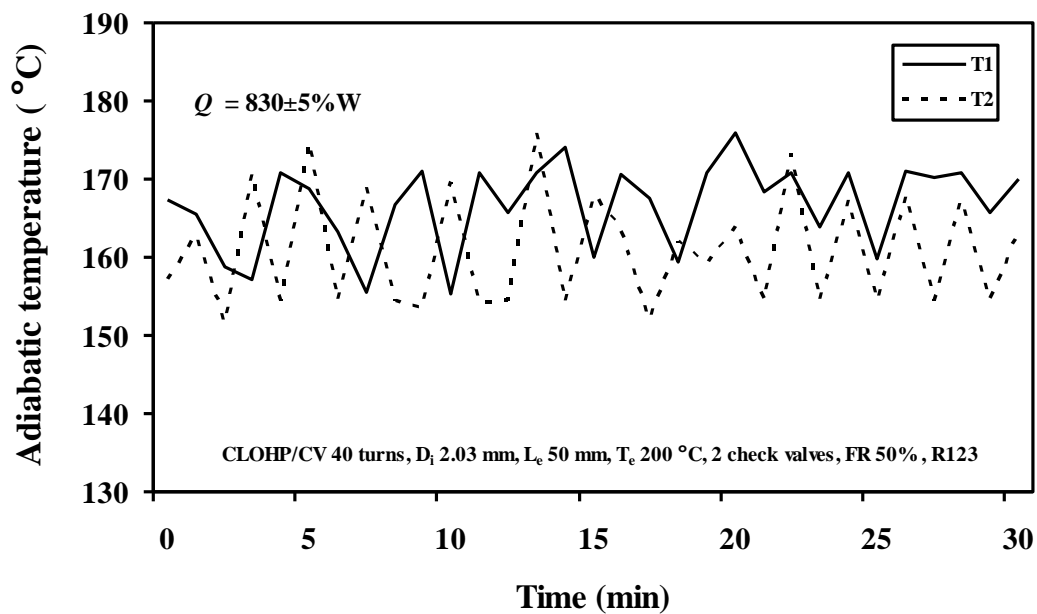
Figure 4.1 Relationship between heat transfer rate and inclination angles of the CLOHP/CV



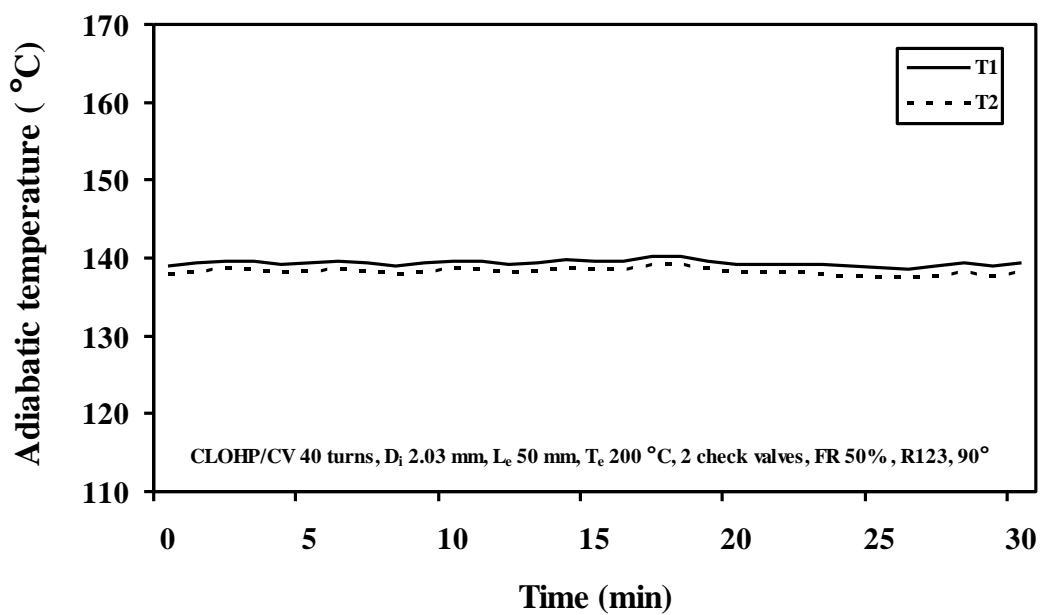
Previous study [19, 22, 27] has shown that CLOHPs operated as a heat transfer device only when the working fluid was able to flow (oscillating and/or circulating flow) in the capillary tube because the fundamental mechanism of the oscillating heat pipe's heat transfer results from the working fluid oscillating that incorporates a phase change of the working fluids. The operation can be done if/and there is a coexistence of liquid plugs and vapor bubbles throughout the length of the tube. When an oscillating heat pipe is operated, there is evaporation at the side that contacts the high temperature resulting in higher vapor pressure and vapor bubble size. The change in size of the bubble causes the driving force, pushing the liquid slug to the condenser, which has the lower temperature. In addition, the condensation at the condenser will make the increase in pressure different between both sides. It should be noted that oscillating heat pipes are made from a single tube; therefore, the movement of the liquid slug and vapor bubble in a particular turn will cause the other turns to move as well. Furthermore, when the liquid is pushed by the vapor into the condenser section, the liquid and vapor in the next turn will also be pushed into the evaporator section. The liquid and vapor that are pushed back to the evaporator will have a higher pressure resulting in a restoring force. The cooperation between the driving and restoring force generates the oscillating flow along the tube axis. This feature can be seen from the oscillatory variation of adiabatic temperatures in adjacent tubes. Similar results can be observed in the operation of the CLOHP/CV in this study as shown in Figure 4.2. If the CLOHP/CV is able to transfer heat ( $Q = 830 \pm 5\%$  W and  $Q_{cond} = 172$  W), as shown in Figure 4.2(a), the adiabatic temperatures of adjacent tubes (T1 and T2) always alternate so that T1 is sometimes higher than T2 and vice versa. This indicates that the flow of the working fluid does not occur in one fixed flow direction. When the CLOHP/CV is unable to operate, T1 and T2 are nearly equal and constant as shown in Figure 4.2(b). It was clearly seen that the CLOHP/CV worked under normal operating condition.







(a) CLOHP/CV can operate



(b) CLOHP/CV cannot operate

Figure 4.2 Adiabatic temperatures in adjacent tubes of CLOHP/CV



## 4.2 Results of internal pressure

After completing all experiments on the operation of the CLOHP/CV, the influences of the various experimental parameters on the internal pressure and the thermal performance were investigated.

### 4.2.1 Inclination angle

Figure 4.3 shows the relationship between inclination angles and internal pressure, it was found from the experimental results that the inclination angles affected the internal pressure of the CLOHP/CVs. The effect of the inclination angles on the internal pressure of a CLOHP/CV can be considered based on the working temperature of 200 °C and inner diameter of 2.03 mm. The result showed that at high working temperature would affect working fluid temperature in the tube and directly affect the internal high pressure at an inner diameter of 2.03 mm. This might be because at the vertical axis (90°), the working fluid was driven by the driving force that acts directly against the pressure difference of the evaporator and condenser sections. The bubbles easily moved to the condenser section at a very high speed. The oscillating of the vapor bubbles between the evaporator and condenser was sufficiently strong. Thus, a high amount of heat could easily be transferred at the vertical axis. When the inclination angle increased from 20° to 90°, the internal pressure also increased. The maximum internal pressure of these working fluids was obtained at an inclination angle of 90°, the values were 7.53, 4.00 and 1.7 MPa for R123, ethanol and distilled water respectively. However, as the inclination angle decreased, the internal pressure was lower than 90°. This might have been because the moving capability of these working fluids mainly depended on the pressure difference between the evaporator and condenser sections. In addition, at the inclination angle, since there was the effect of a gravitational force, the frequency of oscillation of the vapor bubbles and liquid slugs was comparatively low. Thus, the heat transfer rate decreased.



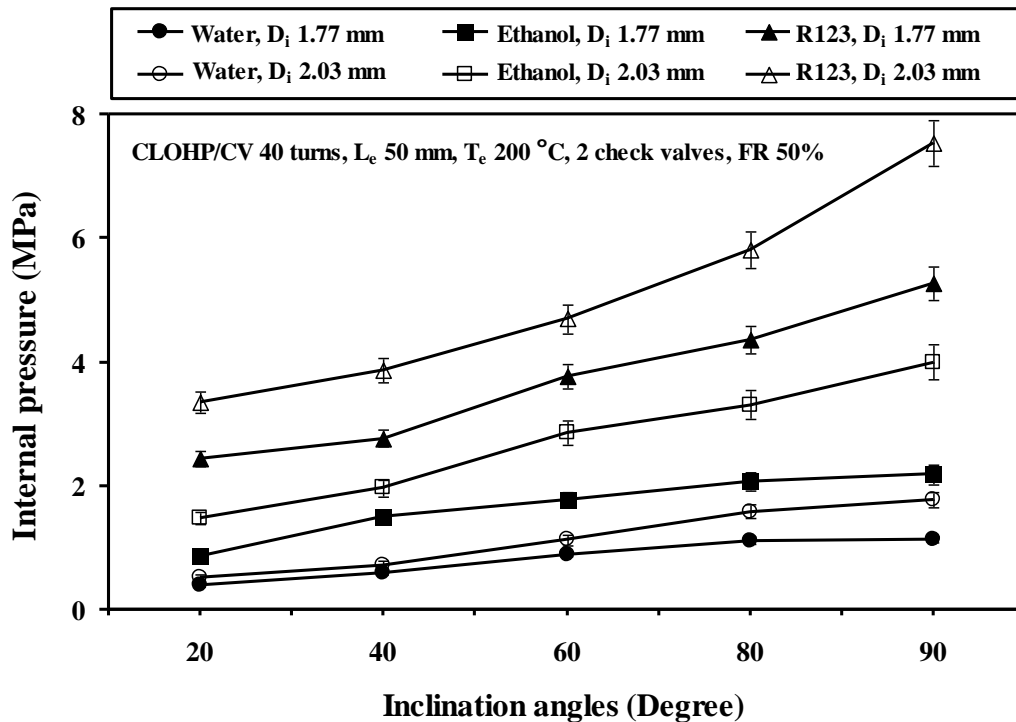


Figure 4.3 Relationship between inclination angles and internal pressure

Figure 4.4 shows the effect of working temperature difference on the internal pressure and from this it can be seen that as the working temperature increases from 100 to 200 °C and the inclination angle increases from 20° to 90°, the internal pressure increases. The working temperature directly affects the internal pressure because the working fluid receives more heat that causes their properties to change with respect to their density, surface tension, viscosity and latent heat of vaporization. Concerning these four properties, the latent heat of vaporization is the major property that has the greatest effect on the motion of the liquid slugs and vapor bubbles in a tube, as well as directly affects the internal pressure increase of the CLOHP/CV. As a result, at an inclination angle of 90°, working temperature of 200 °C, inner diameters of 2.03 mm and R123 as the working fluid beget the internal pressure was 7.53 MPa.



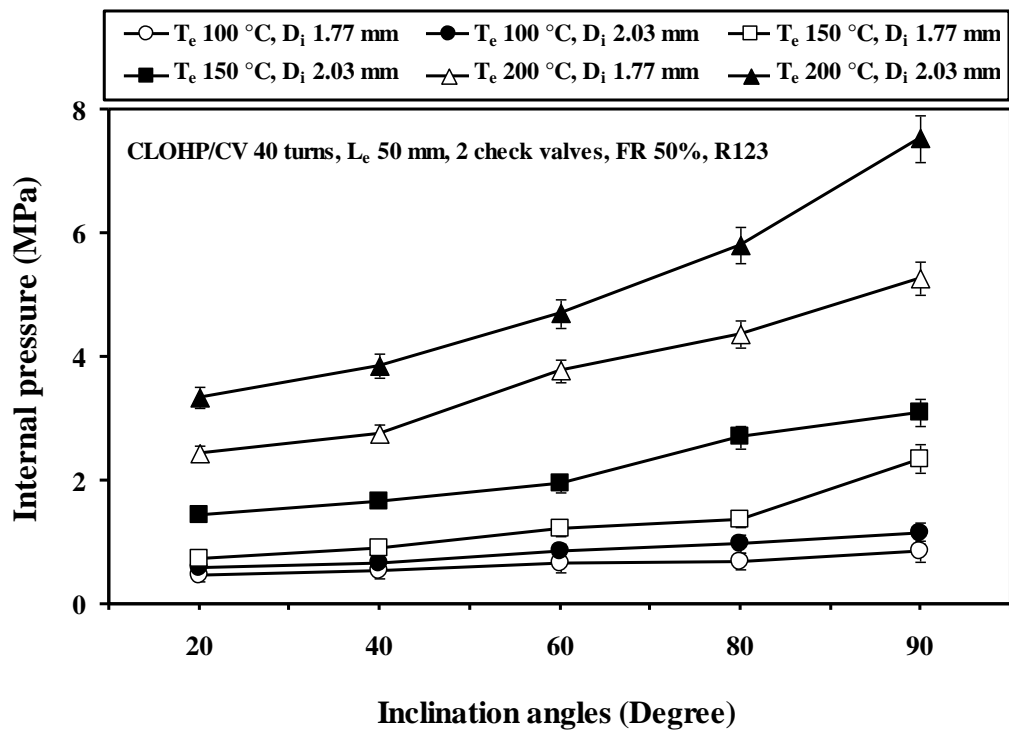


Figure 4.4 Effect of working temperature difference on the internal pressure

Figure 4.5 shows the relationship between the inclination angles and the thermal resistance of the CLOHP/CV for three working fluids (distilled water, ethanol, and R123) at the working temperature of 200 °C. It was found that as the inclination angle increased from 20° to 90°, the thermal resistance decreased and the thermal performance was improved. This is because of the oscillation of the vapor bubbles between the evaporator and the condenser sections were sufficiently strong for the large inclination angle. The CLOHP/CV with R123 as the working fluid at the working temperature of 200 °C worked at the highest performance for both inner diameters of 1.77 and 2.03 mm. The minimal thermal resistance was 0.147 °C/W and 0.048 °C/W for the inner diameters of 1.77 and 2.03 mm, respectively. Figure 4.6 shows the effect of working temperature difference on the thermal resistance.



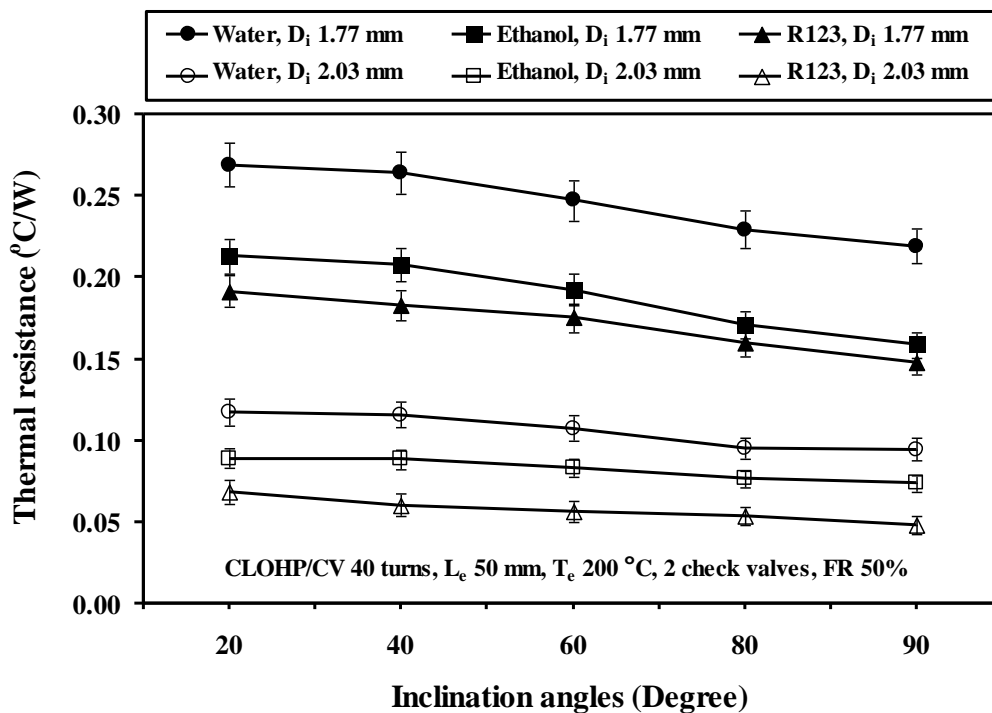


Figure 4.5 Relationship between inclination angles and thermal resistance

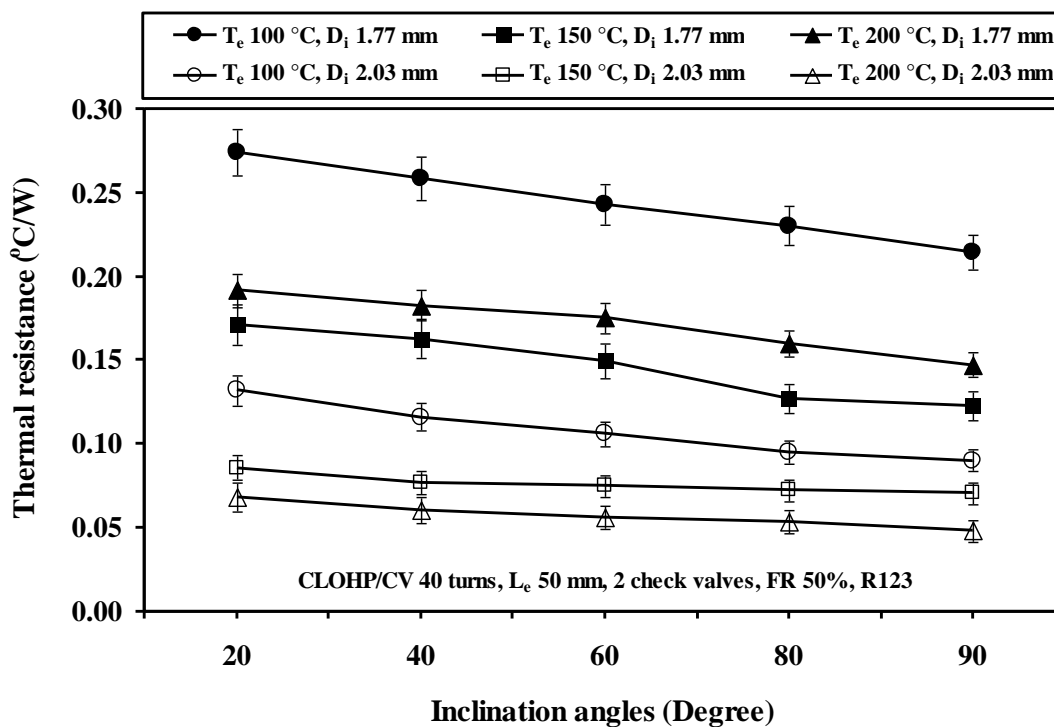


Figure 4.6 Effect of working temperature difference on the thermal resistance



#### 4.2.2 Evaporator length

Figure 4.7 shows the relationship between the evaporator lengths and the internal pressure for the CLOHP/CV with inner diameters of 2.03 and 1.77 mm, working temperature of 200 °C and the inclination angle of 90°. The evaporator, adiabatic and condenser lengths were the same. The experimental result clearly shows the effect of the evaporator length on the internal pressure. When the evaporator length decreases, the effective length between the condenser and the evaporator section also decreases. It was seen that as the evaporator length increased, the internal pressure decreased for every working fluid. The highest internal pressure was obtained for the shortest evaporator length of 50 mm and the inner diameter of 2.03 mm. Internal pressures of 7.53, 4.00 and 1.78 MPa for R123, ethanol and distilled water as the working fluid were found, respectively. Under these conditions, the best heat transfer performance was attained.

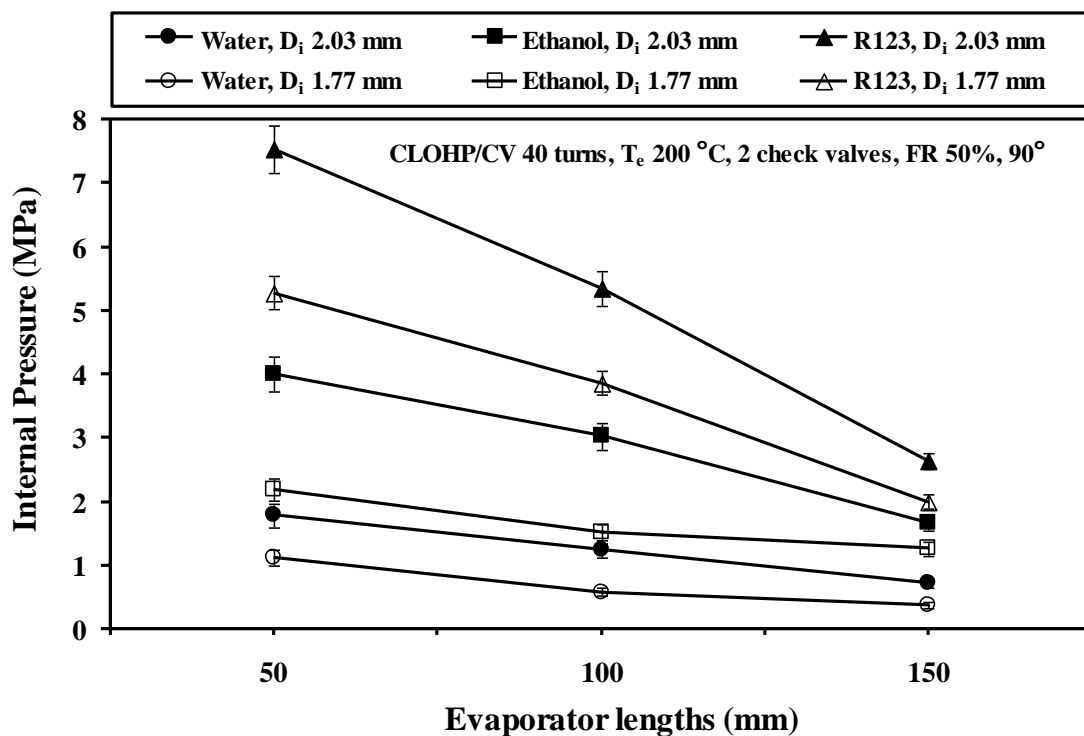


Figure 4.7 Relationship between evaporator lengths and internal pressure



Figure 4.8 shows the dependence of the thermal performance on the evaporator lengths for the CLOHP/CV with 40 turns and  $T_e$  of 200 °C. When the evaporator length was long, the thermal resistance clearly increased. Since the evaporator, adiabatic and condenser lengths were the same, the evaporator length directly related to the effective length of the fluid flow path between the evaporator and condenser sections,  $L_e$ . Thus, the thermal performance improves with a decrease in the evaporator length and effective length. The maximum performance occurred at the shortest evaporator length of 50 mm. This may be because for shorter effective lengths, the frictional pressure drop of the fluid flow is reduced; and thus, the working fluid has more chance to flow from the evaporator to the condenser.

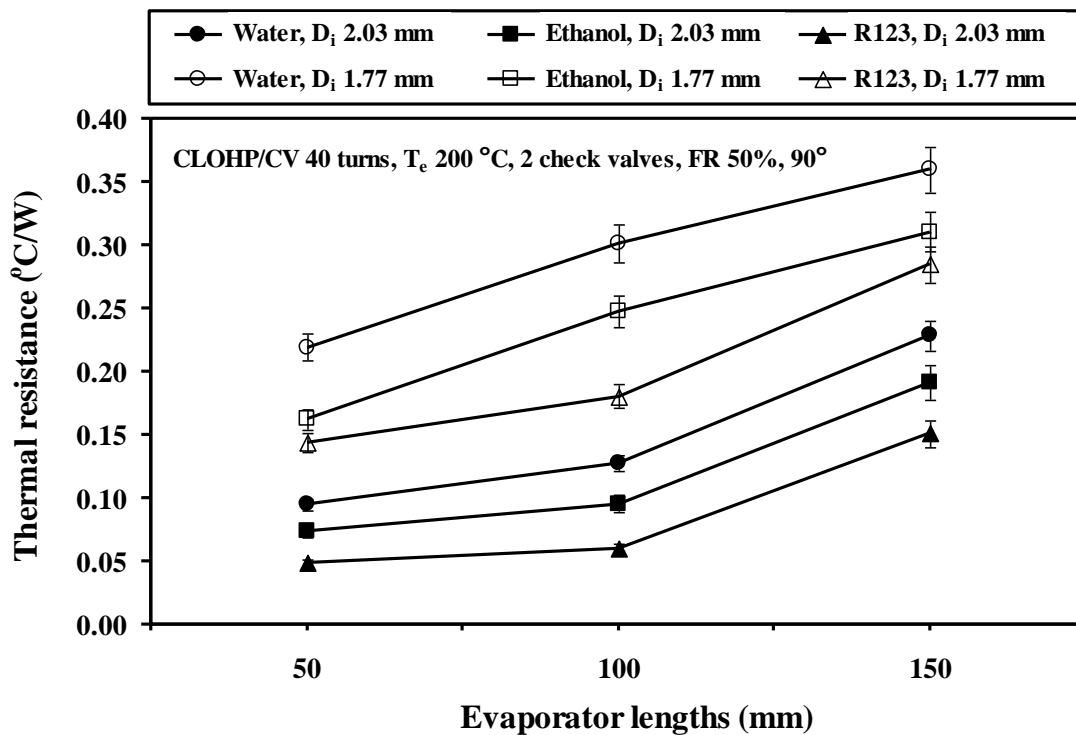


Figure 4.8 Relationship between evaporator lengths and thermal resistance

#### 4.2.3 Inner diameter

Figure 4.9 shows the relationship between the inner diameters and the internal pressure of the CLOHP/CV for three working fluids (distilled water, ethanol, and R123) and a working temperature between 100 and 200 °C. The result showed that



as the inner diameter increased from 1.77 to 2.03 mm, the internal pressure increased for both cases with working temperatures of 100 and 150 °C. In the case of the working temperature of 200 °C, the internal pressure became higher, which affected the working fluid movement in the tube; it was a difficulty movement because of the high surface tension and the internal pressure in the heat pipe that dropped if the internal diameter increased and then the working fluid boiled and moved rapidly. Due to the working fluid properties, when the temperature rises, the density of the working fluid drops and the surface tension and the shear force also drop, but the driving force increases. As a result, the heat transfer performance and thus, the heat transfer rate would increase when the internal pressure increased. It can be concluded that the CLOHP/CV with R123 as the working fluid, working temperature at 200 °C and inner diameter of 2.03 mm, gave the highest internal pressure of 7.53 MPa.

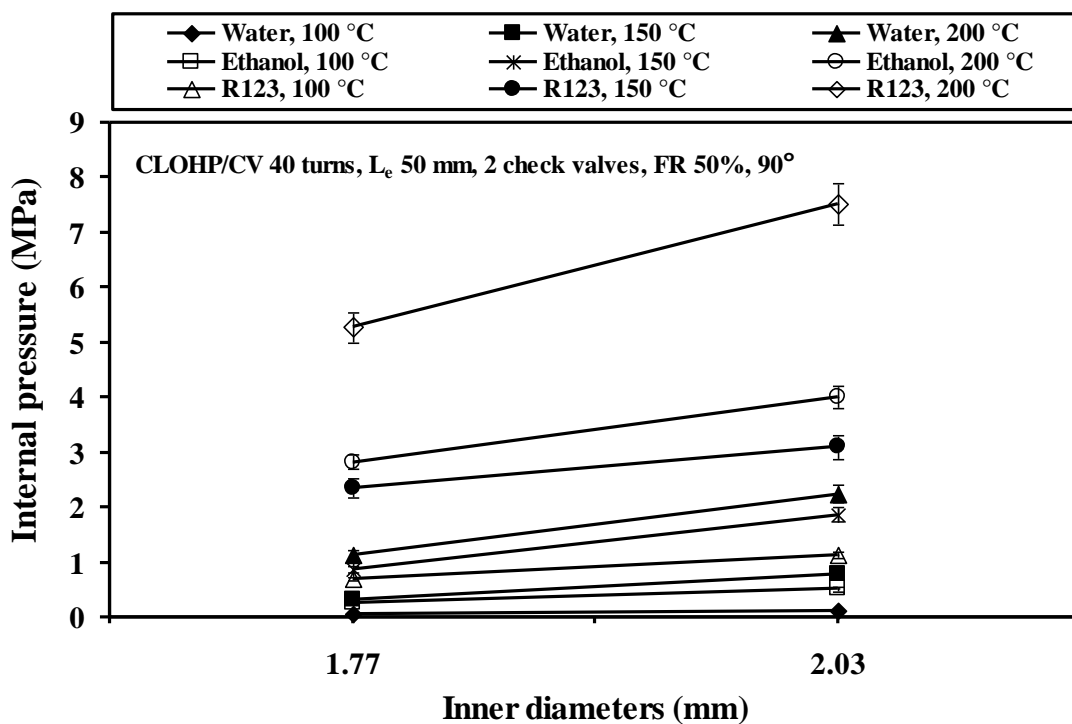


Figure 4.9 Relationship between inner diameters and internal pressure

Figure 4.10 shows the effect of the tube inner diameters on the thermal performance of the CLOHP/CV with three kinds of working fluids (distilled water, ethanol and R123) at working temperatures between 100 and 200 °C. It can be seen that





when increasing the inner diameter from 1.77 to 2.03 mm, the thermal resistance decreased. The effect of operational orientation becomes relatively weak or insignificant when decreasing the inner diameter, because the surface tension dominates the fluid flow and vapor bubbles cannot move to the condenser section easily in the smaller tube. The heat transfer performance of the CLOHP/CV with an inner diameter of 2.03 mm was investigated for all working fluids. The hypothesis proposed by (Maezawa et al., 1996) was used to estimate the optimum inner diameter of the CLOHP/CV, when it was thought that the vapor slug filled the cross section area within the tube. It was, in reality, found that the internal wall of the tube was covered by a liquid film; therefore, the optimum inner diameter of the tube can be slightly larger than the value estimated in the reference. In conclusion, for the case of the working temperature at 200 °C and an inner diameter of 2.03 mm, the highest thermal performance 0.048 °C/W was achieved for R123, which was better than that of distilled water and ethanol.

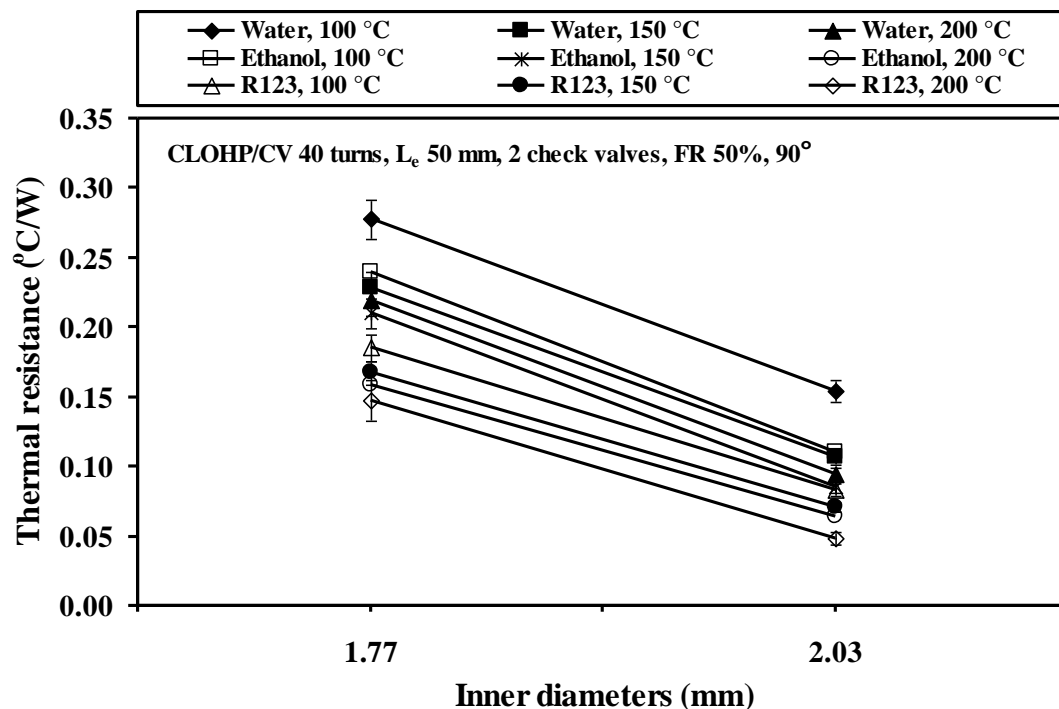


Figure 4.10 Relationship between inner diameters and thermal resistance



#### 4.2.4 Working fluids

In this study, distilled water, ethanol and R123 were used as the working fluids. Their properties are different, namely their densities, surface tensions, viscosities and latent heats of vaporization. Concerning these four properties, the latent heat of vaporization is the dominant property that has a strong effect on the CLOHP/CV. A low latent heat will cause the liquid to evaporate more quickly at a given temperature and a higher vapor pressure; the liquid slug oscillating velocities will be increased and the heat transfer performance of the CLOHP/CV will be improved.

Figure 4.11 shows the result of the internal pressure variation for the three working fluids. The highest internal pressure, 7.53 MPa, was attained when the working fluid was R123 with an inner diameter of 2.03 mm and a working temperature of 200 °C and thus the highest thermal performance is expected to be achieved for this working fluid. It is the medium for the transferring of heat from the high temperature to the low temperature. When the working fluids at the evaporator section receive the heat from the heat source, they will evaporate and produce vapor and then move to the condenser section. When the vapor contacts the cool surface of the condenser, the latent heat of the vapor will be transferred to the inner surface of the condenser. Then, it will condense to a liquid and flow back to the evaporator section again. This has the highest thermal conductivity and lowest latent heat of vaporization. Due to this excellent property, active motions of the liquid slug and vapor bubbles are induced in the tube, which results in a high heat transfer rate.



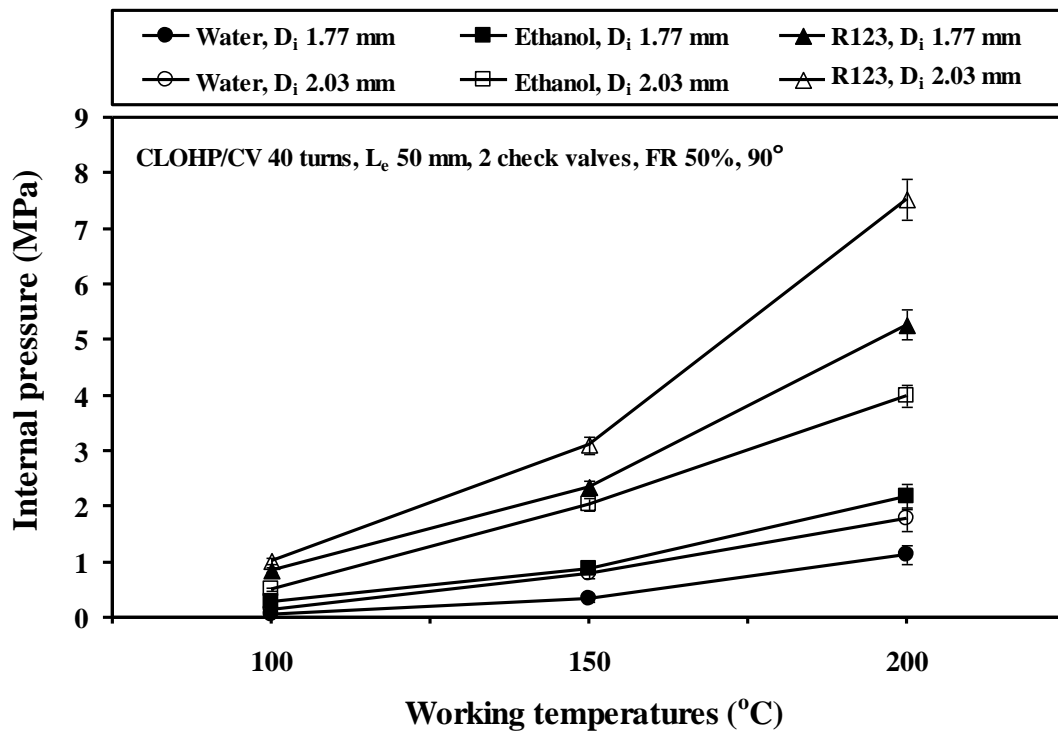


Figure 4.11 Relationship between working temperatures and internal pressure

Figure 4.12 shows the relation between the working temperatures and the thermal resistance for the three working fluids. If the heat input to the evaporator increases, both the evaporator temperature and the fluid temperature will increase gradually, which causes the surface tension and latent heat to decrease. Higher surface tension will allow the use of a larger tube diameter and then the pressure in the tube drops. A larger tube diameter would allow for improved performance and causes the pressure to drop. However, if the pressure drops a large amount, greater bubble pumping force is required and thus higher heat input is also required to maintain pulsating flow. Low latent heat will cause much more liquid evaporation at a given temperature. The liquid slug oscillation velocity will increase and thus the heat transfer performance of the PHP will be improved. More vapors are generated to cause faster vapor flow. R123 as the working fluid, which has the highest internal pressure and resulted in the highest thermal performance of a CLOHP/CV, will cause the lowest thermal resistance, which was  $0.048 \text{ }^\circ\text{C/W}$ .



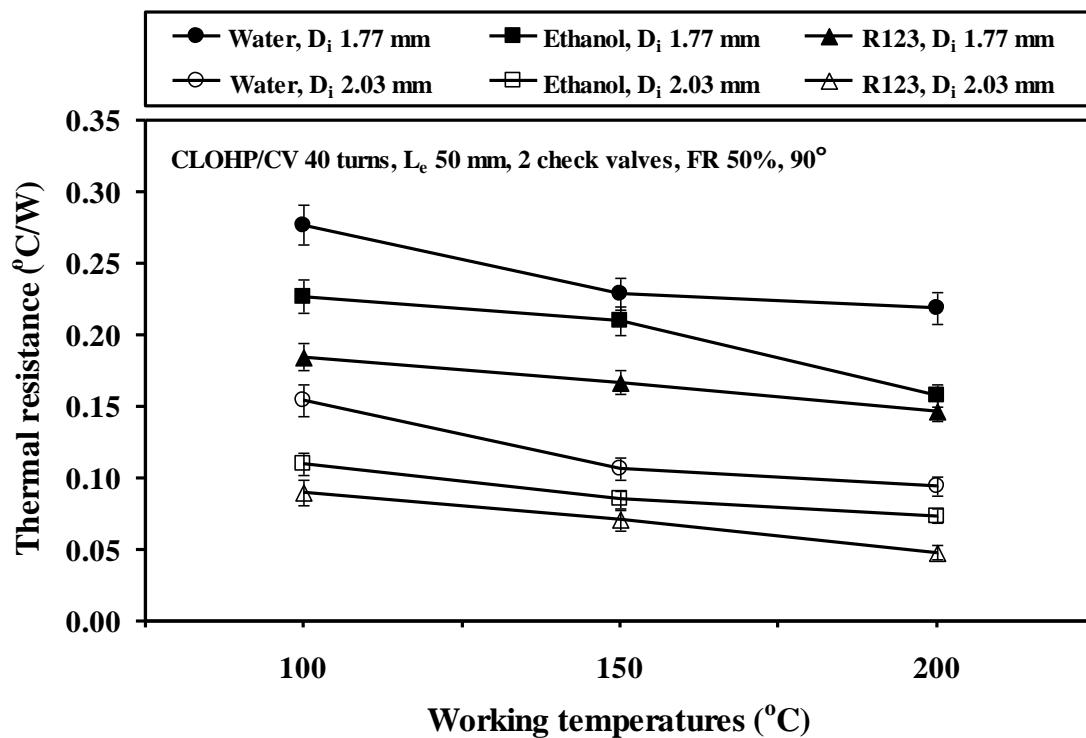


Figure 4.12 Relationship between working temperatures and thermal resistance

#### 4.2.5 Working temperature

Figure 4.11 shows the relationship between the working temperatures and the internal pressure for the CLOHP/CV with three working fluids: distilled water, ethanol and R123, an inner diameter of either 1.77 or 2.03 mm. The result shows that as the working temperature increases from 100 to 200 °C, the internal pressure increases. The working temperature directly affects the internal pressure and thus, the temperature rise results in an increase of the heat transfer rate accordingly. The CLOHP/CV, with R123 as the working fluid, an inner diameter of 2.03 mm, an inclination angle of 90° and a working temperature of 200 °C resulted in the highest internal pressure of 7.53 MPa. When the CLOHP/CV was heated in the evaporator section, the working fluid evaporates and increases the vapor pressure, thus causing the bubbles in the evaporator zone to grow. This pushes the liquid towards the low-temperature area in the condenser section. Cooling of the condenser results in a reduction of vapor pressure and condensation of bubbles in that section of the heat pipe. The growth and collapse of bubbles in the evaporator and condenser sections results in an oscillating motion within the tube. Heat is transferred through latent heat in the vapor and through sensible heat



transported by the liquid slugs. At higher temperatures, R123 has a lower boiling point and thus higher internal pressure than ethanol and distilled water as the working fluid, high heat input causes high internal pressure in the evaporator section. Heat input in the evaporator is the energy source that provides the driving force in the direction of motion in the tube that causes fluid flow to the condenser section. When heat is extracted in the condenser section, the working fluid returns to the evaporator section.

Figure 4.12 shows the relationship between the working temperatures and the thermal resistance for the CLOHP/CV with three kinds of working fluids: distilled water, ethanol and R123 and an inner diameter of either 1.77 or 2.03 mm. The result showed that as the working temperature increased from 100 to 200 °C, the thermal resistance decreased. In the case of R123 as the working fluid and a working temperature of 200 °C, the lowest thermal resistances were 0.147 °C/W and 0.048 °C/W for the inner diameters of 1.77 and 2.03 mm, respectively. The thermal resistance of the CLOHP/CV with R123 as the working fluid, a working temperature of 200 °C and an inner diameter of 2.03 mm was lower than those with ethanol and distilled water as the working fluid. As the working temperature increased, the heat transfer rate increased and the thermal resistance decreased. For R123, the thermal conductivity increases and the heat capacity increases. Moreover, with the increase of the temperature, the heat transfer rate increased because the buoyancy force decreased when the temperature increased. In conclusion, as the working temperature increases the thermal resistance decreases and accordingly, the heat transfer rate increases.

#### 4.2.6 Comparison of the performance of CLOHPs

Figure 4.13 shows a comparison of the heat transfer between the CLOHP/CV and the CLOHP without check valves (CLOHP, Charoensawan et al. 2003). The comparison results show the effect of the performances of the heat transfer between both the heat-pipe for the three working fluids (distilled water, ethanol and R123) and the inner diameter of 2.0 mm in a vertical orientation 90°. It was found that the heat transfer of the CLOHP/CV was more than the CLOHP because the CLOHP/CV provides a higher heat transfer through the addition of check valves that prevent bidirectional flow. Under normal oscillating heat-pipe operating conditions, the liquid slug and vapor plug are effectively located in the condenser and evaporator respectively. The liquid forms U-shaped columns in individual turns of the oscillating heat-pipe and



the oscillations form waves. Under these conditions, effective heat transfer is limited by the amplitude of the waves. When the amplitude of the heat transfer area is not included as part of the waves, an effective working fluid supply to the heat transfer area cannot be obtained and the heat transfer is not maintainable. This operating limit can be overcome by the inclusion of check valves in the CLOHP. The check valves regulate the flow such that it becomes unidirectional and the heat transfer area is not restricted by the amplitude of the oscillating flow. However, the thermal performance is a complex combination of the above, it is certainly difficult to prescribe or proscribe a certain working fluid unless all the boundary conditions are exactly known and individual effects have been explicitly isolated and quantified. The different heat-pipes (CLOHP/CV and CLOHP) are beneficial under different operating conditions. An optimum trade off of various thermo-physical properties has to be achieved depending on the imposed thermo-mechanical boundary conditions. R123 of the CLOHP/CV has the lowest latent heat of vaporization and the highest thermal conductivity when compared to distilled water and ethanol. Therefore, the CLOHP/CV has a higher heat transfer than the CLOHP.



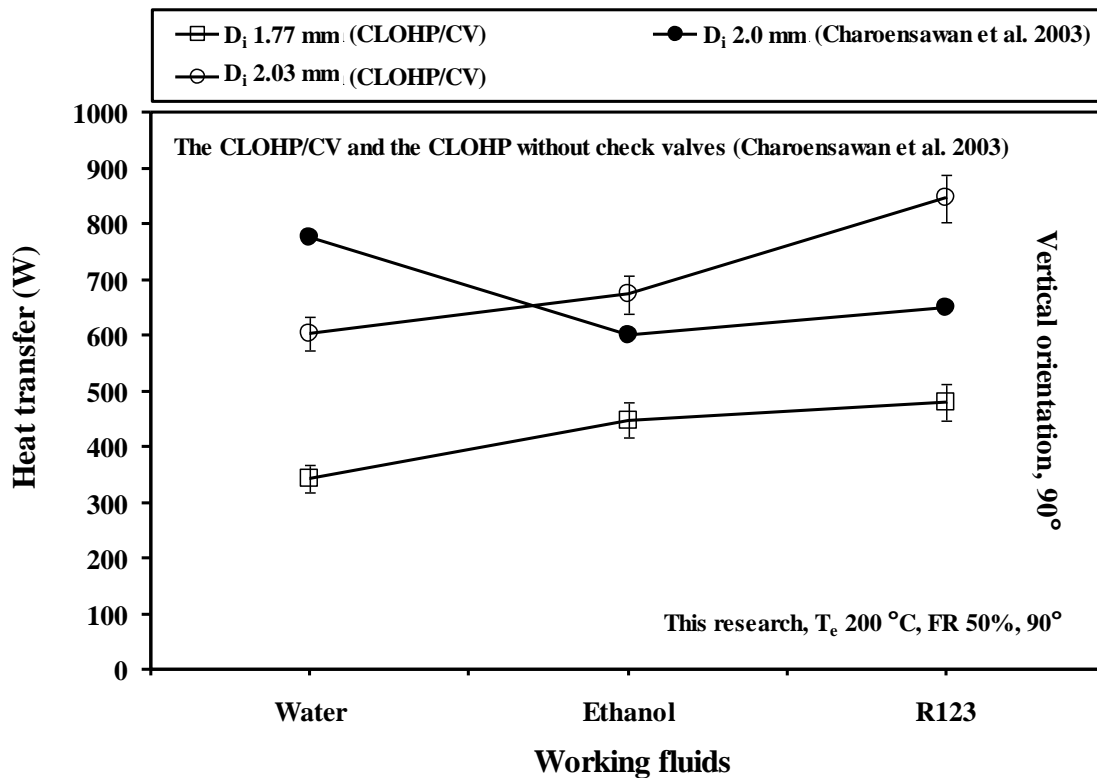


Figure 4.13 Comparison of heat transfer rate

Figure 4.14 shows a comparison of the thermal resistance between the CLOHP/CV and the CLOHP without check valves (CLOHP, Charoensawan et al. 2003). The comparison result shows the performances of the thermal resistance of both heat-pipes. The CLOHPs with three kinds of working fluids, distilled water, ethanol, and R123, with a filling ratio of 50% of the total volume and an inner diameter of 2.0 mm in a vertical orientation 90°. The thermophysical properties of the working fluid coupled with the geometry of the device have profound implications on the thermal performance of the device and the check valves will support the working fluid within the heat-pipe so it flows in the same direction. Thus, it will not cause any collisions between the vapor plug and liquid slug that move back and forth in the heat-pipe, thus affecting thermal performance. It can be seen that the highest performance was at the maximum inner diameter of 2.0 mm. This trend was also seen for all the CLOHP/CVs. This may be because the smaller inner diameter leads to an increased frictional pressure drop and then flow resistance. The comparison results found that the thermal resistance



of the CLOHP/CV with R123 as the working fluid was lower than those of the other CLOHP.

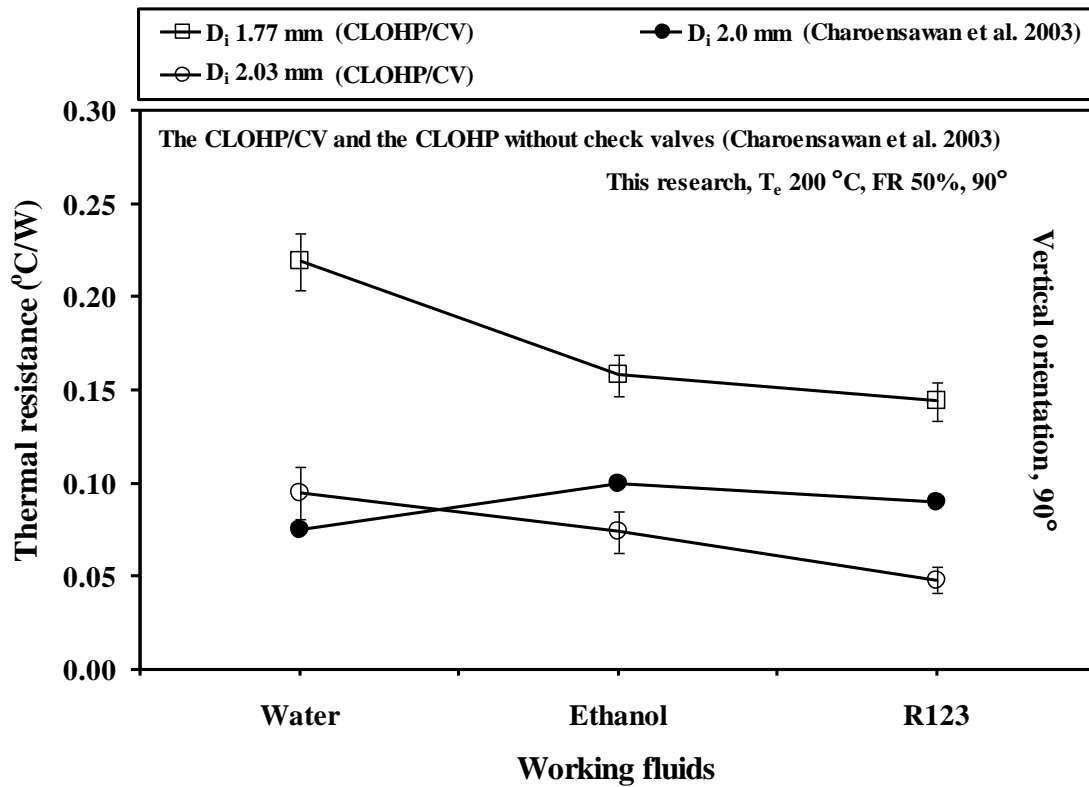


Figure 4.14 Comparison the thermal resistance

### 4.3 Results of copper corrosion

#### 4.3.1 Visual examination

Figure 4.15 shows the photographs of the actual copper tubes, cross-sectional view of copper tubes for the experiment as shown in Figure 4.15(a). A longitudinal view of the sample copper tube in the evaporator section before testing and after testing is shown in Figure 4.15(b-c). The times of the experiments were 500, 1000 and 3000 hours. Distilled water and ethanol were used as the working fluids. As can be seen from Figure 4.15, the characters and compounds deposited on the inner surface of the CLOHP/CV were unable to be observed; so, we needed to use an instrument for accurate photography, which was SEM analysis for surface micrographs of the CLOHP/CV.





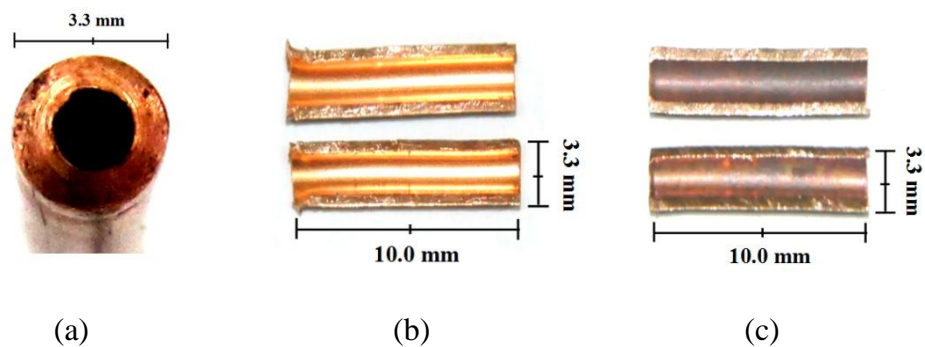


Figure 4.15 Photographs of the actual copper tubes: (a) cross-sectional view copper tube for experiment, (b) inner surface of the copper tube before testing and (c) inner surface of the copper tube after testing

#### 4.3.2 Surface analysis (SEM)

Under the effect of a small pressure difference, the working fluid flows cyclically in a process of phase change of evaporation and condensation inside the sealed space of the CLOHP/CV. The corrosion mechanism of the CLOHP/CV is thus much more complicated than with structural materials immersed in static or even flowing liquid such as those for fast breeder reactors. In order to identify the possible limiting factors on the life of temperature heat pipes, it is necessary to study the corrosion process and its characteristics. As show in Figure 4.16 show the SEM micrographs of the CLOHP/CV inner surface. It can be seen that there is no deposits or corrosion products on the unused surface. The specimen used for comparison was from the evaporator section as it is expected that most of the reaction occurred on this part.



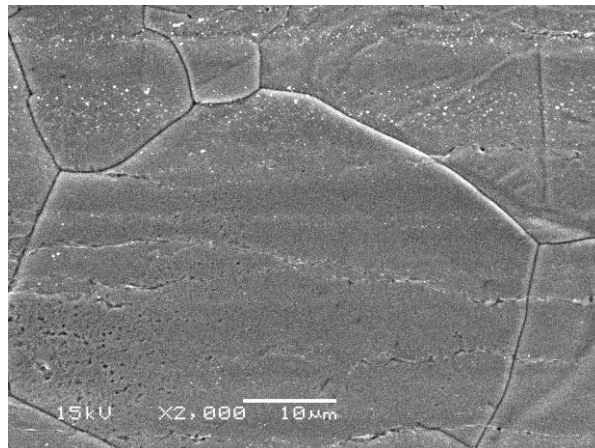


Fig. 4.16 SEM micrographs for CLOHP/CV: before testing

Figure 4.16(a-b) shows the CLOHP/CV tested with distilled water and ethanol as the working fluids, respectively. After the 500 hours time test the analysis with the SEM found that the inner surface of the copper tube character was missing and strong corrosion was clearly visible. The reactions between the internal fluid and tube wall were present at the start of the reaction period; so, there was only corrosion at the thin surface of the tube wall. Figure 4.16(a-b) shows the grain character of the copper tube clearly. The inner surface was smooth and without deposits and corrosion products at the beginning, this study shows that the reaction of the copper was rather elaborate.

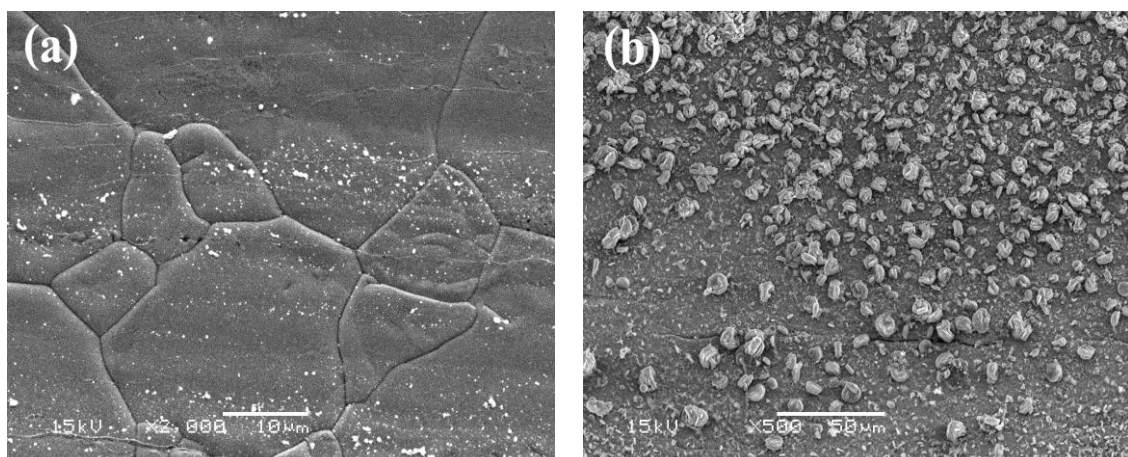


Figure 4.16-1 SEM micrographs for the CLOHP/CV at 500 hours: (a) distilled water as the working fluid and (b) ethanol as the working fluid

Figure 4.16(c-d) shows the CLOHP/CV tested with distilled water and ethanol as the working fluids respectively. At the 1000 hours time test, as can be observed in the SEM micrographs, corrosion products were mainly deposited around the copper tube, in the region of cathodic behavior as determined by the corrosion mechanism. These reactions will cause corrosion volume at the inner surface of the copper tube to increase, which arouses the pit clearly. There were some oxides at the copper surface, which condensed to be a thin layer. The copper ions and electrons will spread out with the oxide at the surface. On the other hand, oxide will spread in the inner copper texture and this affects the loss of the metal texture.

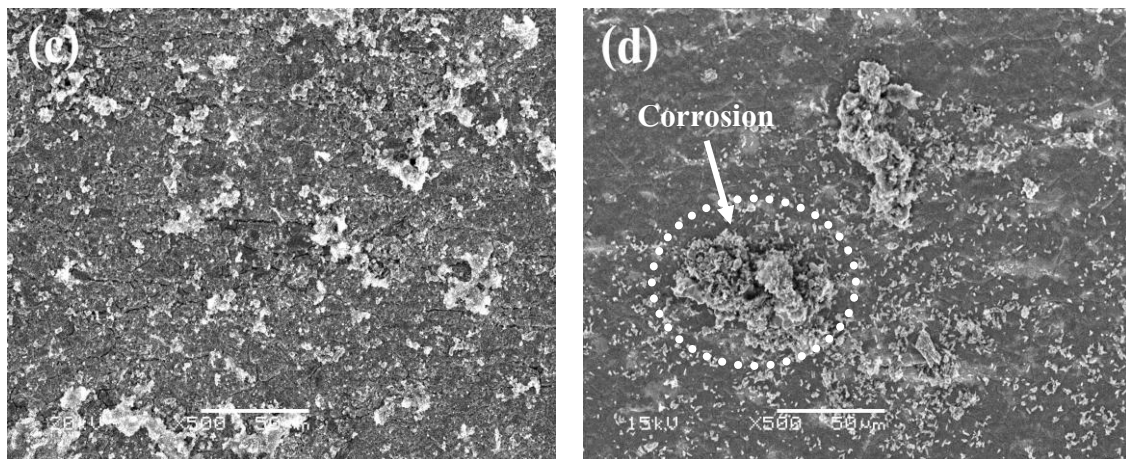


Figure 4.16-2 SEM micrographs for the CLOHP/CV at 1000 hours: (c) distilled water as the working fluid and (d) ethanol as the working fluid

Figure 4.16(e-f) shows the CLOHP/CV tested with distilled water and ethanol as the working fluids, respectively. At the 3000 hours time tests, analysis with SEM found that the inner character of the copper tube was eroded from the layer of the surface tube clearly. These show that, if predicting forward with longer times, the corrosion reaction of the tube will be increased and the materials have all life times that depend on the complement other factors. From the above analysis, one finds that serious corrosion occurs generally in the evaporator section next to the flowing liquid; while, in the condenser part corrosion is slight. Hence, the erosion of the cyclic fluid flow should also be considered as an important factor accelerating the corrosion.





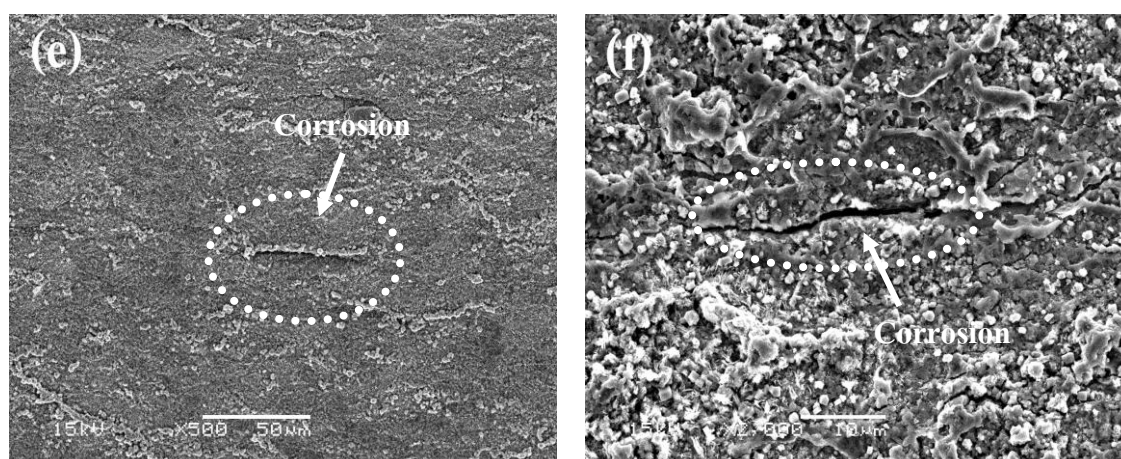


Figure 4.16-3 SEM micrographs for the CLOHP/CV at 3000 hours: (e) distilled water as the working fluid and (f) ethanol as the working fluid

#### 4.3.3 Elemental analysis (EDX)

Figure 4.17 shows the elemental analysis (EDX) for the CLOHP/CV. The experiment analyzed the elements that occurred on the inner surface of the copper tube and tested them with the SEM for the corrosion products that occurred by the reaction between the working fluids and the inner surface of the copper tube as show in (Table 4.1). Then, a comparison of the differences of the tube surface analysis before testing and the transitions after testing in different time periods (500, 1000 and 3000 hours) is shown. In Figure 4.17(a) the results of the EDX that occurred on the inner surface of the copper tube before testing is shown.

Table 4.1 All elements analyzed for the copper tube surface by EDX

Specimen	C	O	P	Cl	Fe	Cu
(a)	6.24	1.01	-	-	-	92.76
(b)	5.20	10.49	-	-	-	84.31
(c)	14.52	8.77	0.88	-	1.61	74.22
(d)	6.87	11.36	-	-	-	81.77
(e)	-	20.84	-	13.70	0.77	64.70
(f)	8.70	9.43	0.44	-	5.57	75.86
(g)	4.98	20.84	0.37	-	25.88	47.93



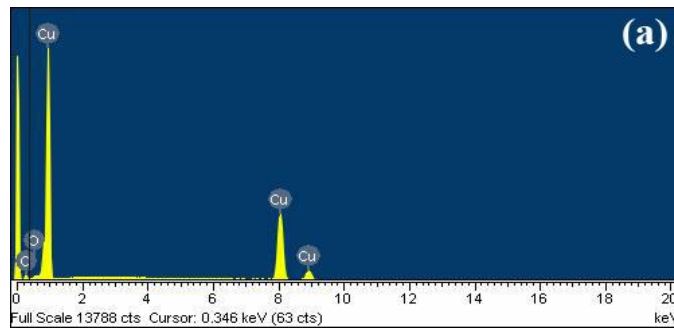


Figure 4.17 EDX for CLOHP/CV: (a) before testing

Figure 4.17(b-c) is the CLOHP/CV after testing with distilled water and ethanol as the working fluids, respectively. At the 500 hours period an analysis with EDX found that the CLOHP/CV with distilled water as the working fluid showed the volume of the copper elements as decreased when compared with Figure 4.17(a) before testing. It was discovered that there was corrosion of the copper tube from an internal reaction, but there was no other element occurring on the surface of the copper tube. In the copper tube that was filled with ethanol as the working fluid, it was found that iron (Fe) and phosphorus (P) occurred from an internal reaction as shown in Figure 4.17(c). Ethanol as the working fluid caused a more rapid reaction than the distilled water as the working fluid. As a result, there was more corrosion. Moreover, the study found that the corrosion occurred at the ball of the check valve of the CLOHP/CV, which is made of iron.

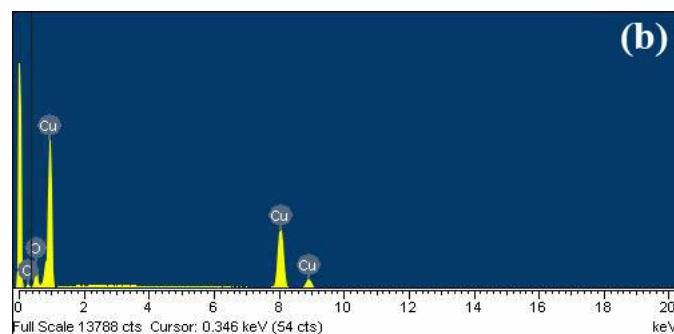


Figure 4.17-1 EDX for CLOHP/CV at 500 hours: (b) distilled water as the working fluid

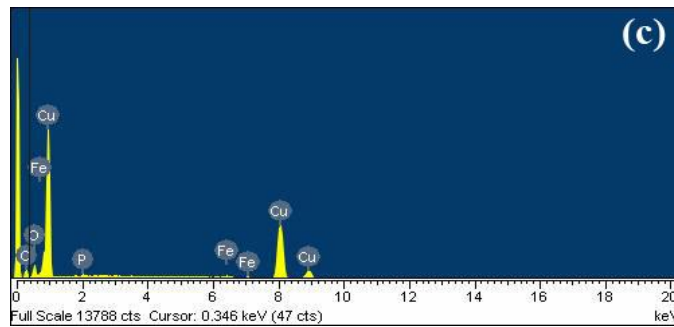


Figure 4.17-2 EDX for CLOHP/CV at 500 hours: (c) ethanol as the working fluid

Figure 4.17(d-e) shows the CLOHP/CV after testing with distilled water and ethanol as the working fluids, respectively. At the 1000 hours time, the test found that the corrosion products were mainly deposited around the copper tube. When analyzed, the inner surface of the CLOHP/CV with ethanol as the working fluid, it was found that the chlorine (Cl) element occurred through the reaction of ethanol as the working fluid. The copper tube and chlorine (Cl) would cause the failure of the heat pipe directly. Accordingly, ethanol as the working fluid reacted more bitterly than distilled water as the working in the same time period.

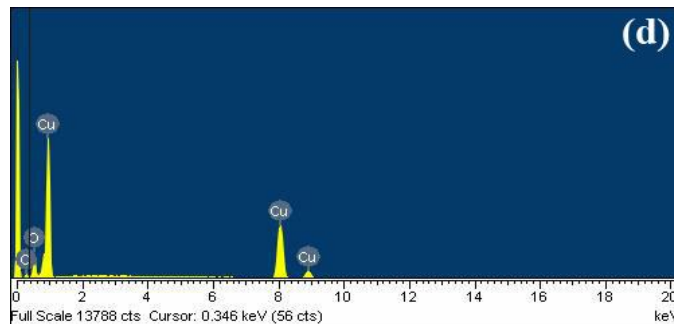


Figure 4.17-3 EDX for CLOHP/CV at 1000 hours: (d) distilled water as the working fluid



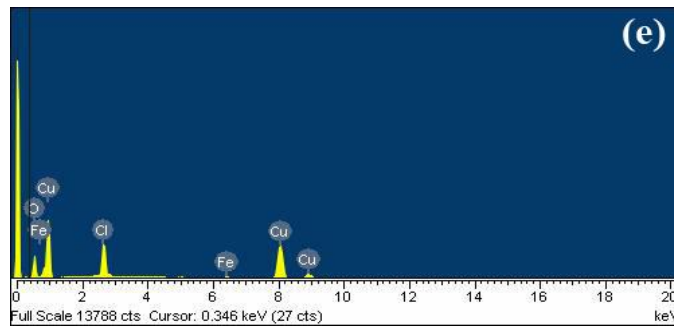


Figure 4.17-4 EDX for CLOHP/CV at 1000 hours: (e) ethanol as the working fluid

Figure 4.17(f-g) shows the CLOHP/CV tested with distilled water and ethanol as the working fluids, respectively. At the 3000 hours time tests, when analysis was done with EDX, it was found that the same element occurred on the inner surface of the copper tube, but there was a different element volume. The CLOHP/CV with ethanol as the working fluid, the copper element volume at the inner tube by analysis was less than the CLOHP/CV with distilled water as the working fluid because there were many corrosion products on the copper surface that occurred from the reaction between the working fluid and the tube surface in the copper tube. It caused more corrosion and further failure of the CLOHP/CV.

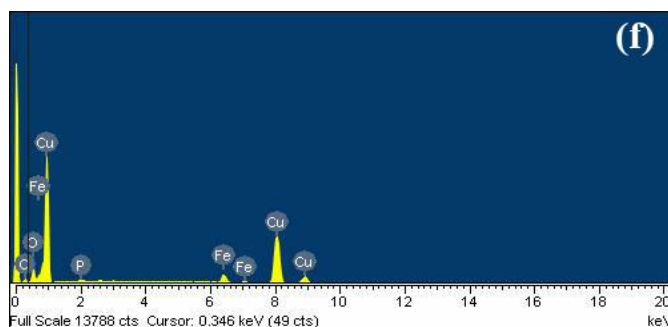


Figure 4.17-5 EDX for CLOHP/CV at 3000 hours: (f) distilled water as the working fluid

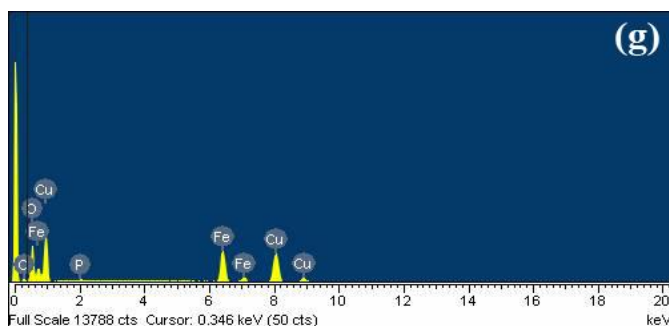


Figure 4.17-6 EDX for CLOHP/CV at 3000 hours: (g) ethanol as the working fluid

#### 4.3.4 Chemical composition analysis (Flame-AAS)

There is a linear relationship between the concentration of the copper ions in a colored solution and the absorbance of the solution. A series of solutions of a copper solution may be prepared with different concentrations. If the absorbance of these solutions are measured and plotted versus solution concentration, the points should form a straight line. This line, called a calibration curve, shows how absorbance changes with the concentration of a solution. Each copper ion has its own unique calibration curve that must be determined experimentally. A calibration curve of copper solution is shown in Figure 4.18.

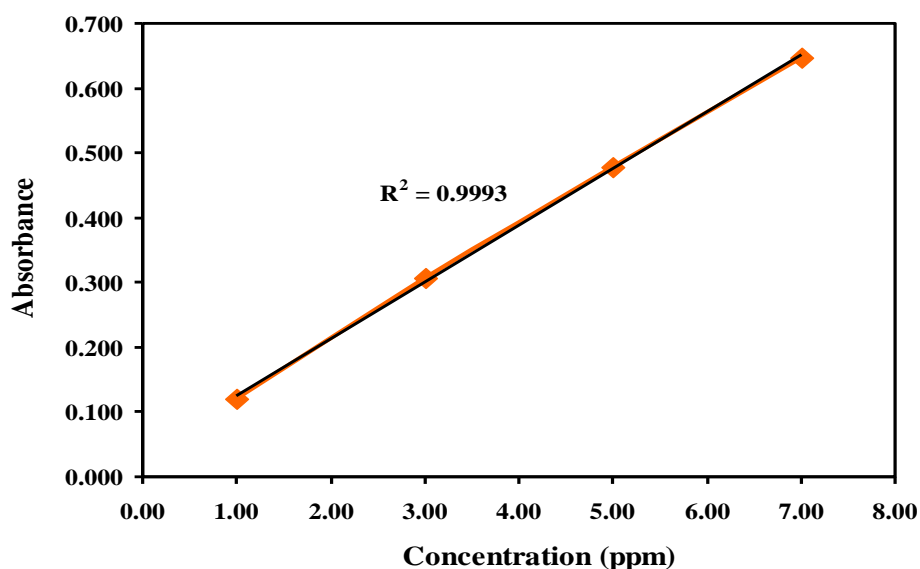


Figure 4.18 Calibration curve of copper solution





A calibration curve is a valuable tool for finding the concentration of a copper solution mix in the working fluids. Once we have a calibration curve, the absorbance of copper can be measured, compared to the calibration curve and the corresponding concentration found. Fig 4.18 shows that, the data has reliability ( $R^2$ ) at 0.9993 when calculating the concentration of copper particles in the working fluid, which are showed in (Table 4.2). Then calculating the volume of copper particles associate with the working fluid at 50% filling capacity or 22 ml of the total internal tube volume.

Table 4.2 Concentration value of copper particles

<b>Working fluid (500 hours)</b>	<b>Concentration (ppm)</b>	<b>Weight of copper (mg)</b>
Distilled Water	0.010712	0.000236
Ethanol	7.39724	0.162767
<b>Working fluid (1000 hours)</b>		
Distilled Water	0.067352	0.001482
Ethanol	16.17504	0.355851
<b>Working fluid (3000 hours)</b>		
Distilled Water	0.097095	0.002136
Ethanol	18.57228	0.408590

The Flame-AAS analysis found that as the duration time went up the concentration of copper particles in the working fluid increased, which causes the internal reaction of the working fluid with the inner wall of the CLOHP/CV. (Table 4.2) shows the concentration of copper in the working fluid at the beginning of the test period to the 1000 hours test period, there are high concentrations and then the concentration of copper will decrease until to 3000 hours test period.

Figures 4.19 and 4.20 show the relationship between the results of the concentrations of copper particles and duration time in the experiment at the working temperature was 200°C, using distilled water and ethanol as the working fluids. This has a relationship for the logarithmic function; the data has reliability ( $R^2$ ) at 0.9082 and 0.8901 respectively, as determined by the following equations (4.1) and (4.2).

$$C_{Cu,W} = 0.0010 \ln(t) - 0.0059 \quad (4.1)$$

$$C_{Cu,E} = 0.129 \ln(t) - 0.6001 \quad (4.2)$$



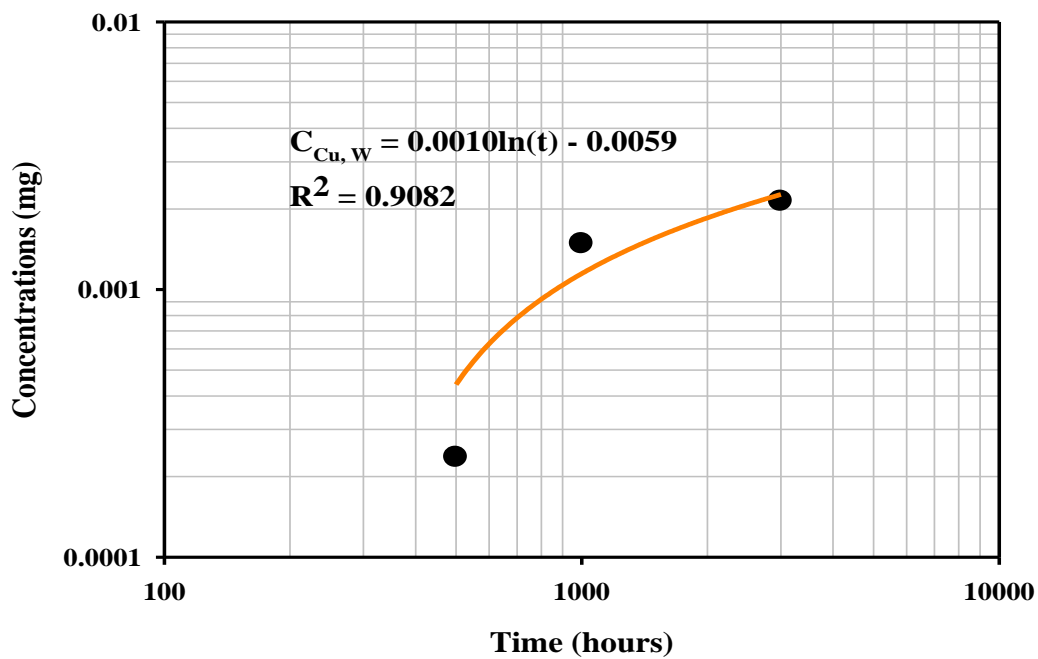


Figure 4.19 Relationship between concentrations of Cu and time with distilled water as the working fluid

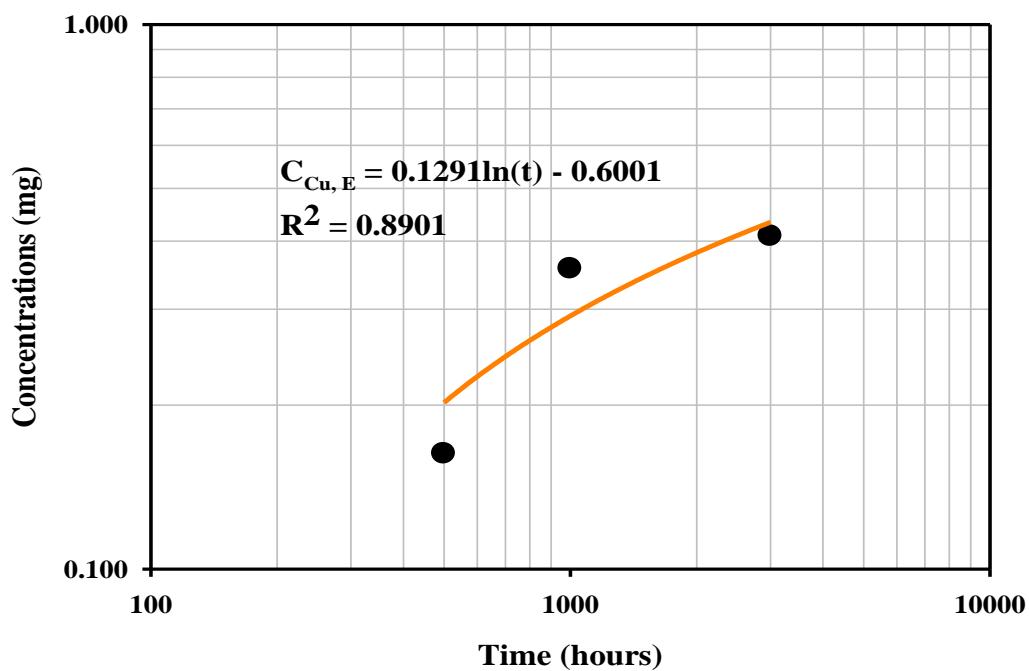


Figure 4.20 Relationship between concentrations of Cu and time with ethanol as the working fluid



In conclusion, there are high reactions to the test at the first time period because there are many volumes of fluid that take part in the reaction that causes the oxygen volume of the oxidation and reduction reactions. As for the corrosion mechanism caused by the oxygen inside the CLOHP/CV, a theory of oxygen recycling in a sealed space is proposed in this study. If the oxygen reaction decreases, the concentration of copper solutions will decrease as well. The table showed that there were greater concentrations of copper particles in ethanol as the working fluid than distilled water as the working fluid, because the boiling point is lower than in distilled water, so it can move faster. When the working fluid moves through at high speed and it has copper particles suspended in it, the speed of the flow will cause the metal particles to collide with the inner wall of the pipe. Hence, the fluid flow should be considered as an important factor accelerating the corrosion. Moreover, oxidation and reduction reactions will cause the corrosion ratio to increase.

#### 4.3.5 Corrosion rate

This result shows that the internal corrosion rates of the CLOHP/CV, which used distilled water and ethanol, can be discussed in two parts. The first one was the time of testing from 500 to 1000 hours where the corrosion rates were greater. The second one was the time of testing from 1000 to 3000 hours where the corrosion rate was lower. From these, relative equations of the corrosion rates with the duration of testing, as in equations (4.3) and (4.4), show the relationship for the polynomial function between the corrosion rates with duration time in experiments at the working temperature of 200 °C, using distilled water and ethanol as the working fluids, by the following equations:

$$Cr_W = -1.2290 \times 10^{-14} (t^2) + 4.4241 \times 10^{-11} (t) - 1.3018 \times 10^{-8} \quad (4.3)$$

$$Cr_E = -8.7107 \times 10^{-13} (t^2) + 2.0812 \times 10^{-9} (t) + 3.3359 \times 10^{-6} \quad (4.4)$$



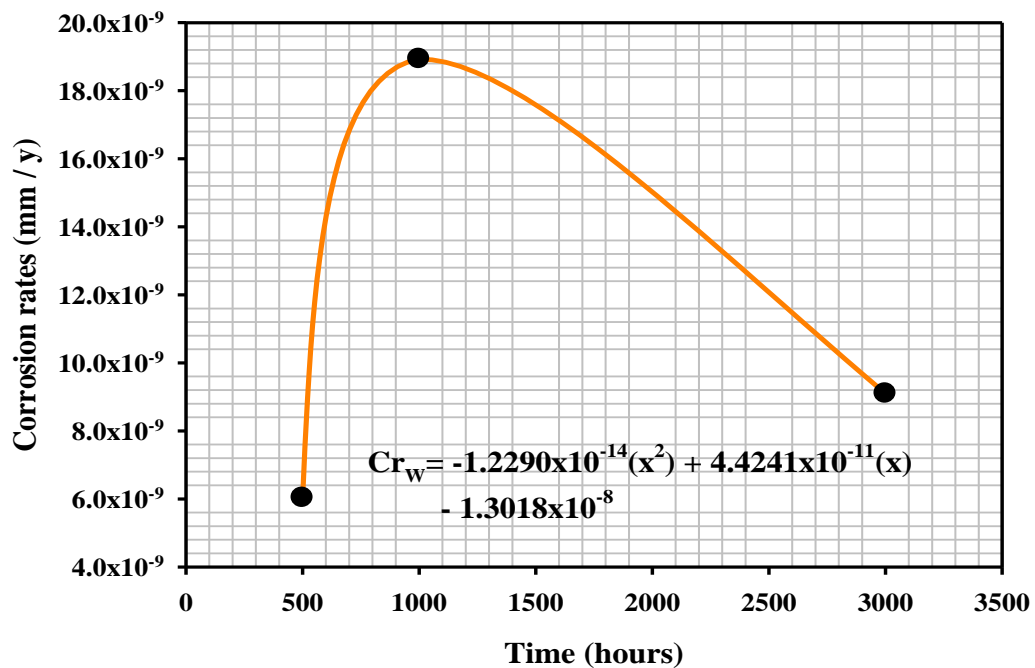


Figure 4.21 Relationship between corrosion rates and time with distilled water as the working fluid

Figure 4.21 shows the results of a time between 500 to 1000 hours for the CLOHP/CV testing, which used distilled water was working fluid. At 200 °C it was found that there were more internal corrosion rates because the volume of oxygen that reacted with the tube wall was at a high rate. This caused the corrosion rates to be high, but when compared with the corrosion rates when the working fluid was ethanol it was found that they were less because of the inner boiling system of the heat pipe, from the working fluid's properties. In the closed system of the CLOHP/CV the effect from the internal temperature, the time of testing that caused the corrosion occurred easily, it affected the corrosion rates of the heat pipe. After 1000 hours testing, the corrosion rates were lower because the volume of oxygen that reacted was lower. This was shown in the relation of the Polynomial functions as in equation (4.3). From equation (4.3) it was found that the corrosion rates were lower after a time of testing of 1000 hours, the corrosion rates of distilled water at the time of testing of 3000 hours caused a corrosion rate that was about  $9.09 \times 10^{-9}$  mm/y.



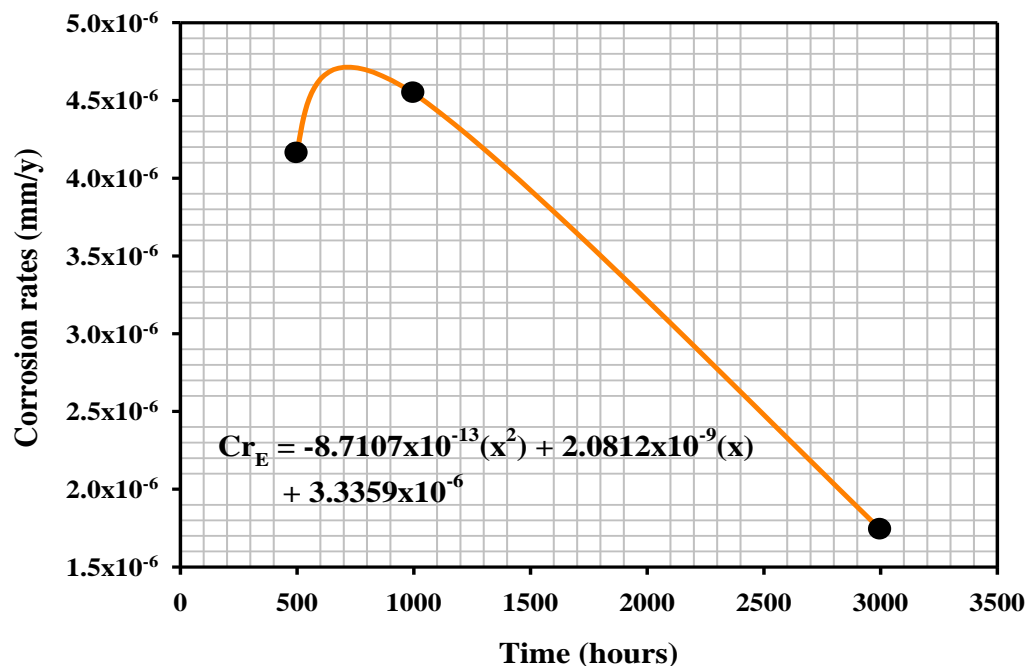


Figure 4.22 Relationship between corrosion rates and time with ethanol as the working fluid

Figure 4.22 shows the times between 500 and 1000 hours for the CLOHP/CV test using ethanol was the working fluid. At 200 °C it was found that during this time the internal corrosion rates occurred more than if distilled water was used at the time of 1000 hours, there was more corrosion at 500 hours when compare with the distilled water, because the substrate reacted with the internal surface more and faster than the distilled water. The ethanol working fluid had greater corrosion properties than the distilled water so it caused corrosion rates that were more and after testing at 1000 hours, the corrosion rates would be lower down with the distilled water. This was shown in the relation of the Polynomial functions as in equation (4.4). From equation (4.4) it was found that the corrosion rate would be lower after 1000 hours. At the time of testing, 3000 hours caused corrosion rates that were about  $1.74 \times 10^{-6}$  mm/y and resulted in copper oxide, which was a product of the corrosion. Copper oxide can be referred to as copper (I) oxide (cuprous oxide,  $\text{Cu}_2\text{O}$ ), which is a red powder, or copper (II) oxide (cupric oxide,  $\text{CuO}$ ), which is a black powder. The patina shields the metal from corrosion. Upon strong heating, it forms a black solid copper oxide. The



experiments conducted with pure oxygen have also shown that the overall corrosion damage and the rate of corrosion of copper tube depend on the concentration of the solution and the time of exposure. From the above analysis, one finds that serious corrosion occurs generally in the condenser section next to the flowing liquid; while, in the evaporator part corrosion is slight. Hence, the erosion of the cyclic fluid flow should also be considered as an important factor accelerating the corrosion. The high temperature corrosion caused by the working fluid in the high temperature heat pipes is attributed to the recycling effect of the oxidizing agents and the erosion of the working fluid inside the heat pipes. Serious corrosion occurs mainly in the condenser section due to the flowing liquid.

#### **4.4 Results of fatigue on copper tube**

##### 4.4.1 S-N curves of copper tube (C1220) in fatigue test

Since the amplitude of the cyclic loading has a major effect on the fatigue performance, the S-N relationship is determined for specific loading amplitude. The amplitude is expressed as the R ratio value, which is the minimum peak stress divided by the maximum peak stress. It is most common to test at an R ratio of curves, with each curve at a different R ratio being often developed. A variation to the cyclic stress controlled fatigue test is the cyclic strain controlled test. In this test, the strain amplitude is held constant during cycling. Strain controlled cyclic loading is more representative of the loading found in thermal cycling, where a component expands and contracts in response to fluctuations in the operating temperature. It should be noted that there are several shortcomings of S-N fatigue data. First, the condition of the test specimens does not always represent actual service conditions. For example, components with surface conditions, such as pitting from corrosion, which differs from the condition of the test specimens that will have significantly different fatigue performance. Furthermore, there is often a considerable amount of scatter in fatigue data even when carefully machined standard specimens out of the same lot of material are used. Since there is considerable scatter in the data, a reduction factor is often applied to the S-N curves to provide conservative values for the design of components. For some components, the crack propagation life is neglected in design because stress levels are high and/or the critical



flaw size small. For other components, the crack growth life might be a substantial portion of the total life of the assembly. Moreover, preexisting flaws or sharp design features may significantly reduce or nearly eliminate the crack initiation portion of the fatigue life of a component. The useful life of these components may be governed by the rate of subcritical crack propagation.

Fatigue, as one of the most important failure modes in bulk structural materials, has been investigated for a long time. Transition from the traditional engineering to micro/nano technology has driven the research interests in fatigue toward small-scale materials. On the small scale, the design and reliability of the materials do not follow the conventional theories since the fatigue behavior of small scale materials has been proven to be different from that of bulk materials due to size effects. Failure cycles applied for specimens are also shown in (Table 4.3).

Table 4.3 Summary of fatigue tests

<b>Model Type</b>	<b>Temp (°C)</b>	<b>Specimen Type/Screw or Flange</b>	<b>Failure Cycle (<math>N_f</math>)</b>
<b>Uniform</b>	<b>200</b>	<i>S</i>	47,591
<b>One-wave</b>	<b>200</b>	<i>S</i>	55,854
<b>One-wave</b>	<b>300</b>	<i>S</i>	53,550
<b>Uniform</b>	<b>15</b>	<i>F</i>	307,984
<b>One-wave</b>	<b>15</b>	<i>F</i>	436,757
<b>Two-wave</b>	<b>15</b>	<i>F</i>	203,535
<b>Uniform</b>	<b>200</b>	<i>F</i>	271,131
<b>One-wave</b>	<b>200</b>	<i>F</i>	168,950
<b>Two-wave</b>	<b>200</b>	<i>F</i>	68,791
<b>Uniform</b>	<b>300</b>	<i>F</i>	107,756
<b>One-wave</b>	<b>300</b>	<i>F</i>	13,174
<b>Two-wave</b>	<b>300</b>	<i>F</i>	10,393

Figure 4.23 shows the graph of the S-N curve of a copper tube (C1220) that illustrates the stress values and the number of cycles to failure ( $N_f$ ) values, which is known as an S-N curve. A log scale is almost always used for the number of cycles to failure ( $N_f$ ). It was found that a stress of 200 MPa, one-wave type specimen values at a



temperature of 200 °C was more than the one-wave type specimen values at a temperature of 300 °C and uniform type specimen values at a temperature of 200 °C degrees Celsius. The number of cycles to failure ( $N_f$ ) were 55854, 53550 and 47591, respectively and at the a temperature of 200 °C for the one-wave type specimen, the  $N_f$  value was greater. Due to the higher temperature, that affects the molecular structure of the copper tube was less when taken together, so it caused the fracture uncomplicatedly. When the copper tube is heated, it would be the one procedure with the metallic material was a linear expansion. By that, the material would expand in the axis that affected the thickness of the copper tube, at the higher temperatures, there was more expansion and the uniform-type at a temperature of 200 °C was small because the fracture of the specimen occurred in the screw area and did not occur in the center of the specimen. As this area was fragile by design of the tensile-compress load, so the fracture would be uncomplicated more than the center of the specimen, which caused the screw-model specimen to have a damage problem in this area that is showed in Figure 4.25. This shows that the fracture surfaces obtained from the screw-model specimen at relatively stress levels of 200 MPa for the one-wave type specimen at 300 °C and uniform type specimen at 200 °C. Therefore, the study would design the specimen in a flange-model, which explains the experiment results of the specimen in Figure 4.26. Comparing with the graph of the DHP of the copper that found the stress of 200 MP has a number of cycles to failure ( $N_f$ ) values as approaching the DHP annealed copper values. (DHP copper was from material of copper solid material ingots formed parts to fatigue which is the standard value of the fatigue test specimen comparing with copper tube.)





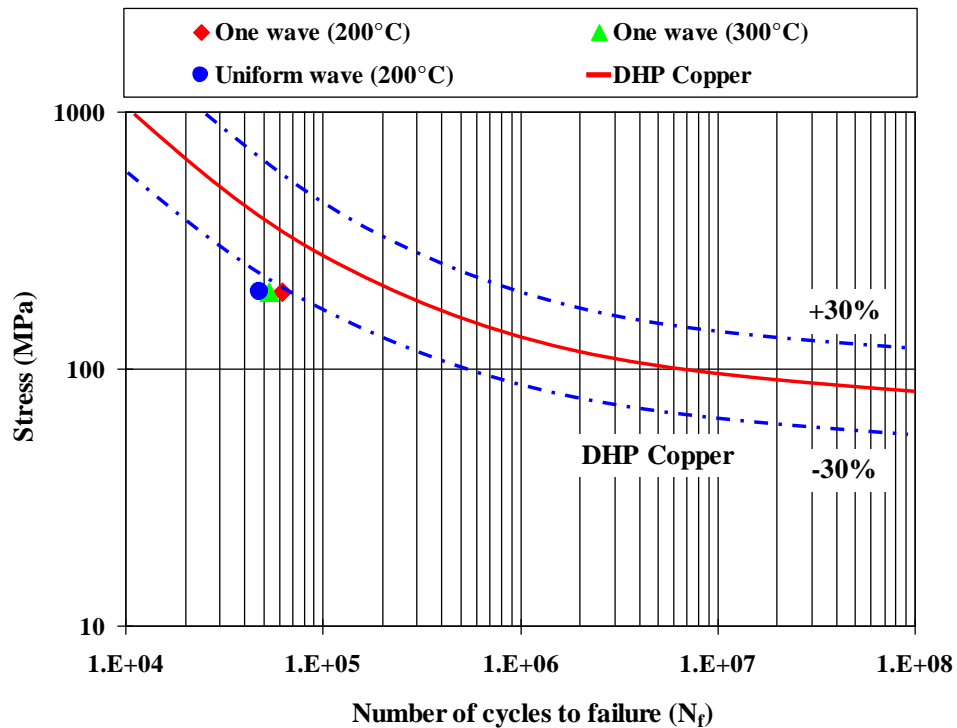


Figure 4.23 S-N curves for DHP and C1220 copper in fatigue test (screw-model)

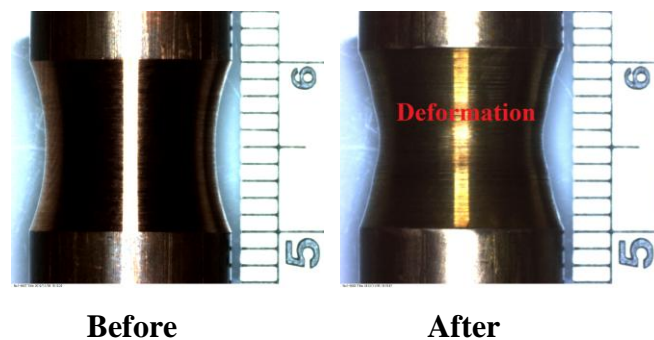


Figure 4.24 Photographs of before and after the fatigue test (one-wave type, 200 °C)

Figure 4.24 shows the before and after photographs of the fatigue test for a one-wave type specimen at 200 °C in the screw-model, stress levels of 200 MPa, in which it can be seen that after the test the copper tube has deformation. It was found that fatigue was a major factor in the copper tube specimen because the plastic deformation range will have first undergone elastic deformation, which is reversible, and so the object will return part way to its original shape. Soft thermoplastics have a

rather large plastic deformation range, as does the copper tube specimen as it was a ductile metal. Under tensile stress, plastic deformation is characterized by a strain region and a necking region, before finally fracture (also called rupture). During the strain, the material becomes stronger through the movement of atomic dislocations. The necking phase is indicated by a reduction in the cross-sectional area of the specimen. Necking begins after the ultimate strength is reached. During necking, the material can no longer withstand the maximum stress and the strain in the specimen rapidly increases. Plastic deformation ends with a fracture in the material.

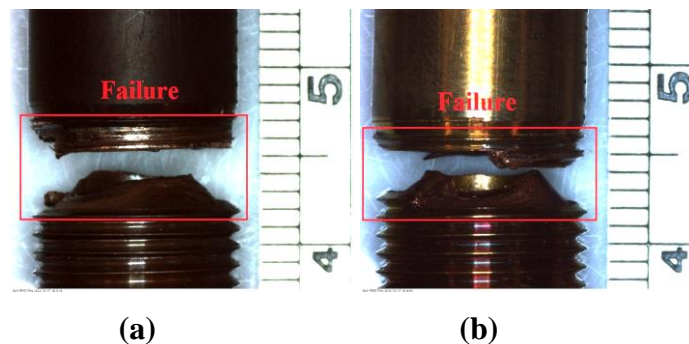


Figure 4.25 Photographs of (a) one-wave type 300 °C and (b) uniform-type 200 °C fatigue test

Another deformation mechanism is metal fatigue, which occurs primarily in ductile metals. It was originally thought that a material deformed only within the elastic range and returned completely to its original state once the forces were removed. However, faults are introduced at the molecular level with each deformation. After many deformations, cracks will begin to appear, followed soon after by a fracture and as deformation occurs, internal inter-molecular forces arise that oppose the applied force. If the applied force is not too large, these forces may be sufficient to completely resist the applied force, allowing the object to assume a new equilibrium state and to return to its original state when the load is removed. A larger applied force may lead to a permanent deformation of the object, or even to its structural failure.



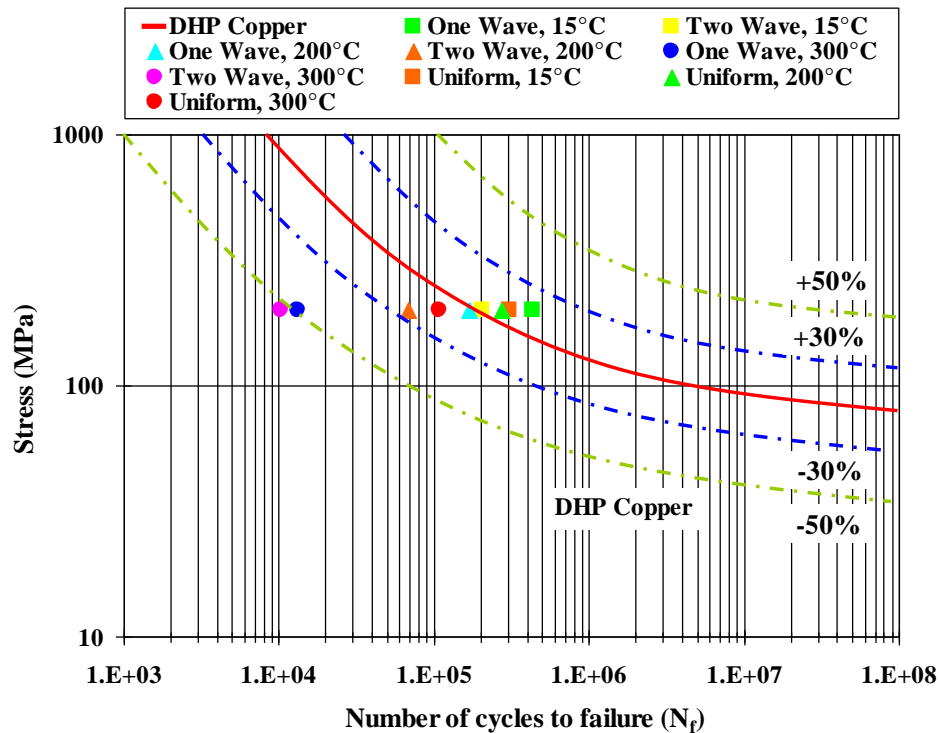


Figure 4.26 S-N curves for DHP and C1220 copper in fatigue test (flange-model)

The number of cycles to failure ( $N_f$ ) values for the S-N curves with the specimens at 200 MPa were compared with those from standard size specimens of DHP copper tubes tested at high temperature. As seen in Figure 4.26, the number of cycles to failure ( $N_f$ ) values for the specimens were equal to or slightly greater than those from standard smooth bar specimens. No strong effect of specimen size on the number of cycles to failure ( $N_f$ ) was found for this specimen. It can be said that the number of cycles to failure ( $N_f$ ) of the two-wave type specimen at 300 °C, hourglass shaped specimen was rather sensitive to fatigue motion during testing (cyclic tension-compression loading). On the other hand, it was rather insensitive to the lateral displacement and the increased temperature affected the structure of the copper tube, which caused the material damage to occur quickly. Most materials expand somewhat when heated through a temperature range that does not produce a change in phase. When the added heat increases, the average amplitude of vibration of the atoms in the material will increase with the average separation between the atoms. Suppose an object of length undergoes a temperature change of a magnitude, if the temperature



difference is reasonably small, the change in length is generally proportional to the length and temperature difference. Stated mathematically, the material will have the same expansion in all directions for a given temperature change. This is true for each of the copper tube materials that were used (materials that exhibit this type of behavior, are called linear expansion), so linear expansion has an effect on the copper tube specimen when increasing the temperature. The S-N curve found that the one-wave type specimen at room temperature had the highest number of cycles to failure ( $N_f$ ) value because at normal temperature the structure of the copper tube has a few changes that are able to bear the fatigue life more than specimens tested at 200 and 300 °C. When there are changes in the hourglass shaped specimen, they will be extended to the fatigue specimen with the two-wave type specimen components and the uniform-type specimen. The results showed that the effect is a direct extension of the specimen and the hourglass shaped as it was found that the temperature has the greatest impact. Then the focus was on the part of the specimen test group compared with the curve of the DHP copper at the stress of 200 MPa with the control range values  $\pm 30\%$ , one-wave and two-wave specimen at 300 °C with the control range values  $\pm 50\%$  because the temperature and hourglass shaped have affected to failure: the number of cycles to failure ( $N_f$ ) value was similar. The properties of the copper tube (C1220) and the deoxidized high phosphorus copper (DHP copper) are similar, so they are in the same range and the information can be used for applications in future devices. This is a particularly important development for the future.

#### 4.4.2 Photograph observations on the fracture surface of the specimens

Photograph observations on the fracture surface of the specimens that failed at different temperature levels, reveal that different crack propagations operate at different levels of temperature and are shown in Figure 4.27(a-h). The specimen surface was measured using photographs taken by the CCD video camera. The crack initiated at the specimen surface and propagated. The crack surface was observed to be almost perpendicular to the loading direction. Fatigue striations were observed on the surfaces. The fracture surfaces of the miniaturized specimens were similar to those of the standard sized specimens.

Figure 4.27(a) and (b) show the fracture surfaces obtained from the flange-model specimen at relative stress levels of 200 MPa for the uniform-type specimen at



room temperature (15 °C). On a macroscopic scale, the surfaces in both the figures are oriented normal to the main principal stress (longitudinal axis of the specimen) and exhibit planar topography with gradually increasing roughness as the crack propagates. The region of the crack propagation was characterized by a smooth and bright fractured surface, vividly captured in Figure 4.29(a). The area of the final fracture is rather small in these cases owing to relatively lower applied stress. The geometry and macroscopic orientation of the fractured surface (tensile) crack propagation and uniform-type specimen at 200 °C and 300 °C have the same fracture surfaces as the uniform-type at room temperature, but it has a difference in the number of cycles to failure because the temperature affects the structure of the copper's linear expansion. The important feature is the shape of the fracture as viewed from the side. If the stress concentration is relatively insignificant, the fracture face will essentially be a flat plane. However, if the stress concentration played an important part in causing the failure, such as a sharp corner on a step in a shaft, the fracture face will be curved in that area affected by the stress concentration. The sketch in Figure 4.29(a) shows a side view of a shaft and the concave fracture face indicates that there was a serious stress concentration. (If there had been an adequate radius on the shaft and a low stress concentration factor, the fracture face would have been essentially flat, or the failure may not have happened at all.)

Figure 4.27(b) shows the position at the beginning of the fracture in the copper tube, the start of a fracture is determined by the cracking tendencies at the tip of the crack. If a plastic deformation flaw existed at the tip, the structure was not endangered because the metal mass surrounding the crack would support the stress. When brittle fracture occurs (under the conditions for brittle fracture stated above), the crack will initiate and propagate through the material at great speeds (speed of sound). It should be noted that smaller grain size, higher temperature and lower stress tend to mitigate crack initiation. Larger grain size, lower temperatures and higher stress tend to favor crack propagation. There is a stress level below which a crack will not propagate at any temperature. This is called the lower fracture propagation stress. As the temperature increases, a higher stress is required for a crack to propagate.

Figure 4.27(c) shows the fracture obtained in the flange-model specimen at a relative stress level of 200 MPa for the one-wave type specimen at a temperature of



200 °C. Figure 4.29(d) shows the fracture obtained in the flange-model specimen for the one-wave type specimen at room temperature (15 °C). From the experiment on the copper tube at the room temperature it can be seen what the fracture surface of the copper tube will look like: the surface is not smooth because the copper has the property of toughness, when compared to the fracture surface that occurs when there is a temperature difference. This can be seen from the surface of the fracture of specimen.

Figure 4.27(e) shows the fracture surface in cross section of the one-wave type specimen at a temperature of 200 °C. It was found that a closer examination of the failure surfaces provided more information regarding the nature of the fractures and the condition; the specimens failed due to a classic fatigue crack initiation and growth mechanism. The fatigue striations were clearly evident on the failure surfaces indicating that the crack advanced through the specimen. The clear indication of intersection flow lines over the entire material's surface indicates the extent to which the plastic deformation was distributed around the neck specimen region. While necking was seen under the conditions, the nature of the final fracture surfaces were similar when observed with the CCD camera. A limited amount of plasticity-induced deformation void formation is apparent and the final failures appeared to be relative ductile in nature.

Figure 4.27(f) shows the fracture surface of the one-wave type specimen at a temperature of 300 °C. It was found that the fracture of the specimens was similar to the one-wave type at 200 °C, but occurred faster because of the temperatures used in testing were different. As the temperature affected of copper structure that caused the specimen be expand, it affected the thickness of the specimen. As a result, the one-wave type specimen at 300 °C would fracture more easily than the one-wave type specimen at 200 °C and the number of cycles to failure ( $N_f$ ) value was less.

Figure 4.27(g-h) shows the fracture surface obtained from the flange-model specimen at a relatively stress levels of 200 MPa for the two-wave type specimen at a temperature of 200 °C. It was found that the fracture at the top of specimen shown in the figure in this area was positioned close to the loading. Thus, the fracture specimen was easier than the one-wave type specimen, which caused the value of the number of cycles to failure ( $N_f$ ) to be lower and the temperature to increase, which caused the specimen to fracture faster and the temperature will affect the value of the number of cycles to failure ( $N_f$ ).



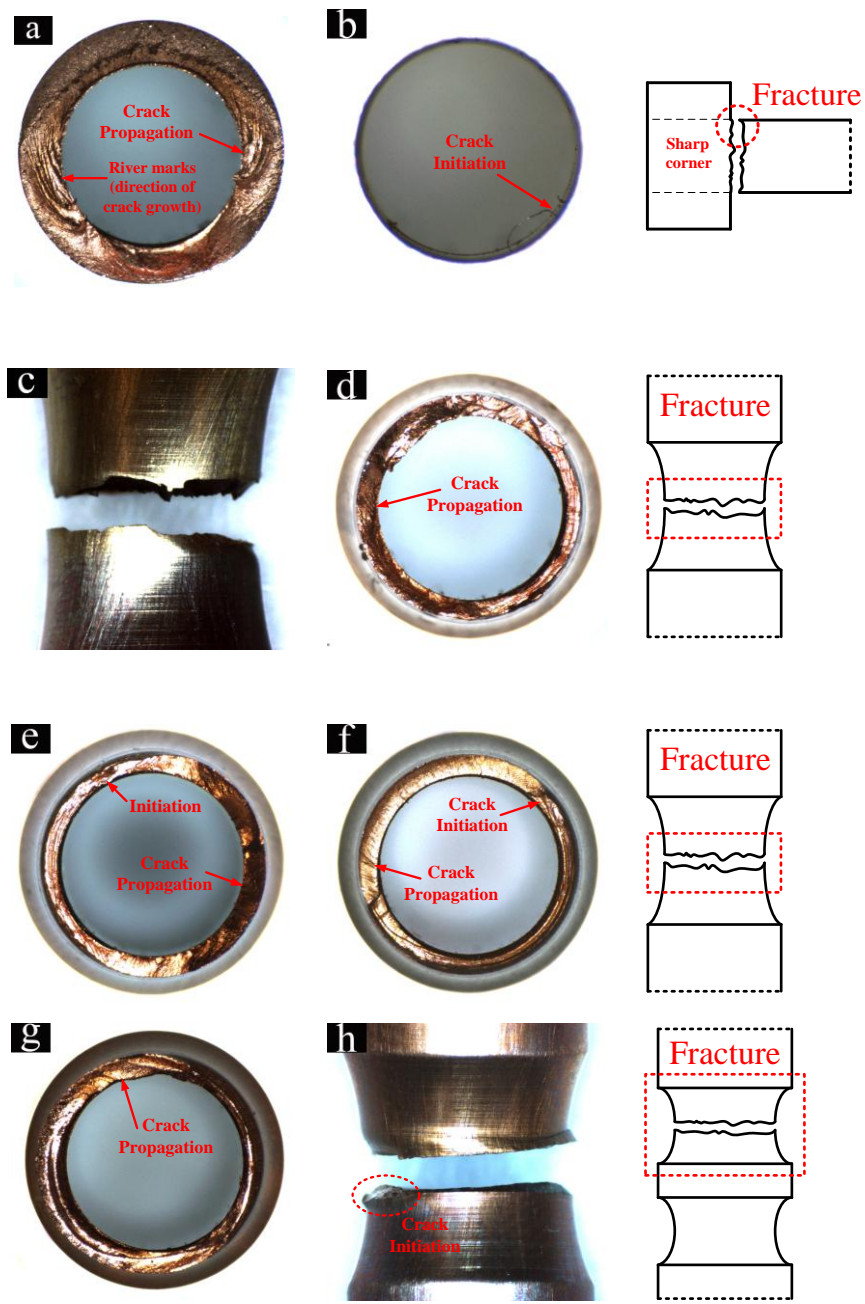


Figure 4.27 Fracture surfaces of specimens (Flange-model)



## CHAPTER 5

### Conclusions and Suggestions

#### 5.1 Conclusions

##### 5.1.1 Conclusion of the internal pressure

An experimental study was performed on a CLOHP/CV to investigate the effects of inclination angle, evaporator length, inner diameter, working fluid and working temperature on the internal pressure and thermal performance. The major results were:

5.1.1.1 The optimum inclination angle for obtaining the highest internal pressure and the thermal performance was  $90^\circ$ .

5.1.1.2 The maximum internal pressure and thermal performance occurred at the short evaporator length of 50 mm. For longer evaporator sections, the thermal resistance clearly increased.

5.1.1.3 Both the CLOHP/CVs with 1.77 mm or 2.03 mm inner diameters were operated successfully at all three working temperatures, showing excellent performances. The CLOHP/CV consisting of 2.03 mm ID tube had the highest internal pressure of 7.53 MPa and the lowest thermal resistance of  $0.048\text{ }^\circ\text{C/W}$ .

5.1.1.4 The working fluid has major effects on the thermal performance. The highest internal pressure and thermal performance appeared for a CLOHP/CV with R123 as the working fluid.

5.1.1.5 The internal pressure and thermal performance of a CLOHP/CV was improved by increasing the working temperature and at  $200\text{ }^\circ\text{C}$  the lowest thermal resistance was recorded.

5.1.1.6 The performance of the CLOHP/CV was more than the CLOHP, but the CLOHPs can be beneficial under different operating conditions. An optimum trade off of various thermo-physical properties has to be achieved depending on the imposed thermo-mechanical boundary conditions.





### 5.1.2 Conclusion of CLOHP/CV corrosion

It can be summarized that:

5.1.2.1 The analysis with the SEM after 3000 hours testing found that the character corrosion on the inner surface of the CLOHP/CV was being pitting. In the CLOHP/CV with distilled water and ethanol as the working fluids and an increase in the test time affected the corrosion of the tube.

5.1.2.2 The analysis with the Flame-AAS found that from the beginning of the test until 1000 hours the concentration of copper particles in the distilled water and ethanol as working fluids were more than after 1000 and 3000 hours, because the oxygen volume in the working fluid caused many reactions at the beginning. When the oxygen decreased after 1000 hours, this caused the reaction to decrease as well and the concentration of the copper particles was 18.57228 ppm or 0.408590 mg.

5.1.2.3 The corrosion rates of the internal tube of the CLOHP/CV were found for the duration of the experiment at the working temperature of 200 °C, using distilled water and ethanol as the working fluids. They had a relationship of a polynomial function that caused the corrosion rates at 3000 hours that were about  $9.09 \times 10^{-9}$  and  $1.74 \times 10^{-6}$  mm/y respectively.

5.1.2.4 From the experiment it was found that the concentrations of copper particles and corrosion rates in the CLOHP/CV, with water and ethanol as the working fluids, were inversely proportional to time.

### 5.1.3 Conclusion of fatigue of CLOHP/CV

An experimental study investigated the effect of fatigue failure on the copper tube used to fabricate the CLOHP/CV at operated temperature. The major results are summarized as follows:

5.1.3.1 The factors that influence the fatigue life of structures are such as mean and stress, hourglass shaped and temperature effect. Some methods have been developed for improving the fatigue performance, which is also evaluated. Good quality design and fabrication of a welded structure can significantly affect the fatigue life.

5.1.3.2 Structural components during their life time are exposed to dynamic loading. Significant cost savings can be gained by including effects of fabrication and details of fatigue robustness in the design phase. The performance of a structure is largely determined by the initial design.



5.1.3.3 From the comparison to the total fatigue life of the specimen it can be concluded that in the case of specimens tested under the cycle fatigue, the crack propagation phase constitutes the major proportion of the fatigue life and analysis of experimental results may help to define the fatigue strength for a given number of cycles to failure.

## **5.2 Suggestions**

5.2.1 The employment of equipment and instruments: for future work it will be necessary to use more accurate equipment and instruments to record data.

5.2.2 In order to clearly observe the generation of the new NCG once the old NCG was purged, future experiments should be performed.

5.2.3 Future experiments should also be carried out to find a suitable release valve material that will be compatible with the system.



## **REFERENCES**



## REFERENCES

- [1] Akachi, H., Notoya, S. and Maezawa, S. "Thermal performance of capillary tunnel type flat plate heat pipe". Proceedings of the 9<sup>th</sup> International Heat Pipe Conference, Albuquerque. New Mexico: 1995. p. 88-96.
- [2] Akachi, H., Polasek, F. and Stulc, P. "Pulsating heat pipe". Proceedings of the 5<sup>th</sup> International Heat Pipe Symposium. Australia: 1996. p. 208-217.
- [3] Baker, E. "Prediction of long-term heat pipe performance from accelerated life tests". AIAA Journal 1973; 11(9): 1345-1347.
- [4] Bastidas, J.M., Cano, E. and Mora, N. "Copper corrosion-simulated uterine solutions". Contraception 2000; 61: 395-399.
- [5] Bhuwakietkumjohn, N., Rittidech, S. and Pattiya, A. "Heat-transfer characteristics of a top heat mode closed-loop oscillating heat pipe with a check valve (THMCLOHP/CV)". Journal of Applied Mechanics and Technical Physics 2012; 53(2): 224-230.
- [6] Charoensawan, P. Heat transfer characteristics of closed-loop oscillating heat pipe. [Thesis for Doctor of Philosophy in Mechanical Engineering] Chiang Mai: Chiang Mai University; 2003.
- [7] Charoensawan, P. and Terdtoon, P. "Thermal performance of horizontal closed-loop oscillating heat pipes". Applied Thermal Engineering 2008; 28(5-6): 460-466.
- [8] Charoensawan, P., Terdtoon, P., Tantakom, P., Ingsuwan, P. and Groll, M. "Effects of inclination angles, filling ratios and total lengths on heat transfer characteristic of a closed-loop oscillating heat pipe". Proceedings of the 6<sup>th</sup> International Heat Pipe Symposium. Chiang Mai Thailand; 2000. p. 422-430.
- [9] Charoensawan, P., Terdtoon, P. and Chaitep S. "Corrosion of Tubes Used in Thermosyphon Heat Exchanger for Waste Heat Recovery System: A Case of Internal Surface". Heat Transfer Engineering 2001; 22(7): 18-27.
- [10] Davis, J.R. "Corrosion: Understanding the Basics". ASME International USA. 2000.
- [11] Dobson, R.T. "Theoretical and experimental modeling of an open oscillatory heat pipe including gravity". Thermal science 2004; 43: 113-119.



- [12] Dunn, P. and Reay, D. Heat Pipe. n.p.: Pergamon International Library; 1982.
- [13] Gi, K., Sato, F. and Maezawa, S. “Flow visualization experiment on oscillating heat pipe”. Proceedings of the 11<sup>th</sup> International Heat Pipe Conference, Tokyo Japan: 1999. Unpage.
- [14] Hollmark, H.M., Keech, P.G., Vegelius, J.R., Werme, L. and Duda, L.-C. “X-ray absorption spectroscopy of electrochemically oxidized Cu exposed to Na<sub>2</sub>S”. Corrosion Science 2012; 54: 85-89.
- [15] Kai, M., Baoming, W. and Zhang, Z. “Study on prolonging the life-time of carbon steel-water heat pipe”. Proceeding of the 7<sup>th</sup> International Heat Pipe Conference; May 21-25; Minsk, U.S.S.R.: 1990. Unpage
- [16] Khandekar, S., Dollinger, N. and Groll, M. “Understanding operational regimes of closed loop pulsating heat pipe: an experimental study”. International Journal of Applied Thermal Engineering 2003; 23: 707-719.
- [17] Kuźnicka, B. “Erosion–corrosion of heat exchanger tubes”. Engineering Failure Analysis 2009; 16: 2382-2387.
- [18] Lee, S., Kim, J. and Koo, J. “Investigation of pitting corrosion of a copper tube in a heating system”. Engineering Failure Analysis 2010; 17: 1424-1435.
- [19] Lee, W.H., Jung, H.S., Kim, J.H. and Kim, J.S. “Characteristics of pressure oscillation in self-excited oscillating heat pipe based on experimental study”. Proceedings of the 6<sup>th</sup> International Heat Pipe Symposium. Chiang Mai Thailand, 2000: p. 394-403.
- [20] Maezawa, S., Gi, K.Y., Minamisawa, A. and Akachi, H. “Thermal performance of capillary tube thermosyphon”. Proceedings of the 9<sup>th</sup> International Heat Pipe Conference. Albuquerque, New Mexico: 1996. p. 791-795.
- [21] Miyazaki, Y., Polasek, S. and Akachi, H. “Oscillating heat pipe with check valves”. Proceedings of the 6<sup>th</sup> International Heat Pipe Symposium. Chiang Mai Thailand: 2000. p. 389-393.
- [22] Miyazaki, Y. and Akachi, H. “Heat transfer characteristics of looped capillary heat pipe”. Proceedings of the 5<sup>th</sup> International Heat Pipe Symposium. Melbourne, Australia: 1996. p. 378–383.



- [23] Murakami, M. and Arai K. “Statistical Prediction of Long-Term Reliability of Copper-Water Heat Pipe from Accelerated Test Data”. Proceedings of the 6<sup>th</sup> International Heat Pipe Conference. Grenoble, France: 1987. p. 2194-2199.
- [24] Novotna, I., Nassler, J. and Zelko, M. “Contribution to Compatibility of Steel-Water Heat Pipes”. Proceedings of the 3<sup>rd</sup> International Heat Pipe Symposium. Tsukuba, Japan: 1988. p. 319-327.
- [25] Pipatpaiboon, N., Rittidech, S., Sukna, T. and Suddee, P. “Effect of inclination angle working fluid and number of check valves on the characteristics of heat transfer in a closed-looped oscillating heat-pipe with check valves (CLOHP/CV)”. Proceeding of 1<sup>st</sup> International Seminar on Heat Pipe and Heat Recovery Systems. Kuala Lumpur, Malaysia: 2004. p. 83-87.
- [26] Qu, W., Ma, T., Miao, J. and Wang, J. “Effects of radius and heat transfer on the profile of evaporating thin liquid film and meniscus in capillary tubes”. Heat and Mass Transfer 2002; 45: 1879-1887.
- [27] Qu, W. and Ma, T. “Experimental investigation on flow and heat transfer of a pulsating heat pipe”. Proceedings of the 12<sup>th</sup> International Heat Pipe Conference. Moscow Russia: 2002. Unpage.
- [28] Rittidech, S. “Heat transfer characteristics of a closed-end oscillating heat pipe” [Thesis for Doctor of Philosophy in Mechanical Engineering] Chiang Mai: Chiang Mai University, Thailand, 2002.
- [29] Rittidech, S. Heat Pipe Technology. Mahasarakham: Mahasarakham University, Thailand (in thai), Department of Mechanical Engineering; 2011.
- [30] Rittidech, S., Pipatpaiboon, N. and Thongdaeng, S. “Thermal performance of horizontal closed-loop oscillating heat-pipe systems with check valves (HCLOHPs/CVs)”. Journal of Mechanical Science and Technology 2010; 24(2): 545-550.
- [31] Rittidech, S., Pipatpaiboon, N. and Terdtoon, P. “Heat transfer characteristics of a closed loop oscillating heat pipe with check valves”. Applied Energy 2007; 84: 565–577.



- [32] Rittidech, S., Terdtoon, P., Tantakom, P., Murakami, M. and Jompakdee, W. "Effect of inclination angles, evaporator section lengths and working fluid properties on heat transfer characteristics of a closed-end oscillating heat Pipe". Proceedings of the 6<sup>th</sup> International Heat Pipe Symposium. Chiang Mai Thailand: 2000. p. 413-421.
- [33] Rodbumrung, A., Rittidech, S. and Bubphachot, B. "Influence of working fluids, working temperature and evaporator length on internal pressure and damage behavior of the close loop oscillating heat pipe with check valves (CLOHP/CV)". Australian Journal of Basic and Applied Sciences 2011; 5: 1411-1417.
- [34] Tu, S., Zhang, H. and Zhou, W. "Corrosion failures of high temperature heat pipes". Engineering Failure Analysis 1999; 6: 363-370.
- [35] Tong, B.Y., Wong, T.N. and Ooi, K.T. "Closed-loop pulsating heat pipe". Applied Thermal Engineering 2001; 21: 1845-1862.
- [36] Ujiro, T., Satoh, S., Staehle, R.W. and Smyrl, W.H. "Effect of alloying Cu on the corrosion resistance of stainless steels in chloride media". Corrosion Science 2001; 43: 2185-2200.
- [37] Watanabe, O. and Koike, T. "Creep-fatigue life evaluation method for perforated plates at elevated temperature". Journal of Pressure Vessel Technology 2006; 128: 17-24.
- [38] Watanabe, O., Bubphachot, B., Kawasaki, N. and Kasahara, N. "Fatigue strength evaluation of perforated plate at elevated temperature using stress redistribution locus method". Proceedings of the ASME Pressure Vessels & Piping Conference. San Antonio Texas USA: 2007. p. 323-331.
- [39] Watanabe, O., Bubphachot, B. and Matsuda, A. "Stress and strain locus of perforated plate in inelastic deformation strain controlled loading case". Proceedings of the ASME Pressure Vessels & Piping Division. Bellevue Washington USA: 2010. p. 1-9.
- [40] Yang, H., Khandekar, S. and Groll, M. "Operation limit of closed loop pulsating heat pipe". Applied Thermal Engineering 2008; 28: 49-59.
- [41] Zhang, Y. and Faghri, A. "Advances and unsolved issues in pulsating heat pipes". Heat Transfer Engineering 2008; 29(1): 20-44.



- [42] Zhang, Y. and Faghri, A. "Heat transfer in a pulsating heat pipe with open end". *International Journal of Heat and Mass Transfer* 2002; 45: 755-764.
- [43] Zhang, Y., Faghri, A. and Shafii, M.B. "Analysis of liquid–vapor pulsating flow in a u-shaped miniature tube". *International Journal of Heat and Mass Transfer* 2002; 45: 2501-2508.
- [44] Zhao, Y., Qi, Z., Wang, Q., Chen, J. and Shen, J. "Effect of corrosion on performance of fin-and-tube heat exchangers with different fin materials". *Experimental Thermal and Fluid Science* 2011; 37: 98-103.
- [45] "Uniform corrosion". [Online]. n.d. [cited June 2013]; Available from: <http://octane.nmt.edu/WaterQuality/corrosion/uniform.aspx>.
- [46] "InE191 Engineering Material". [Online]. n.d. [cited June 2013]; Available from: <http://www.rmutphysics.com/charud/pdf-learning/2/material/2Corrosion.pdf>.
- [47] "Crevice corrosion". [Online]. n.d. [cited June 2013]; Available from: <http://coxengineering.sharepoint.com/Pages/Crevice.aspx>.
- [48] NASA Kennedy Space Center. "Filiform Corrosion". [Online]. n.d.(a). [cited June 2013]; Available from: <http://corrosion.ksc.nasa.gov/filicor.htm>.
- . "Intergranular Corrosion". [Online]. n.d.(b). [cited June 2013]; Available from: <http://corrosion.ksc.nasa.gov/intercor.htm>.
- . "Stress Corrosion Cracking". [Online]. n.d.(c). [cited June 2013]; Available from: <http://corrosion.ksc.nasa.gov/stresscor.htm>.
- . "Erosion Corrosion". [Online]. n.d.(d). [cited June 2013]; Available from: <http://corrosion.ksc.nasa.gov/eroscor.htm>.
- . "Fretting Corrosion". [Online]. n.d.(e). [cited June 2013]; Available from: <http://corrosion.ksc.nasa.gov/fretcor.htm>
- . "Dealloying". [Online]. n.d.(f). [cited June 2013]; Available from: <http://corrosion.ksc.nasa.gov/dealloying.htm>.
- [49] Siam Kewkamsai. "galvanic-corrosion". [Online]. 23 May 2010. [cited June 2013]; Available from: <http://siamkaewkumsai.blogspot.com/2010/05/galvanic-corrosion.html>.
- [50] "Hydrogen Embrittlement". [Online]. n.d. [cited June 2013]; Available from: <http://www.hydrogen-generators.ws/hydrogen-embrittlement.htm>.





- [51] “Typical S-N Curves”. [Online]. n.d. [cited June 2013]; Available from: <http://www.keytometals.com>.



## **APPENDIX**



**APPENDIX A**  
**Calculation**



### The calculation of inner diameter of oscillating heat pipe

In this study the maximum inner diameter of tube can be calculation as follow:  
 The temperature at the evaporator section was 200 °C and the temperature of dry air at the inlet of condenser section was 25 °C. The operating temperature for calculation =  $\frac{(200+25) \text{ }^{\circ}\text{C}}{2} = 112.5 \text{ }^{\circ}\text{C}$ . From properties of distillate water at temperature was 112.5 °C have  $\sigma = 0.056475 \text{ N/m}$ ,  $\rho = 949.05 \text{ kg/m}^3$

$$\begin{aligned} \text{From formula } D_i &\leq 2 \sqrt{\frac{\sigma}{\rho g}} \\ D_i &\leq 2 \sqrt{\frac{0.056475}{(949.05) \times (9.81)}} \\ D_i &\leq 4.93 \text{ mm} \end{aligned}$$

Therefore, the inner diameter of tube was less than 4.93 mm

### The calculation of volume for filling of working fluid into the CLOHP/CV

The inner diameter of tube in this study was 2.03 mm. The evaporator section was 50 mm. The volume of tube can be calculated as follow:

$$\begin{aligned} V &= \pi r^2 L \\ L &= (80 \times 150) + (\pi \times 10 \times 40) + 58 \text{ (58 mm was} \\ &\text{the total length of loops)} \\ &= 13,314 \text{ mm} \\ V &= \pi \times (2.03/2)^2 \times 13,314 \\ &= 43,091 \text{ mm}^3 \\ &= 43.091 \text{ cm}^3 \end{aligned}$$

The working fluid was filled at 50% = 21.545 cm<sup>3</sup>



### The calculation of the heat flux of the CLOHP/CV

The heat flux can be calculated by equation.

$$q = \frac{Q}{A_c}$$

When  $Q = \dot{m}C_p(T_{c,out} - T_{c,in})$

In this study  $\dot{m} = 0.0057 \text{ kg/s}$

**Example** The CLOHP/CV was made with evaporator length of 50 mm, inner diameter of copper tube was 2.03 mm, distillate water as working fluid and filling ratio 50% of total volume of the CLOHP/CV. The working temperature for testing was 200 °C. The inclination angle was 90° from horizontal axis. The heat flux was calculated as follow:

$C_p$  of ambient air temperature (26.3 °C) was 1.007 kJ/kg.°C,

$T_{c,out}$  was 126.1 °C and  $T_{c,in}$  was 26.3 °C

$$\begin{aligned} Q &= (0.0057) \times 1.007 \times (126.6 - 26.3) \\ &= 0.575 \text{ kW} \end{aligned}$$

The heat flux was calculated by equation

$$\begin{aligned} q &= \frac{0.575}{0.052} = 11.06 \text{ kW/m}^2 \\ &= 11.06 \text{ kW/m}^2 \end{aligned}$$

The heat flux was evaporator length of 50 mm = 11.06 kW/m<sup>2</sup>



### The calculation of the thermal resistance of the CLOHP/CV

The thermal resistance ( $R$ ) would be equal to temperature difference between condenser section and evaporator section to the heat transfer rate.

$$R = \frac{T_e - T_c}{Q}$$

Where  $T_e$  and  $T_c$  are the wall temperatures of the evaporator section and the condenser section, respectively.

**Example** The CLOHP/CV was made with evaporator length of 50 mm, inner diameter of copper tube was 2.03 mm, distillate water as working fluid and filling ratio 50% of total volume of the CLOHP/CV. The working temperature for testing was 200 °C. The inclination angle was 90° from horizontal axis. The heat flux was calculated as follow:

$$T_e \text{ was } 200 \text{ °C, } T_c \text{ was } 145.4 \text{ °C and } Q \text{ was } 0.575 \text{ kW}$$

The thermal resistance was calculated by equation

$$\begin{aligned} R &= \frac{T_e - T_c}{Q} = \frac{200 - 26.3}{0.575} \\ &= 94.96 \text{ °C/kW or } 0.095 \text{ °C/W} \end{aligned}$$

The thermal resistance was evaporator length of 50 mm = 0.095 °C/W

### The calculation of the thermal efficiency of the CLOHP/CV

Thermal efficiency of the CLOHP/CV is a measure from the heat output divided by the heat input in a system.

**Example** Calculate the thermal efficiency ( $\varepsilon$ ) of the CLOHP/CV given by the following equation.

$$\frac{\text{Heat Output}}{\text{Heat Input}} = \frac{Q_{acl}}{Q_{max}} = \frac{C_c(T_{co} - T_{ci})}{C_{min}(T_{hi} - T_{ci})}$$



The best value of the CLOHP/CV for the case of the working temperature of 200 °C, the inner diameters of 2.03 mm, the inclination angle 90°, the evaporator length 50 mm and R123 as working fluid.

The temperature at the evaporator section was 200 °C ( $T_{hi}$ )

The temperature of dry air at the inlet of condenser section was 25 °C ( $T_{ci}$ )

Property of dry air,

$$\rho = 1.1856 \text{ kg/m}^3, C_p = 1,005 \text{ J/kg.K}$$

Determination of the heat capacity ( $C_c$ ) from,

$$C_c = m_a \times C_p$$

$$\therefore m_a = \rho AV$$

$$\begin{aligned} \therefore C_c &= 1.1856 \text{ kg/m}^3 \times 0.01 \text{ m}^2 \times 0.6 \text{ m/s} \times 1,005 \text{ J/kg.K} \\ &= 7.15 \text{ W/K} \end{aligned}$$

$$\therefore C_{\min} = C_c = 7.15 \text{ W/K}$$

$$\begin{aligned} \therefore Q_{\max} &= C_{\min} (T_{hi} - T_{ci}) \\ &= 7.15 \times (200 - 25) \\ &= 1,251.25 \text{ W} \end{aligned}$$

And  $Q_{acl} = C_c (T_{co} - T_{ci})$ , the temperature of dry air at the exit of condenser section was 141.2 °C ( $T_{co}$ )

$$= 7.15(141.2 - 25)$$

$$= 830.83 \text{ W}$$

$$\therefore \varepsilon = \frac{Q_{acl}}{Q_{\max}}$$

$$= \frac{830.83}{1,251.25}$$

$$= 0.66$$

$\therefore$  Thermal efficiency ( $\varepsilon$ ) of the CLOHP/CV was 0.66 or 66%



## **APPENDIX B**

### **Data analysis**





Table B.1 Experimental data of CLOHP/CV (Di 2.03 mm, Distillate water)

$L_e$ (mm)	$T_e$ (°C)	$I_a$ (°)	Condenser			$Q$ (kW)	$q$ (kW/m <sup>2</sup> )	$R$ (°C/W)	$P$ (MPa)
			$T_{out}$ (°C)	$T_{in}$ (°C)	$m$ (kg/s)				
50	100	20	60.4	26.0	0.0057	0.198	3.80	0.174	0.017
		40	61.6	25.9		0.206	3.95	0.168	0.034
		60	63.0	25.9		0.214	4.11	0.161	0.053
		80	63.9	26.1		0.218	4.20	0.158	0.091
		90	64.8	26.1		0.223	4.29	0.154	0.130
	150	20	75.6	26.1	0.0057	0.285	5.48	0.175	0.118
		40	80.9	26.4		0.314	6.04	0.159	0.132
		60	88.7	26.4		0.359	6.90	0.139	0.186
		80	101.0	26.2		0.431	8.29	0.116	0.235
		90	107.6	26.0		0.470	9.03	0.106	0.790
	200	20	106.4	26.1	0.0057	0.463	8.91	0.117	0.126
		40	107.9	26.2		0.471	9.05	0.116	0.225
		60	114.2	26.2		0.507	9.74	0.107	0.322
		80	126.1	26.3		0.572	11.00	0.095	0.377
		90	126.6	26.3		0.575	11.06	0.095	1.780
100	100	20	57.7	26.5	0.0057	0.180	1.73	0.191	0.011
		40	59.8	26.5		0.192	1.84	0.180	0.022
		60	60.0	26.5		0.193	1.86	0.178	0.034
		80	60.0	26.5		0.193	1.86	0.178	0.060
		90	60.6	26.4		0.197	1.89	0.175	0.085
	150	20	80.2	26.4	0.0057	0.310	2.98	0.161	0.077
		40	81.4	26.2		0.318	3.05	0.157	0.086
		60	81.5	26.3		0.318	3.06	0.157	0.122
		80	85.2	26.2		0.340	3.27	0.147	0.154
		90	93.1	26.5		0.384	3.70	0.130	0.517



Table B.1 (Continue)

$L_e$ (mm)	$T_e$ (°C)	$I_a$ (°)	Condenser			$Q$ (kW)	$q$ (kW/m <sup>2</sup> )	$R$ (°C/W)	$P$ (MPa)	
			$T_{out}$ (°C)	$T_{in}$ (°C)	$m$ (kg/s)					
	200	20	98.0	26.7	0.0057	0.411	3.95	0.132	0.082	
		40	104.6	26.7		0.449	4.32	0.121	0.147	
		60	104.8	26.7		0.450	4.32	0.121	0.210	
		80	105.5	26.7		0.454	4.36	0.120	0.246	
		90	110.1	26.8		0.480	4.62	0.113	1.164	
150	100	20	46.9	26.8	0.0057	0.116	0.74	0.488	0.057	
		40	46.1	26.8		0.111	0.71	0.497	0.036	
		60	45.0	26.8		0.105	0.67	0.589	0.034	
		80	45.0	27.0		0.104	0.67	0.608	0.030	
		90	44.9	27.0		0.103	0.66	0.627	0.032	
	150	150	20	67.2	27.1	0.0057	0.231	1.480	0.366	0.027
			40	68.0	27.0		0.236	1.512	0.365	0.034
			60	70.6	27.0		0.251	1.611	0.267	0.035
			80	72.1	27.0		0.260	1.664	0.259	0.050
			90	73.5	26.8		0.269	1.722	0.243	0.056
	200	200	20	83.9	26.8	0.0057	0.329	2.111	0.240	0.015
			40	84.8	26.7		0.335	2.149	0.218	0.017
			60	85.9	26.6		0.342	2.195	0.203	0.022
			80	86.9	26.5		0.348	2.228	0.145	0.042
			90	89.8	26.8		0.363	2.327	0.118	0.051



Table B.2 Experimental data of CLOHP/CV (Di 2.03 mm, Ethanol)

$L_e$ (mm)	$T_e$ (°C)	$I_a$ (°)	Condenser			$Q$ (kW)	$q$ (kW/m <sup>2</sup> )	$R$ (°C/W)	$P$ (MPa)
			$T_{out}$ (°C)	$T_{in}$ (°C)	$m$ (kg/s)				
50	100	20	68.4	26.8	0.0057	0.240	4.62	0.128	0.053
		40	69.7	27.0		0.246	4.73	0.125	0.087
		60	72.3	27.2		0.260	5.01	0.118	0.107
		80	72.8	27.2		0.263	5.06	0.117	0.154
		90	75.6	27.2		0.279	5.37	0.110	0.510
	150	20	88.1	27.2	0.0057	0.351	6.74	0.118	0.223
		40	96.1	27.2		0.397	7.64	0.104	0.258
		60	104.3	27.1		0.445	8.55	0.093	0.311
		80	110.0	26.9		0.479	9.20	0.087	0.438
		90	110.9	26.6		0.486	9.35	0.085	2.040
	200	20	123.4	26.7	0.0057	0.557	10.71	0.089	0.466
		40	124.2	26.7		0.562	10.80	0.088	0.664
		60	130.6	26.8		0.598	11.49	0.083	0.962
		80	139.8	26.8		0.651	12.51	0.076	1.303
		90	143.5	26.7		0.673	12.94	0.074	4.000
100	100	20	63.2	26.6	0.0057	0.211	2.03	0.146	0.035
		40	65.5	26.6		0.224	2.15	0.138	0.057
		60	65.8	26.6		0.226	2.18	0.136	0.070
		80	66.0	26.6		0.227	2.18	0.136	0.101
		90	66.7	26.8		0.230	2.21	0.134	0.334
	150	20	89.1	26.8	0.0057	0.359	3.451	0.116	0.146
		40	91.7	26.8		0.374	3.597	0.111	0.169
		60	92.9	26.6		0.382	3.671	0.109	0.203
		80	93.4	26.8		0.384	3.695	0.108	0.286
		90	99.0	26.8		0.416	3.998	0.100	1.334



Table B.2 (Continue)

$L_e$ (mm)	$T_e$ (°C)	$I_a$ (°)	Condenser			$Q$ (kW)	$q$ (kW/m <sup>2</sup> )	$R$ (°C/W)	$P$ (MPa)	
			$T_{out}$ (°C)	$T_{in}$ (°C)	$m$ (kg/s)					
	200	20	94.0	27.0	0.0057	0.386	3.708	0.129	0.305	
		40	98.6	26.9		0.413	3.971	0.120	0.434	
		60	100.5	26.9		0.424	4.075	0.117	0.629	
		80	101.5	26.9		0.430	4.133	0.115	0.852	
		90	102.9	26.9		0.438	4.207	0.113	2.616	
150	100	20	56.9	26.7	0.0057	0.174	1.11	0.215	0.007	
		40	57.2	26.7		0.176	1.13	0.205	0.024	
		60	58.4	26.6		0.183	1.17	0.191	0.045	
		80	59.2	26.6		0.188	1.21	0.139	0.091	
		90	59.9	26.6		0.192	1.23	0.135	0.101	
	150	150	20	64.9	26.7	0.0057	0.220	1.410	0.275	0.161
			40	66.1	26.9		0.226	1.450	0.251	0.166
			60	66.7	27.0		0.229	1.465	0.222	0.177
			80	70.6	27.0		0.251	1.610	0.192	0.185
			90	75.0	26.9		0.277	1.774	0.163	0.269
	200	200	20	79.1	26.9	0.0057	0.301	1.928	0.083	0.160
			40	80.8	27.0		0.310	1.989	0.082	0.274
			60	83.4	27.0		0.325	2.082	0.082	0.284
			80	86.9	27.0		0.345	2.211	0.078	0.333
			90	87.5	26.9		0.349	2.236	0.077	0.385



Table B.3: Experimental data of CLOHP/CV (Di 2.03 mm, R123)

$L_e$ (mm)	$T_e$ (°C)	$I_a$ (°)	Condenser			$Q$ (kW)	$q$ (kW/m <sup>2</sup> )	$R$ (°C/W)	$P$ (MPa)
			$T_{out}$ (°C)	$T_{in}$ (°C)	$m$ (kg/s)				
50	100	20	75.9	26.6	0.0057	0.284	5.46	0.102	0.320
		40	76.7	26.5		0.289	5.57	0.100	0.521
		60	78.9	26.5		0.302	5.80	0.096	0.639
		80	80.7	26.7		0.311	5.97	0.093	0.923
		90	82.3	26.6		0.321	6.17	0.090	1.020
	150	20	112.0	26.6	0.0057	0.492	9.47	0.079	3.100
		40	114.9	26.7		0.508	9.77	0.077	1.338
		60	116.8	26.6		0.520	10.01	0.075	1.548
		80	120.2	26.5		0.540	10.38	0.072	1.866
		90	122.1	26.5		0.551	10.60	0.071	2.628
	200	20	163.1	26.5	0.0057	0.787	15.13	0.051	3.466
		40	163.2	26.5		0.788	15.15	0.051	3.664
		60	164.2	26.6		0.793	15.24	0.050	3.962
		80	167.4	26.7		0.811	15.59	0.050	4.303
		90	171.0	26.8		0.831	15.97	0.048	7.530
100	100	20	62.4	26.7	0.0057	0.206	1.98	0.141	0.209
		40	71.0	26.6		0.256	2.46	0.113	0.341
		60	77.8	26.6		0.295	2.84	0.098	0.418
		80	78.3	26.6		0.298	2.86	0.097	0.604
		90	80.4	26.6		0.310	2.98	0.093	0.667
	150	20	98.4	26.6	0.0057	0.414	3.980	0.094	0.875
		40	98.7	26.5		0.416	3.996	0.094	1.012
		60	99.6	26.5		0.421	4.046	0.093	1.220
		80	112.8	26.7		0.496	4.772	0.079	1.719
		90	113.5	26.6		0.501	4.819	0.078	2.027



Table B.3 (Continue)

$L_e$ (mm)	$T_e$ (°C)	$I_a$ (°)	Condenser			$Q$ (kW)	$q$ (kW/m <sup>2</sup> )	$R$ (°C/W)	$P$ (MPa)	
			$T_{out}$ (°C)	$T_{in}$ (°C)	$m$ (kg/s)					
200	200	20	146.4	26.8	0.0057	0.689	6.624	0.058	2.267	
		40	153.0	26.8		0.727	6.990	0.055	2.396	
		60	155.7	26.8		0.743	7.146	0.054	2.591	
		80	167.9	26.8		0.813	7.820	0.049	2.814	
		90	168.7	26.8		0.818	7.863	0.049	4.925	
150	100	20	52.3	26.8	0.0057	0.147	0.94	0.177	0.341	
		40	61.0	26.8		0.197	1.26	0.113	0.365	
		60	64.1	26.8		0.215	1.38	0.086	0.499	
		80	66.1	26.7		0.227	1.46	0.078	0.503	
		90	71.1	26.7		0.256	1.64	0.065	0.556	
	150	150	20	84.6	26.8	0.0057	0.333	2.135	0.103	0.458
			40	86.3	26.8		0.343	2.201	0.083	0.470
			60	91.8	26.7		0.375	2.406	0.077	0.872
			80	94.0	26.8		0.387	2.480	0.076	1.203
			90	97.1	26.8		0.405	2.596	0.053	1.306
	200	200	20	121.5	26.8	0.0057	0.546	3.499	0.063	1.038
			40	123.2	26.9		0.555	3.560	0.058	1.040
			60	125.7	27.1		0.568	3.643	0.058	1.061
			80	128.2	27.2		0.582	3.731	0.052	1.121
			90	134.6	27.4		0.618	3.960	0.039	1.237



Table B.4: Experimental data of CLOHP/CV ( $D_i$  1.77 mm, Distillate water)

$L_e$ (mm)	$T_e$ (°C)	$I_a$ (°)	Condenser			$Q$ (kW)	$q$ (kW/m <sup>2</sup> )	$R$ (°C/W)	$P$ (MPa)
			$T_{out}$ (°C)	$T_{in}$ (°C)	$m$ (kg/s)				
50	100	20	46.6	27.9	0.0057	0.108	2.391	0.339	0.045
		40	47.7	27.6		0.116	2.569	0.316	0.051
		60	49.3	27.8		0.124	2.746	0.302	0.057
		80	49.5	27.3		0.128	2.468	0.293	0.060
		90	50.2	27.1		0.133	2.957	0.289	0.079
	150	20	52.6	28.1	0.0057	0.141	3.133	0.278	0.052
		40	57.4	27.9		0.170	3.769	0.227	0.060
		60	64.9	27.8		0.214	4.765	0.198	0.069
		80	77.2	27.4		0.287	6.380	0.170	0.089
		90	83.9	27.5		0.325	7.233	0.146	0.094
	200	20	66.9	26.8	0.0057	0.231	5.128	0.158	0.061
		40	67.8	26.5		0.238	5.291	0.153	0.065
		60	73.8	26.3		0.274	6.092	0.136	0.072
		80	84.9	25.9		0.340	7.548	0.118	0.093
		90	85.1	25.8		0.342	7.611	0.108	0.107
100	100	20	42.1	27.7	0.0057	0.0830	0.9217	0.78	0.016
		40	43.7	27.4		0.0938	1.0427	0.68	0.023
		60	43.7	27.2		0.0950	1.0552	0.65	0.026
		80	43.8	27.3		0.0952	1.0581	0.58	0.027
		90	44.7	27.6		0.0985	1.0943	0.57	0.027
	150	20	54.4	27.8	0.0057	0.1533	1.7037	0.55	0.021
		40	55.1	27.3		0.1603	1.7807	0.54	0.036
		60	54.8	26.9		0.1605	1.7830	0.41	0.037
		80	59.8	28.3		0.1818	2.0201	0.35	0.038
		90	67.1	28.2		0.2243	2.4923	0.32	0.048



Table B.4 (Continue)

$L_e$ (mm)	$T_e$ (°C)	$I_a$ (°)	Condenser			$Q$ (kW)	$q$ (kW/m <sup>2</sup> )	$R$ (°C/W)	$P$ (MPa)	
			$T_{out}$ (°C)	$T_{in}$ (°C)	$m$ (kg/s)					
	200	20	55.2	27.2	0.0057	0.1613	1.7923	0.45	0.047	
		40	61.6	27.2		0.1980	2.2004	0.41	0.050	
		60	61.8	27.3		0.1987	2.2074	0.35	0.052	
		80	62.3	27.2		0.2023	2.2474	0.25	0.055	
		90	66.8	27.2		0.2280	2.5338	0.19	0.061	
150	100	20	29.6	25.0	0.0057	0.0264	0.195	2.07	0.017	
		40	29.6	24.9		0.0272	0.201	2.04	0.021	
		60	29.7	24.9		0.0277	0.205	1.97	0.023	
		80	31.0	24.9		0.0352	0.261	1.53	0.024	
		90	32.0	24.9		0.0408	0.303	1.26	0.025	
	150	150	20	45.9	25.1	0.0057	0.1198	0.887	1.10	0.018
			40	46.9	25.1		0.1255	0.930	0.86	0.022
			60	50.1	25.1		0.1439	1.066	0.77	0.024
			80	51.4	24.9		0.1529	1.133	0.74	0.026
			90	53.3	25.2		0.1620	1.200	0.72	0.032
	200	200	20	50.3	25.1	0.0057	0.1454	1.077	0.83	0.022
			40	51.3	25.1		0.1509	1.118	0.71	0.025
			60	52.8	25.1		0.1595	1.182	0.65	0.029
			80	53.9	25.2		0.1655	1.226	0.50	0.035
			90	56.6	24.9		0.1829	1.354	0.41	0.039





Table B.5 Experimental data of CLOHP/CV ( $D_i$  1.77 mm, Ethanol)

$L_e$ (mm)	$T_e$ (°C)	$I_a$ (°)	Condenser			$Q$ (kW)	$q$ (kW/m <sup>2</sup> )	$R$ (°C/W)	$P$ (MPa)
			$T_{out}$ (°C)	$T_{in}$ (°C)	$m$ (kg/s)				
50	100	20	54.5	27.9	0.0057	0.153	3.409	0.293	0.080
		40	55.8	28.2		0.159	3.535	0.268	0.105
		60	58.4	28.4		0.173	3.852	0.255	0.131
		80	58.5	28.0		0.176	3.908	0.235	0.183
		90	60.7	27.4		0.192	4.269	0.219	0.195
	150	20	66.1	25.1	0.0057	0.236	5.251	0.185	0.249
		40	74.1	25.0		0.283	6.294	0.164	0.251
		60	82.7	25.4		0.330	7.340	0.157	0.257
		80	88.4	25.2		0.364	8.096	0.150	0.291
		90	90.0	25.4		0.372	8.269	0.137	0.380
	200	20	89.1	25.9	0.0057	0.364	8.085	0.156	0.267
		40	90.1	26.2		0.368	8.181	0.151	0.371
		60	96.3	26.2		0.404	8.984	0.135	0.437
		80	105.4	26.1		0.457	10.162	0.114	0.541
		90	109.3	26.0		0.480	10.657	0.101	0.554
100	100	20	46.5	26.5	0.0057	0.1151	1.2787	0.31	0.073
		40	48.6	26.5		0.1274	1.4150	0.30	0.083
		60	49.1	26.5		0.1300	1.4441	0.27	0.090
		80	49.1	26.5		0.1304	1.4494	0.20	0.100
		90	49.7	26.5		0.1337	1.4859	0.19	0.104
	150	20	66.3	26.4	0.0057	0.2298	2.5538	0.26	0.088
		40	68.8	26.4		0.2444	2.7151	0.23	0.104
		60	70.0	26.3		0.2517	2.7971	0.20	0.106
		80	70.5	26.4		0.2541	2.8232	0.19	0.123
		90	75.6	26.3		0.2843	3.1588	0.16	0.135



Table B.5 (Continue)

$L_e$ (mm)	$T_e$ (°C)	$I_a$ (°)	Condenser			$Q$ (kW)	$q$ (kW/m <sup>2</sup> )	$R$ (°C/W)	$P$ (MPa)	
			$T_{out}$ (°C)	$T_{in}$ (°C)	$m$ (kg/s)					
	200	20	56.9	26.3	0.0057	0.1763	1.9592	0.14	0.121	
		40	61.5	26.4		0.2025	2.2498	0.13	0.122	
		60	63.2	26.3		0.2129	2.3659	0.12	0.179	
		80	64.3	26.3		0.2187	2.4300	0.12	0.191	
		90	65.5	26.3		0.2261	2.5118	0.12	0.251	
150	100	20	44.8	25.3	0.0057	0.1125	0.834	0.46	0.037	
		40	45.2	25.4		0.1143	0.847	0.44	0.041	
		60	46.9	25.5		0.1232	0.913	0.37	0.046	
		80	47.8	25.4		0.1292	0.957	0.34	0.048	
		90	48.6	25.4		0.1336	0.989	0.32	0.049	
	150	150	20	49.0	25.6	0.0057	0.1346	0.997	0.71	0.039
			40	50.4	25.8		0.1415	1.048	0.31	0.042
			60	50.8	25.8		0.1440	1.067	0.29	0.049
			80	55.2	25.5		0.1710	1.267	0.28	0.056
			90	60.2	25.4		0.2004	1.485	0.27	0.077
	200	200	20	50.8	24.5	0.0057	0.1514	1.121	0.38	0.055
			40	52.9	24.9		0.1615	1.196	0.28	0.062
			60	56.1	25.1		0.1786	1.323	0.26	0.069
			80	58.9	23.8		0.2024	1.499	0.25	0.073
			90	58.9	23.0		0.2068	1.532	0.23	0.080



Table B.6 Experimental data of CLOHP/CV ( $D_i$  1.77 mm, R123)

$L_e$ (mm)	$T_e$ (°C)	$I_a$ (°)	Condenser			$Q$ (kW)	$q$ (kW/m <sup>2</sup> )	$R$ (°C/W)	$P$ (MPa)
			$T_{out}$ (°C)	$T_{in}$ (°C)	$m$ (kg/s)				
50	100	20	55.6	28.5	0.0057	0.156	3.459	0.274	0.458
		40	56.3	28.4		0.161	3.587	0.259	0.525
		60	58.8	28.6		0.174	3.859	0.243	0.654
		80	59.8	28.0		0.183	4.059	0.230	0.690
		90	62.3	28.8		0.193	4.285	0.214	0.751
	150	20	81.8	26.3	0.0057	0.320	7.116	0.171	0.613
		40	85.5	27.2		0.336	7.463	0.163	0.625
		60	88.3	27.9		0.348	7.735	0.150	0.997
		80	92.5	28.6		0.368	8.170	0.127	1.312
		90	94.4	28.6		0.379	8.418	0.123	1.407
	200	20	97.2	27.3	0.0057	0.403	8.959	0.135	1.227
		40	97.3	27.2		0.404	8.975	0.126	1.264
		60	98.2	27.2		0.409	9.086	0.119	1.286
		80	101.5	27.4		0.427	9.486	0.104	1.389
		90	105.0	27.4		0.447	9.929	0.091	1.496
100	100	20	52.0	26.5	0.0057	0.1467	1.6297	0.18	0.149
		40	52.0	26.5		0.1470	1.6332	0.15	0.193
		60	53.0	26.1		0.1551	1.7232	0.11	0.197
		80	56.3	25.9		0.1753	1.9479	0.10	0.237
		90	57.9	25.9		0.1844	2.0485	0.09	0.245
	150	20	66.0	27.0	0.0057	0.2246	2.4951	0.15	0.197
		40	66.2	27.0		0.2261	2.5124	0.13	0.197
		60	67.2	27.1		0.2311	2.5681	0.12	0.204
		80	80.1	27.4		0.3035	3.3723	0.10	0.218
		90	80.8	27.3		0.3082	3.4240	0.07	0.220



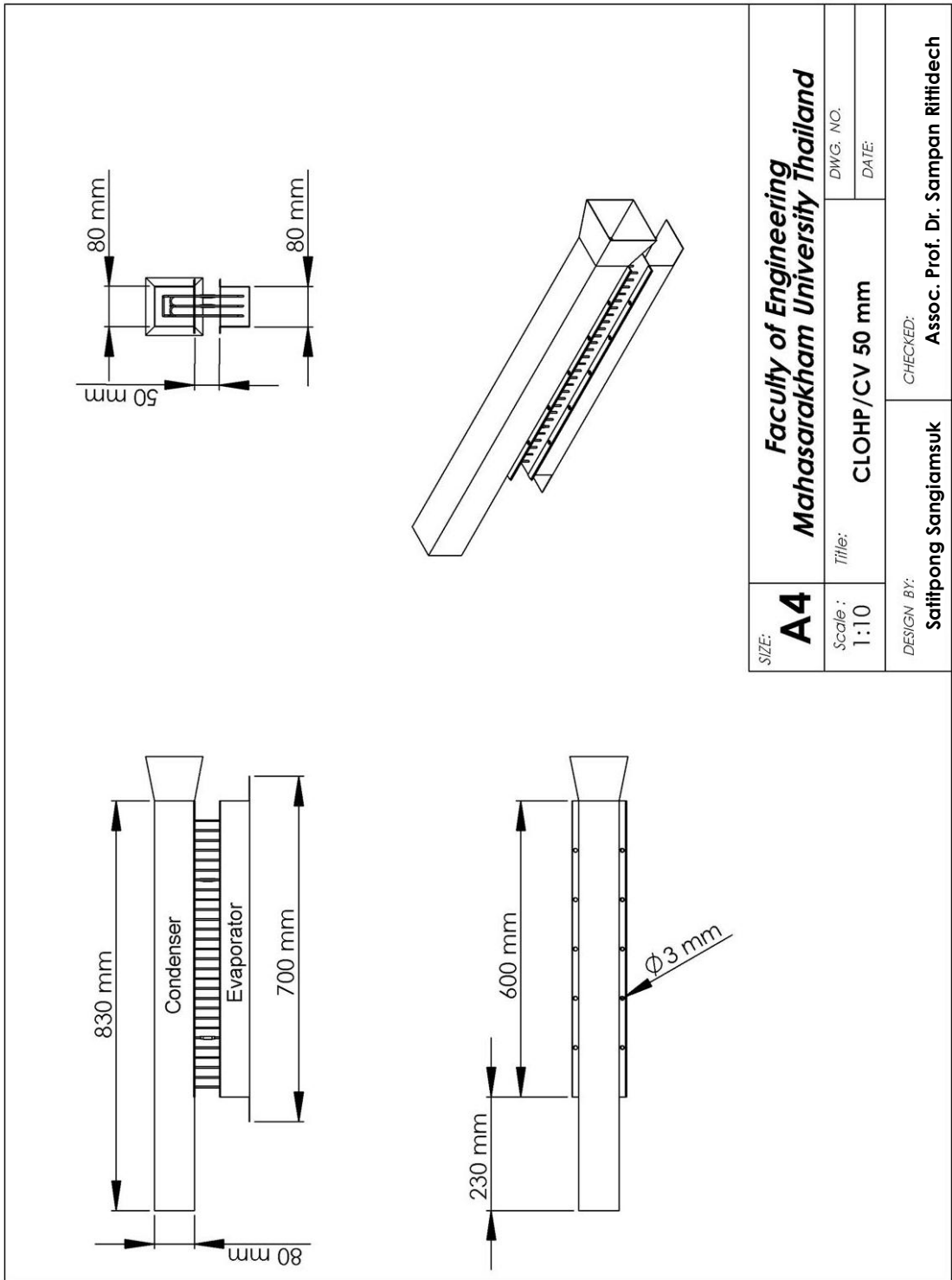
Table B.6 (Continue)

$L_e$ (mm)	$T_e$ (°C)	$I_a$ (°)	Condenser			$Q$ (kW)	$q$ (kW/m <sup>2</sup> )	$R$ (°C/W)	$P$ (MPa)	
			$T_{out}$ (°C)	$T_{in}$ (°C)	$m$ (kg/s)					
	200	20	75.1	27.1	0.0057	0.2766	3.0732	0.11	0.283	
		40	81.4	27.1		0.3131	3.4788	0.11	0.318	
		60	84.1	27.1		0.3287	3.6522	0.09	0.322	
		80	95.7	27.0		0.3959	4.3988	0.09	0.369	
		90	96.2	26.8		0.4001	4.4461	0.06	0.372	
150	100	20	46.9	26.5	0.0057	0.1173	0.869	0.31	0.069	
		40	48.6	26.5		0.1274	0.944	0.23	0.075	
		60	49.0	26.1		0.1321	0.978	0.17	0.078	
		80	49.4	25.9		0.1356	1.005	0.14	0.102	
		90	57.4	25.9		0.1817	1.346	0.13	0.106	
	150	150	20	61.7	25.2	0.0057	0.2101	1.556	0.21	0.091
			40	63.7	25.1		0.2223	1.647	0.18	0.103
			60	70.4	25.2		0.2604	1.929	0.16	0.114
			80	72.3	25.2		0.2712	2.009	0.13	0.126
			90	76.1	25.3		0.2926	2.167	0.10	0.181
	200	200	20	67.1	25.1	0.0057	0.2421	1.794	0.19	0.139
			40	68.9	25.2		0.2521	1.867	0.14	0.147
			60	71.4	25.1		0.2670	1.977	0.13	0.154
			80	73.9	25.2		0.2805	2.078	0.12	0.175
			90	81.2	25.1		0.3231	2.393	0.09	0.257

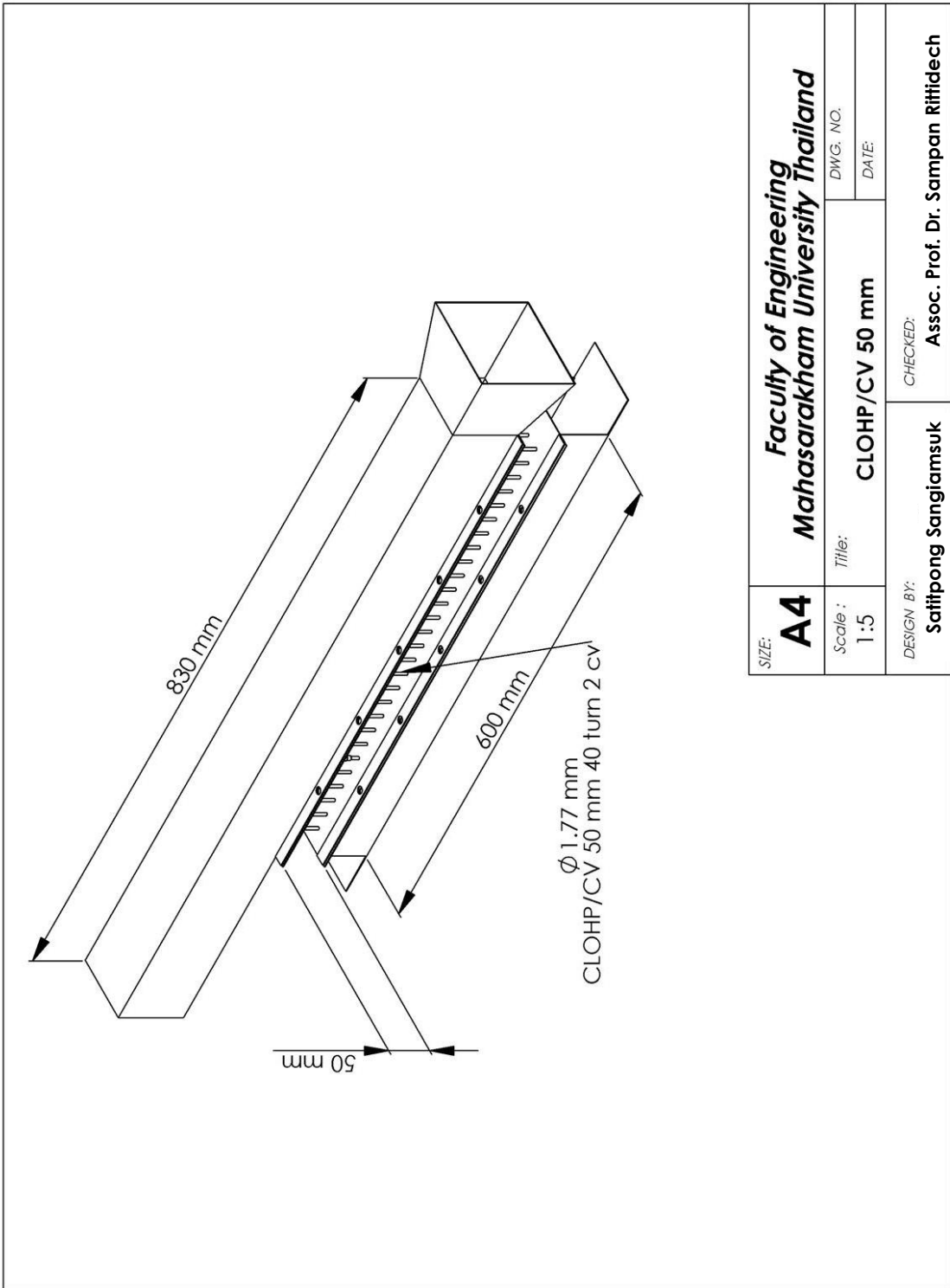


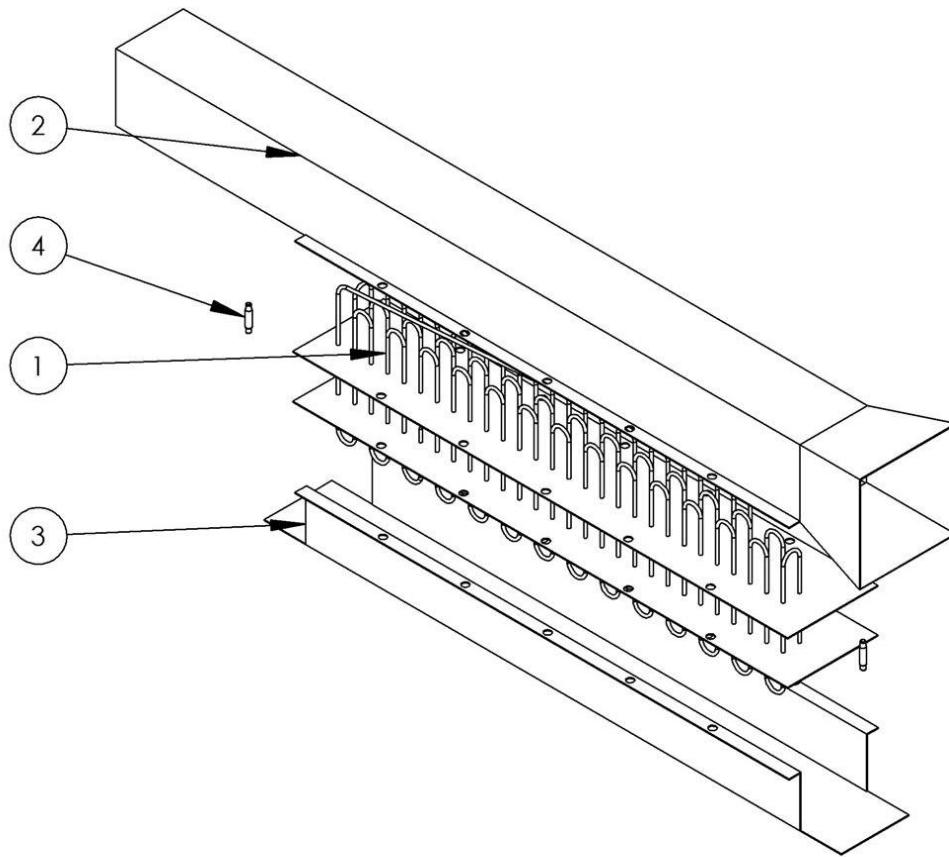
**Appendix C**  
**Experimental Set**





SIZE: <b>A4</b>	<b>Faculty of Engineering          Maharakham University Thailand</b>	
	DWG. NO.	DATE:
Scale : <b>1:10</b>	Title: <b>CLOHP/CV 50 mm</b>	
DESIGN BY: <b>Satitpong Sangiamsuk</b>	CHECKED: <b>Assoc. Prof. Dr. Sampan Ritthidech</b>	

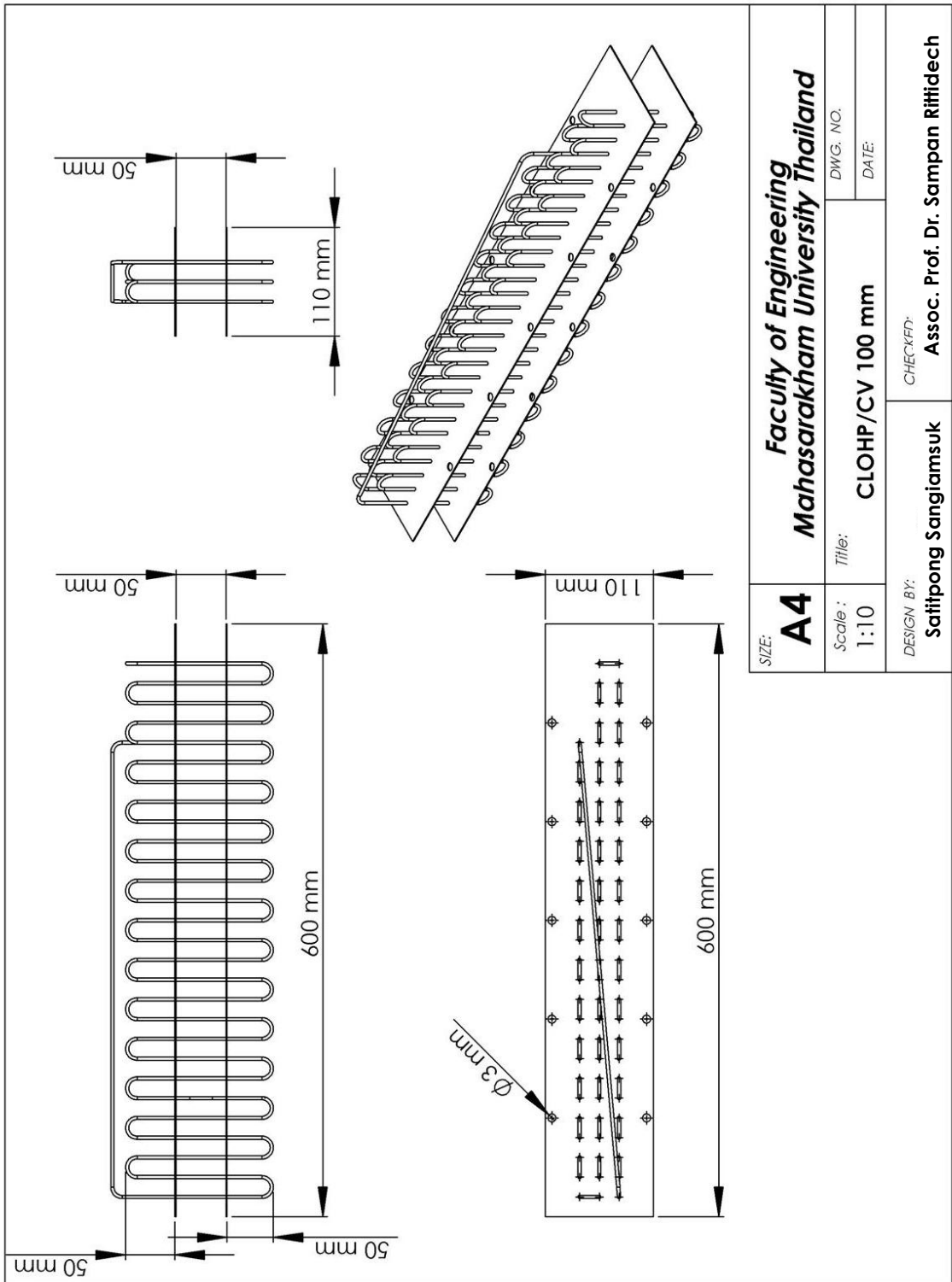


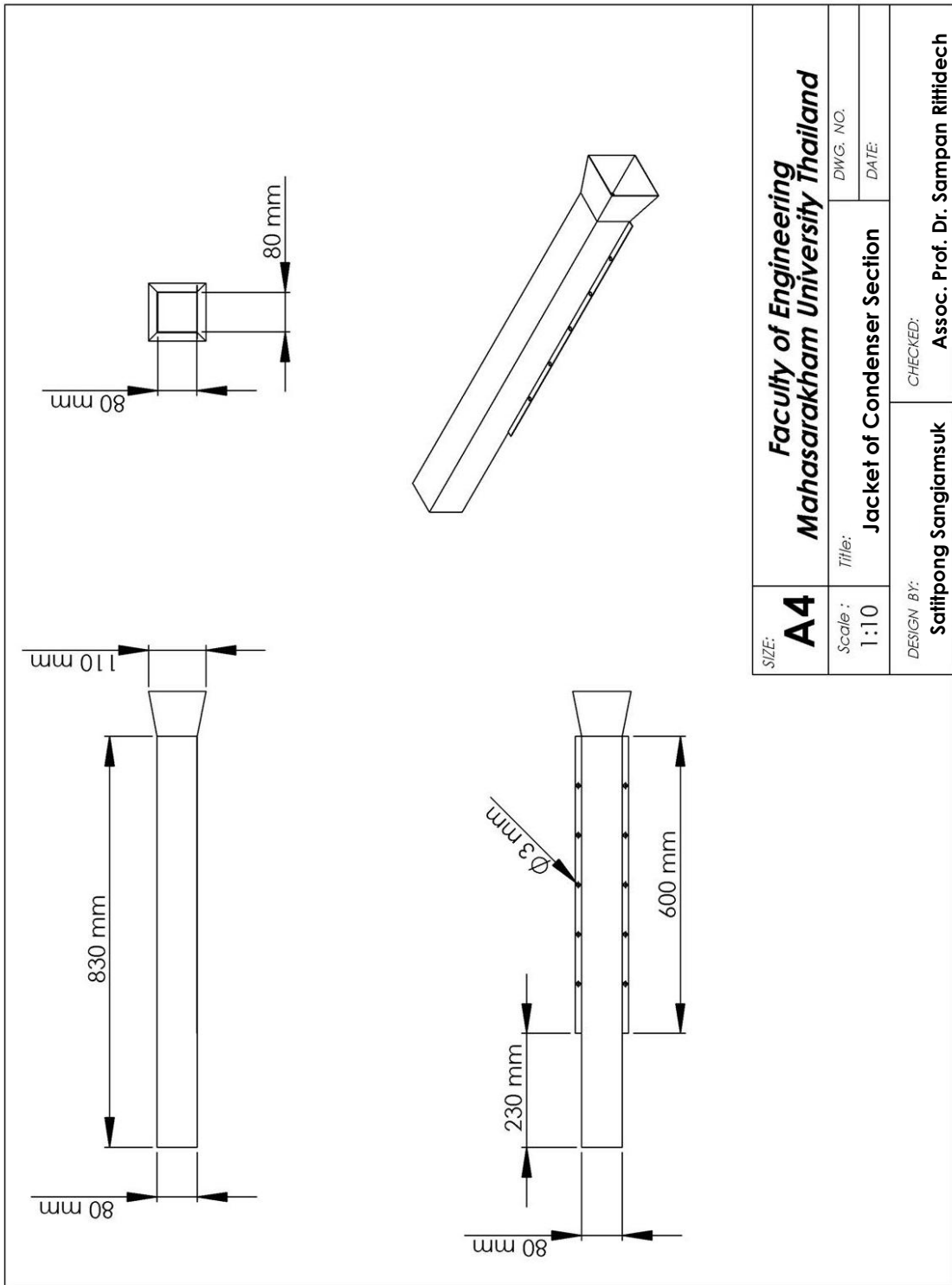


NO	PART	QTY
1	CLOHP/CV 50 mm, 40 turn, 2 CV	1
2	Jacket of Condenser Section	1
3	Jacket of Evaporator Section	1
4	Check valves	2
SIZE: <b>A4</b>		Faculty of Engineering Mahasarakham University Thailand
Scale: 1:5	Title: CLOHP/CV 50 mm	DWR. NO. DATE:
DESIGN BY: Satitpong Sangiamsuk	CHECKED: Assoc. Prof. Dr. Sampan rittidech	

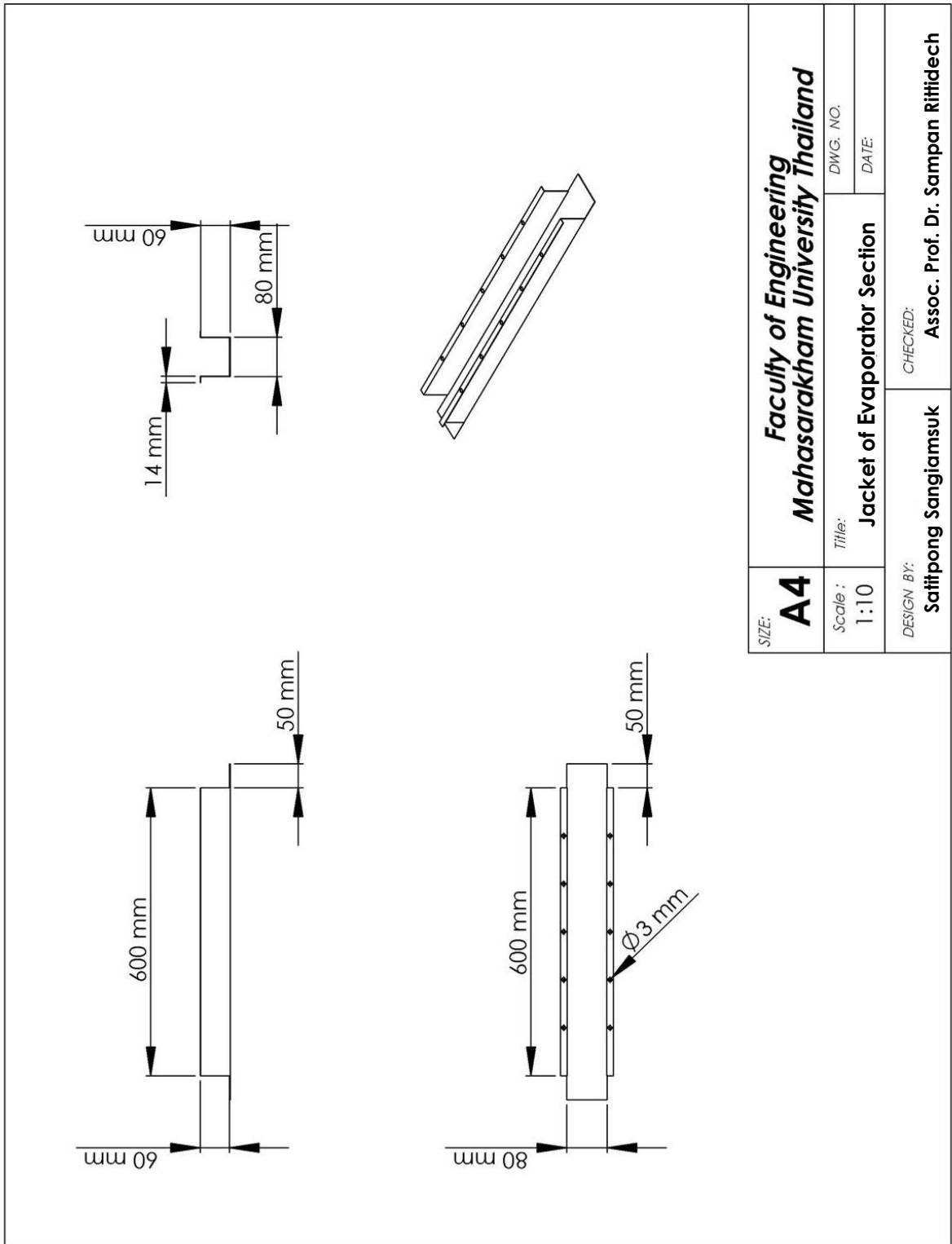




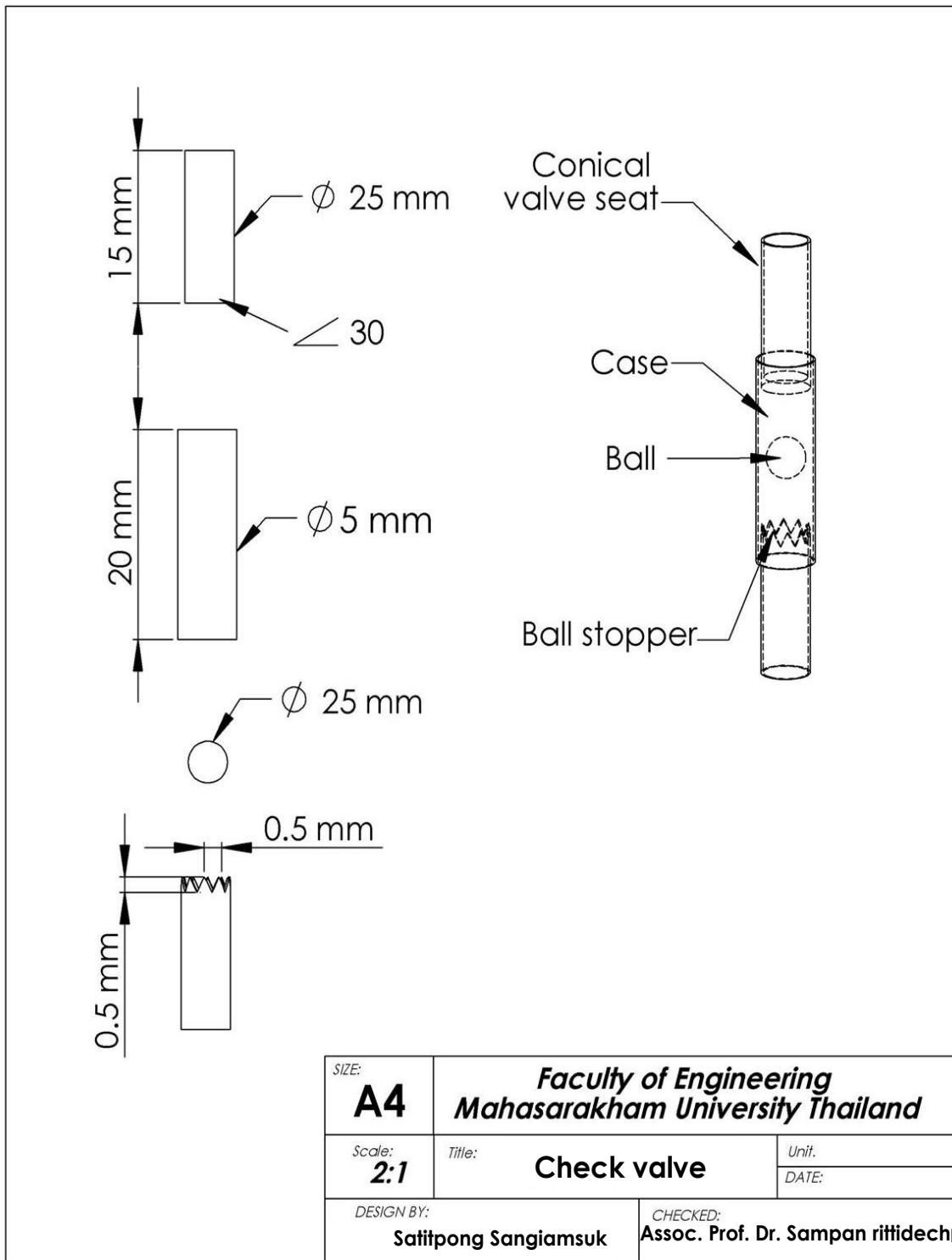


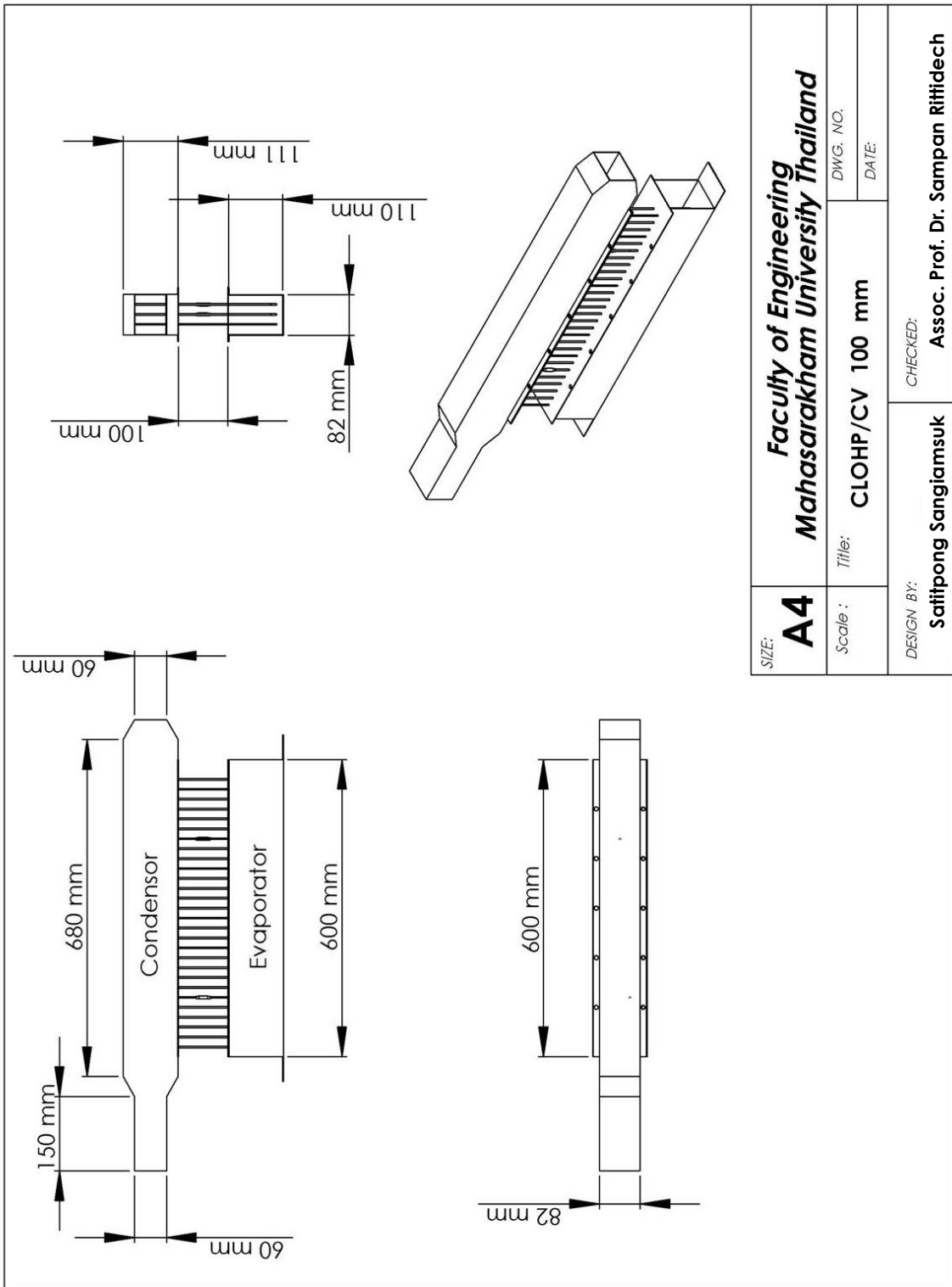


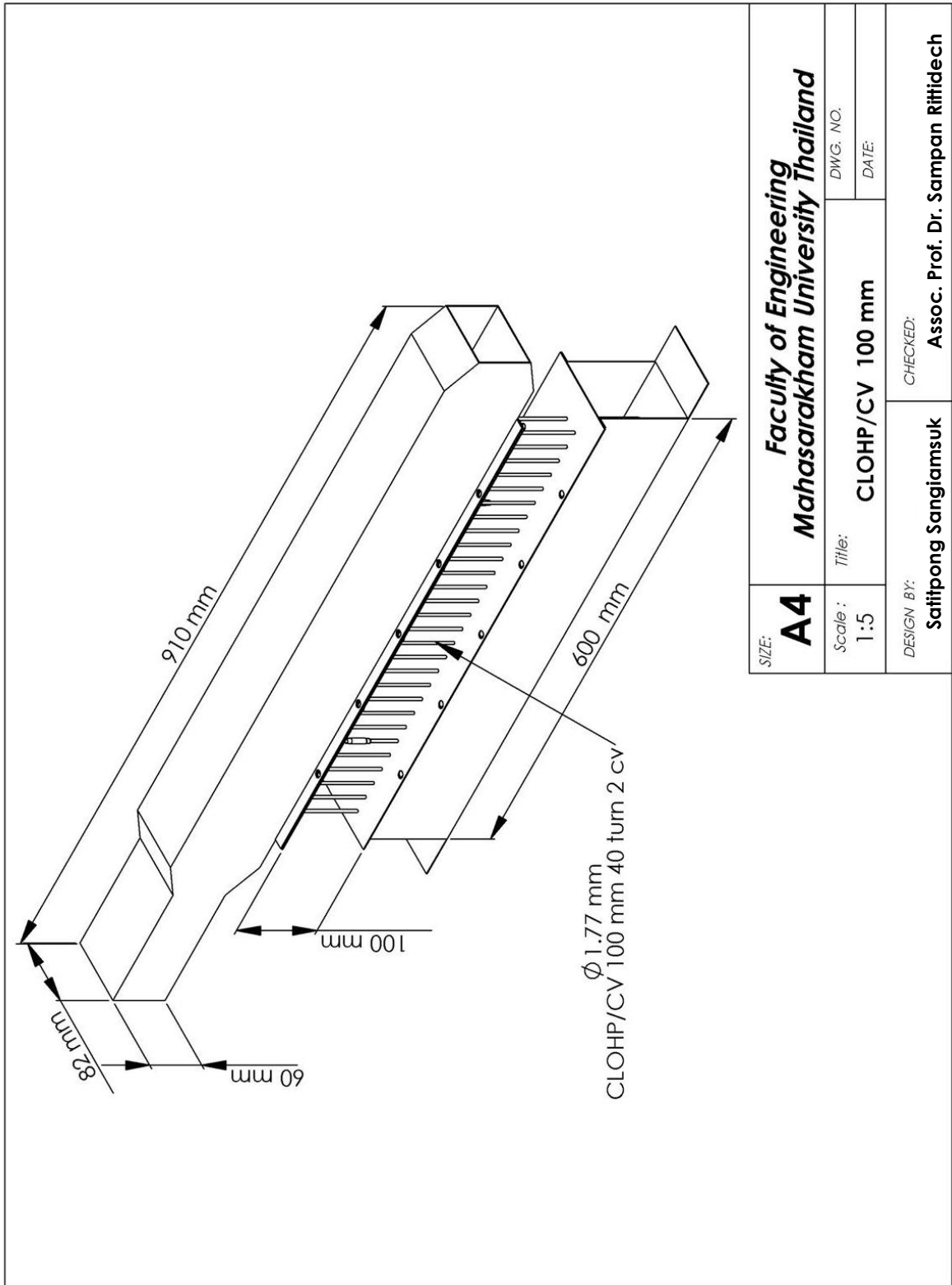
SIZE: <b>A4</b>	Faculty of Engineering Maharakham University Thailand		DWG. NO.:
	Scale : 1:10	Title: <b>Jacket of Condenser Section</b>	DATE:
DESIGN BY: <b>Sattipong Sangiamsuk</b>	CHECKED: <b>Assoc. Prof. Dr. Sampan Rittidech</b>		



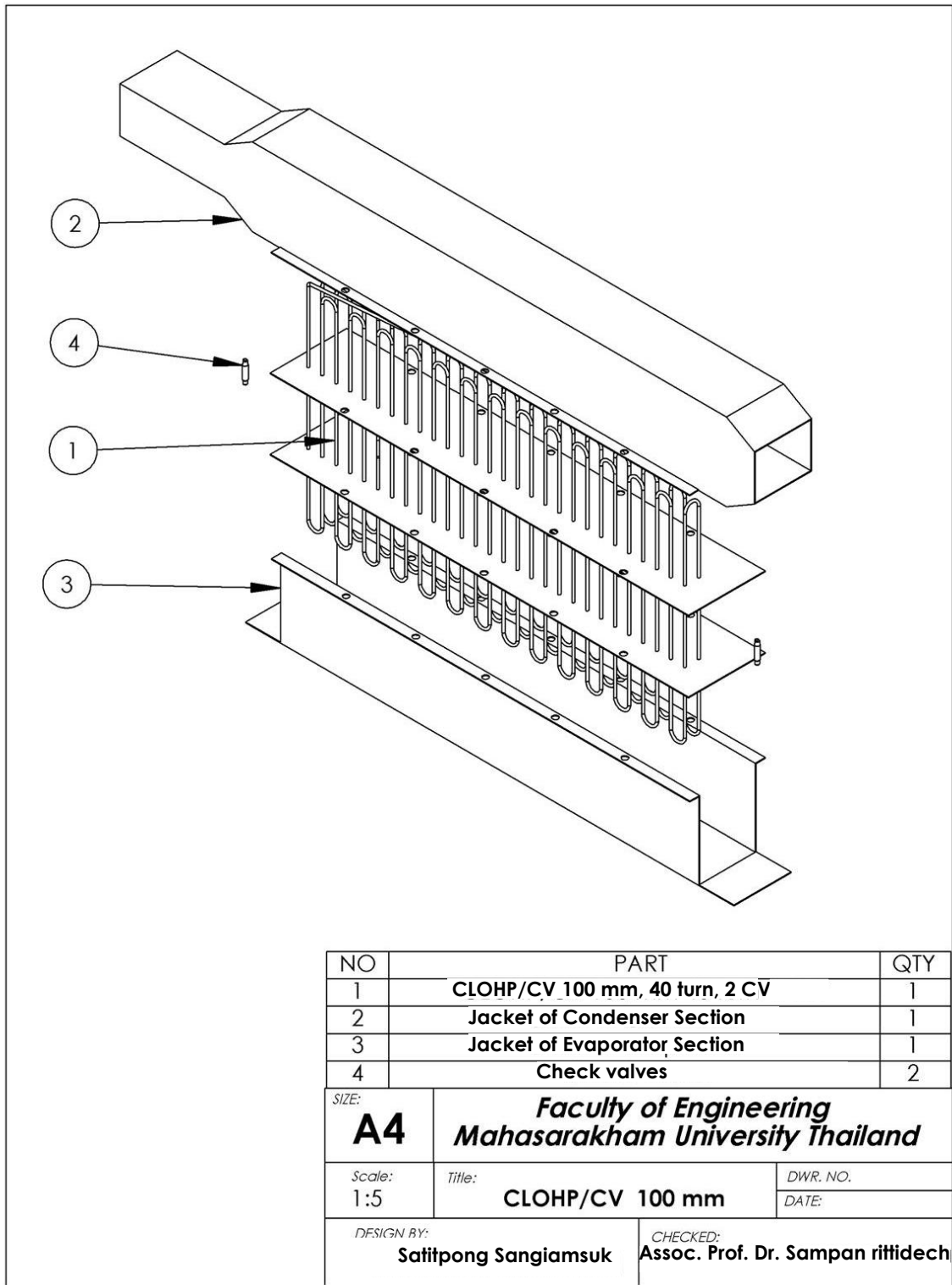
SIZE: <b>A4</b>	<b>Faculty of Engineering</b> <b>Maharakham University Thailand</b>	
	DWG. NO.	DATE:
Scale : 1:10	Title: <b>Jacket of Evaporator Section</b>	
DESIGN BY: <b>Sattipong Sangiamsuk</b>	CHECKED: <b>Assoc. Prof. Dr. Sampan Riffidech</b>	







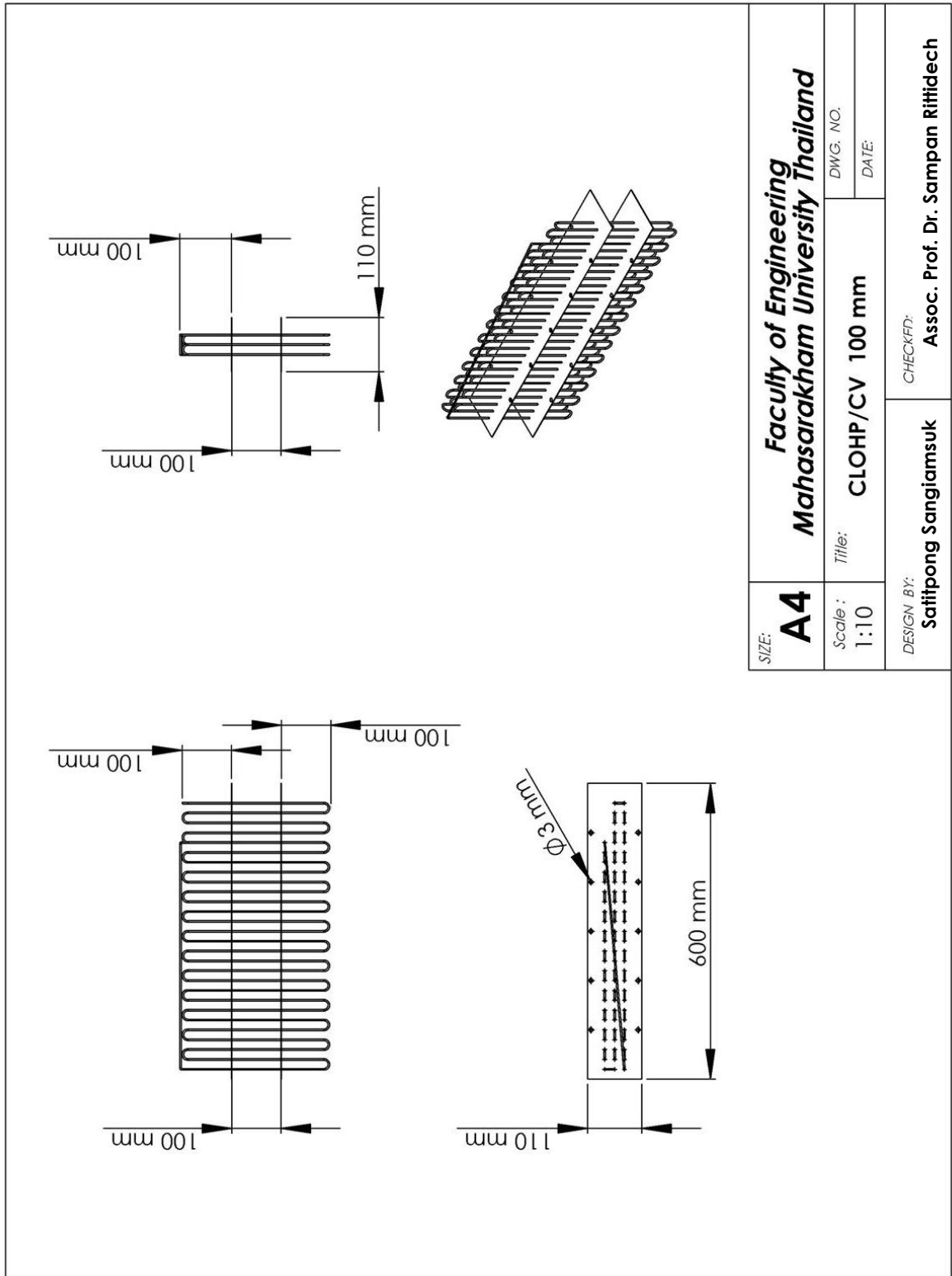
SIZE: <b>A4</b>	Faculty of Engineering Maharakham University Thailand		DWG. NO.
	Scale : 1:5	Title: CLOHP/CV 100 mm	DATE:
DESIGN BY: Sattipong Sangiamsuk	CHECKED: Assoc. Prof. Dr. Sampan Ritthidech		



NO	PART	QTY
1	CLOHP/CV 100 mm, 40 turn, 2 CV	1
2	Jacket of Condenser Section	1
3	Jacket of Evaporator Section	1
4	Check valves	2

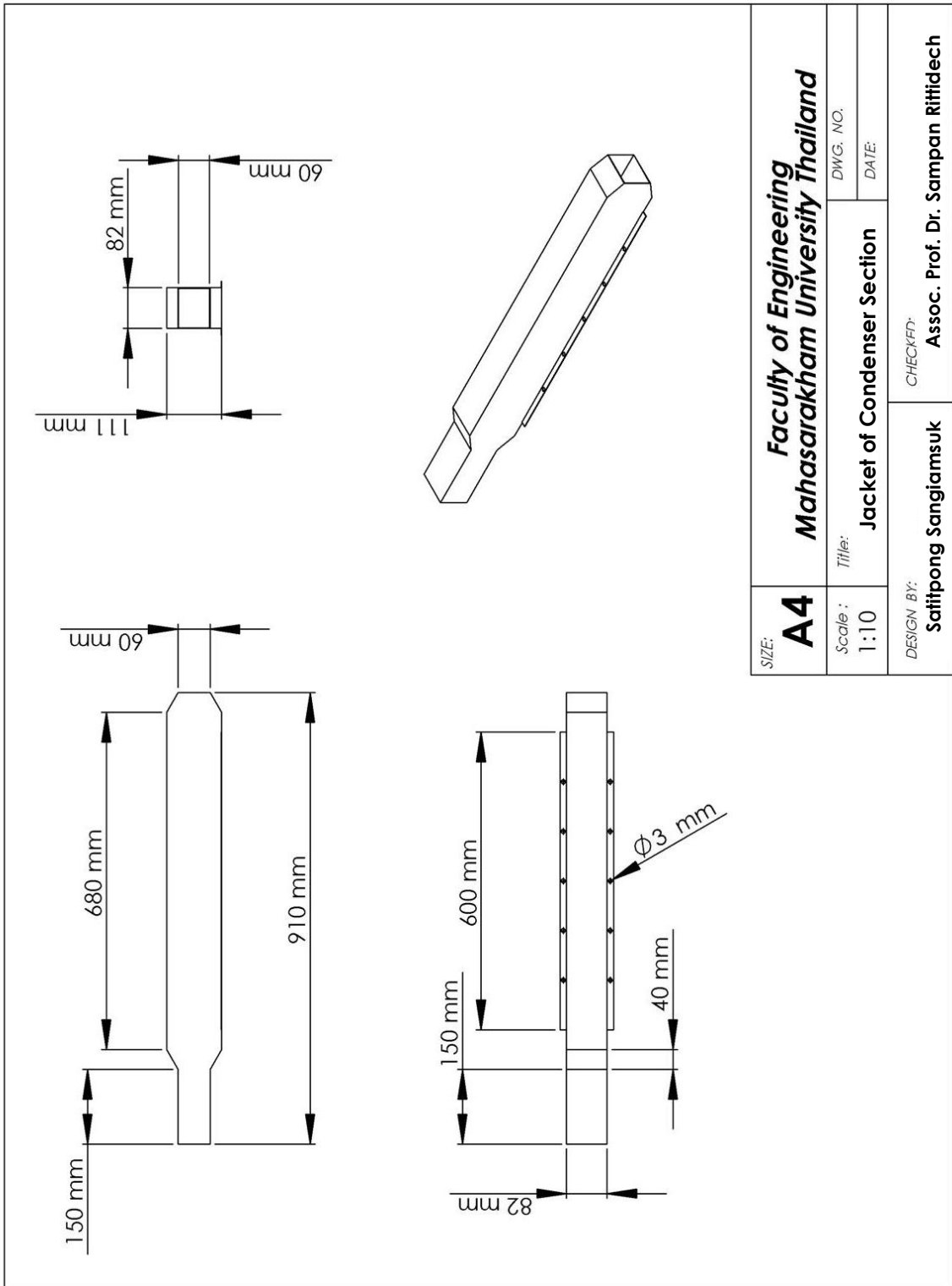
  

SIZE: <b>A4</b>		<b>Faculty of Engineering Mahasarakham University Thailand</b>	
Scale: 1:5	Title: CLOHP/CV 100 mm	DWR. NO.	
		DATE:	
DESIGN BY: Satitpong Sangiamsuk		CHECKED: Assoc. Prof. Dr. Sampan rittidech	

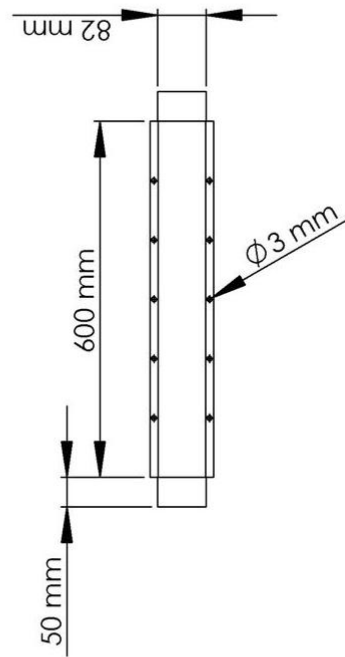
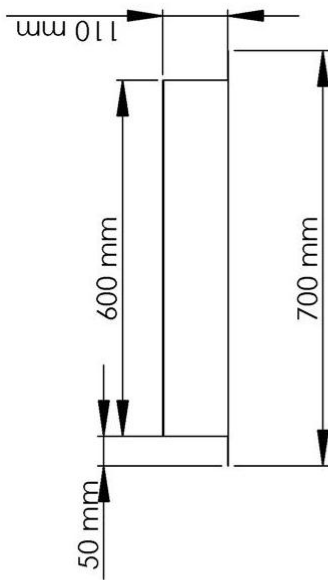
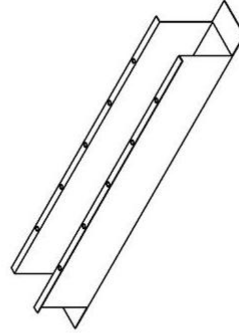
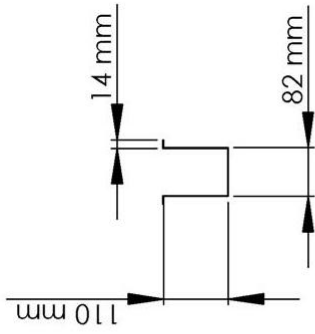


<b>SIZE:</b> <b>A4</b>	<b>Faculty of Engineering</b> <b>Maharakham University Thailand</b>	
	Title: <b>CLOHP/CV 100 mm</b>	DWG. NO. DATE:
Scale : <b>1:10</b>	CHECKED: <b>Assoc. Prof. Dr. Sampan Ritthidech</b>	
DESIGN BY: <b>Satipong Sangiamsuk</b>		

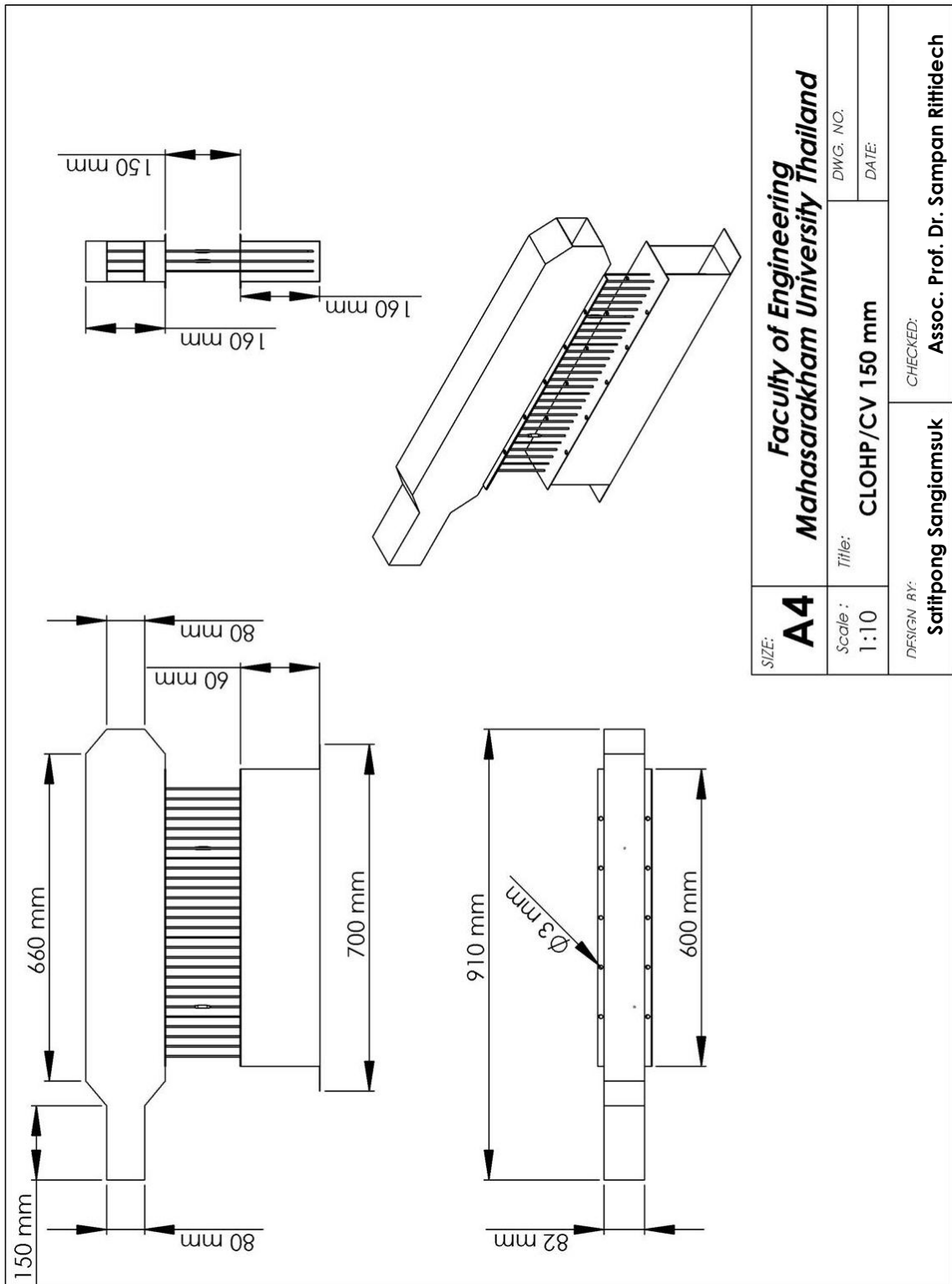




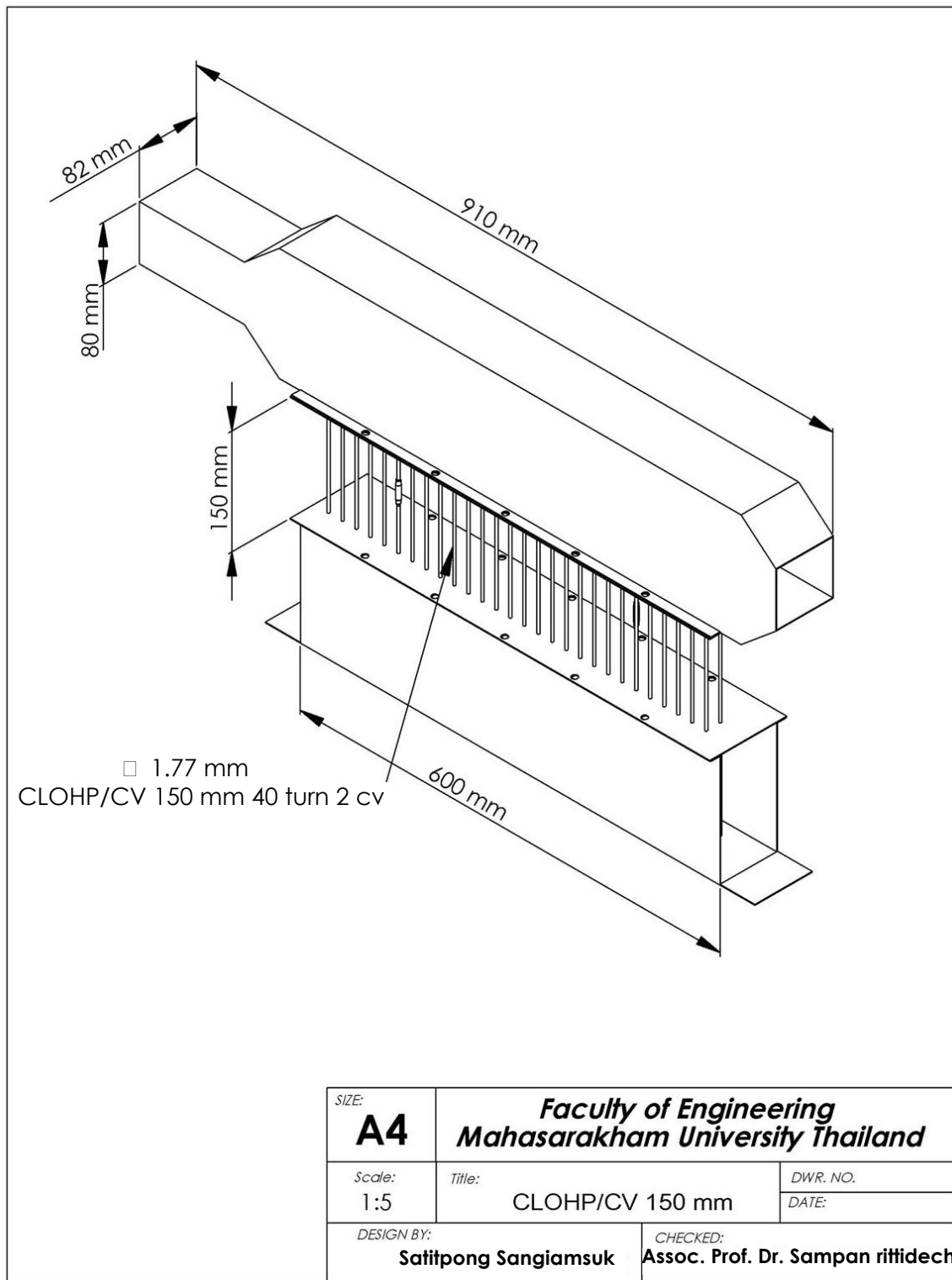
<b>SIZE:</b> <b>A4</b>	<b>Faculty of Engineering</b> <b>Maharakham University Thailand</b>	
	DWG. NO.:	DATE:
<b>Scale :</b> 1:10	<b>Title:</b> <b>Jacket of Condenser Section</b>	
<b>DESIGN BY:</b> <b>Satitpong Sangiamsuk</b>	<b>CHECKED BY:</b> <b>Assoc. Prof. Dr. Sampan Ritthidech</b>	

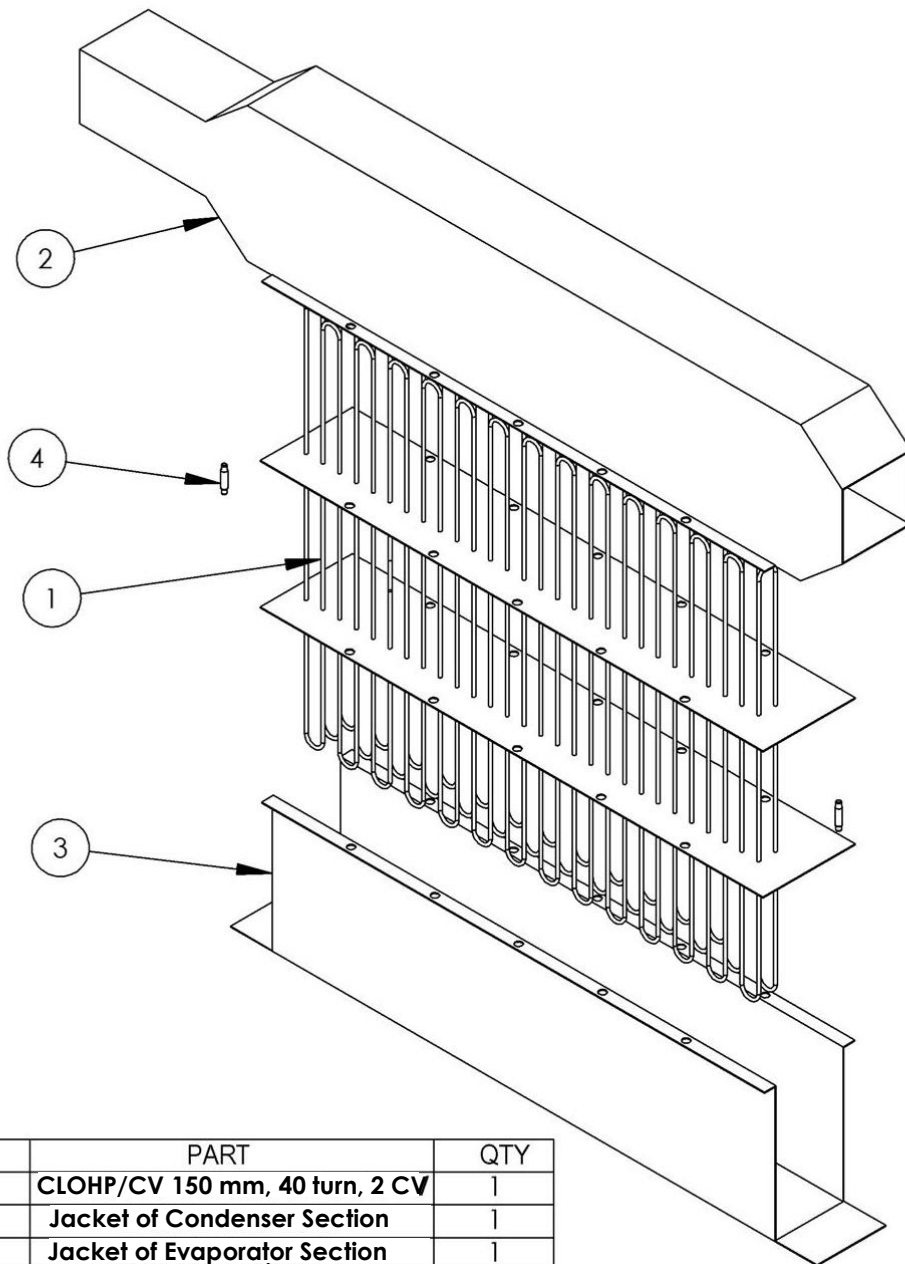


SIZE: <b>A4</b>	Faculty of Engineering Maharakham University Thailand	
	DWG. NO.	DATE:
Scale : 1:10	Title: <b>Jacket of Evaporator Section</b>	
DESIGN BY: <b>Satipong Sangiamsuk</b>	CHECKED: <b>Assoc. Prof. Dr. Sampan Ritfidech</b>	



SIZE: <b>A4</b>	Faculty of Engineering Maharakham University Thailand	
	Scale : 1:10	DWG. NO. _____ DATE: _____
Title: CLOHP/CV 150 mm	CHECKED: Assoc. Prof. Dr. Sampan Ritthidech	
DESIGN BY: Satitpong Sangiamsuk	_____	

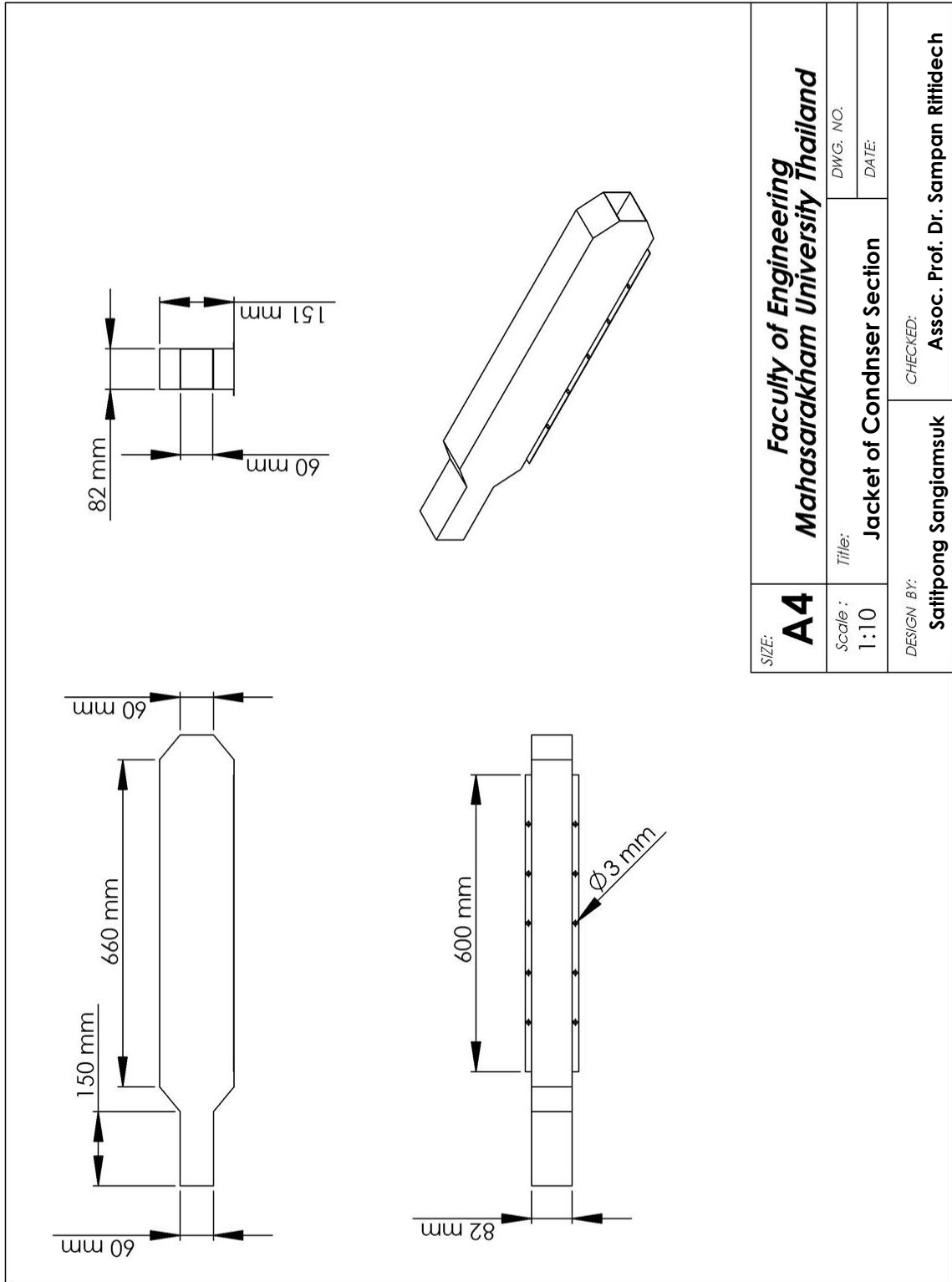




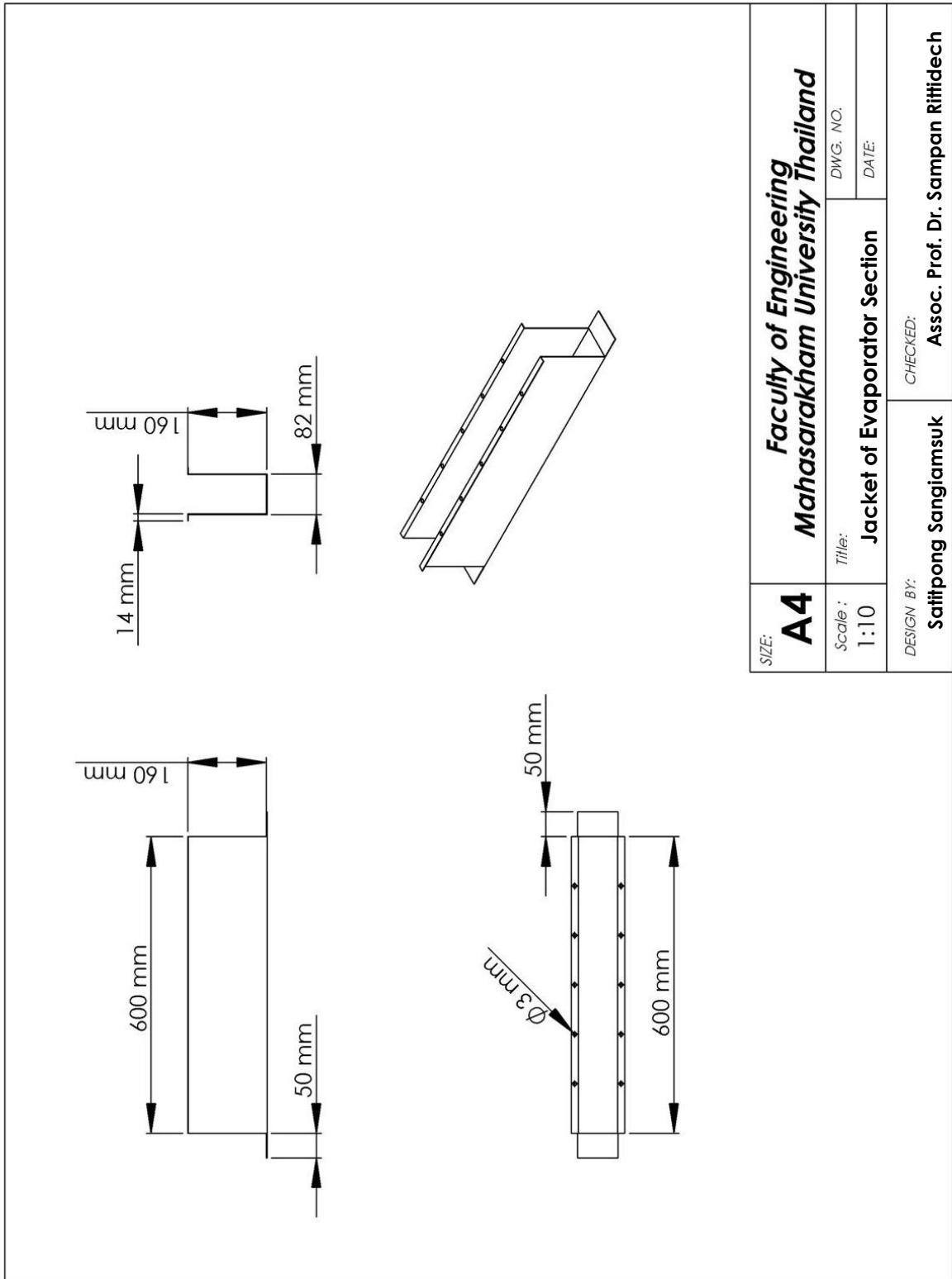
NO	PART	QTY
1	<b>CLOHP/CV 150 mm, 40 turn, 2 CV</b>	1
2	<b>Jacket of Condenser Section</b>	1
3	<b>Jacket of Evaporator Section</b>	1
4	<b>Check valves</b>	2

		SIZE: <b>A4</b>	<b>Faculty of Engineering Mahasarakham University Thailand</b>	
		Scale: 1:5		
DESIGN BY: <b>Satitpong Sangiamsuk</b>		CHECKED: <b>Assoc. Prof. Dr. Sampan rittidech</b>		

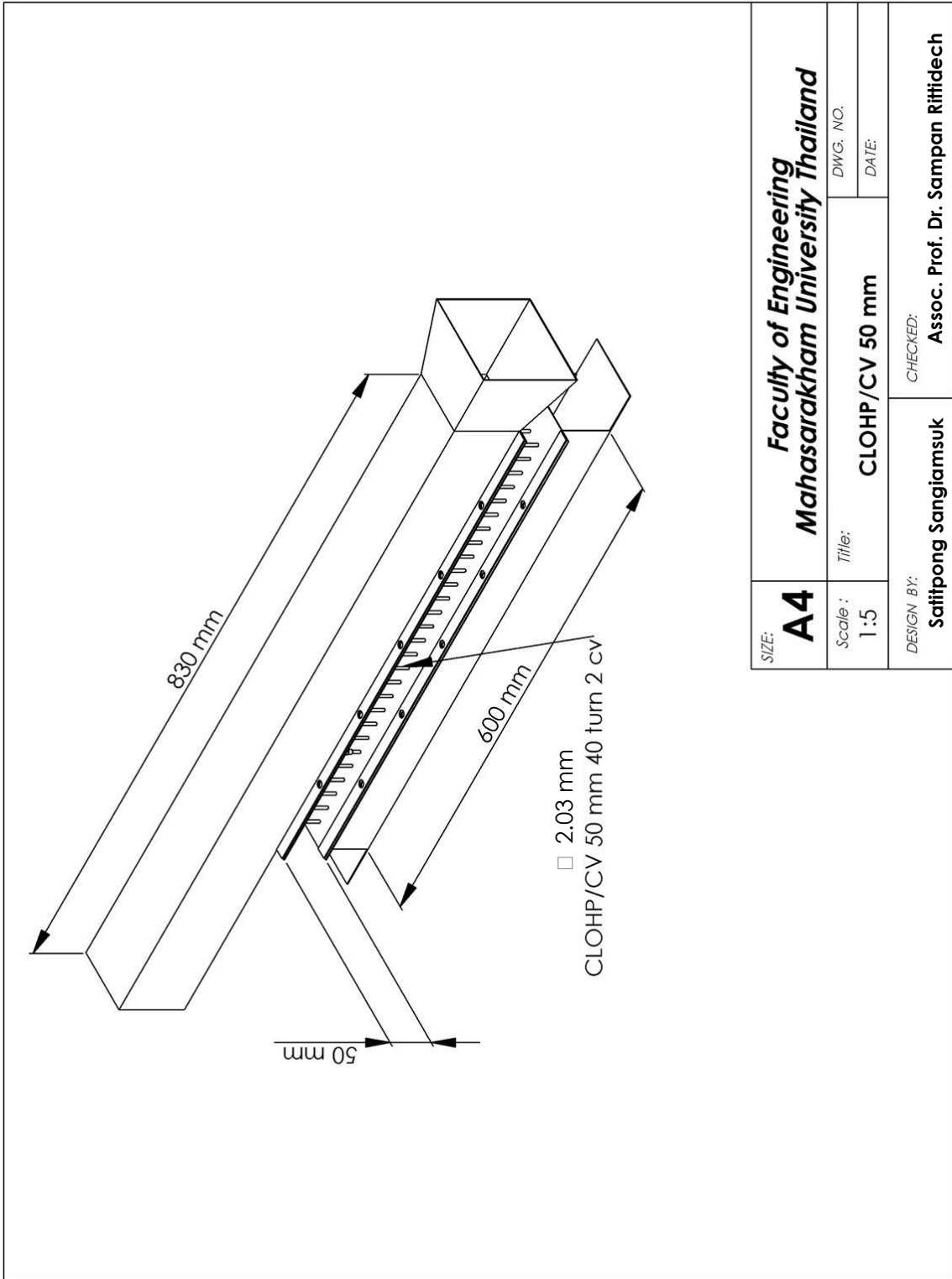




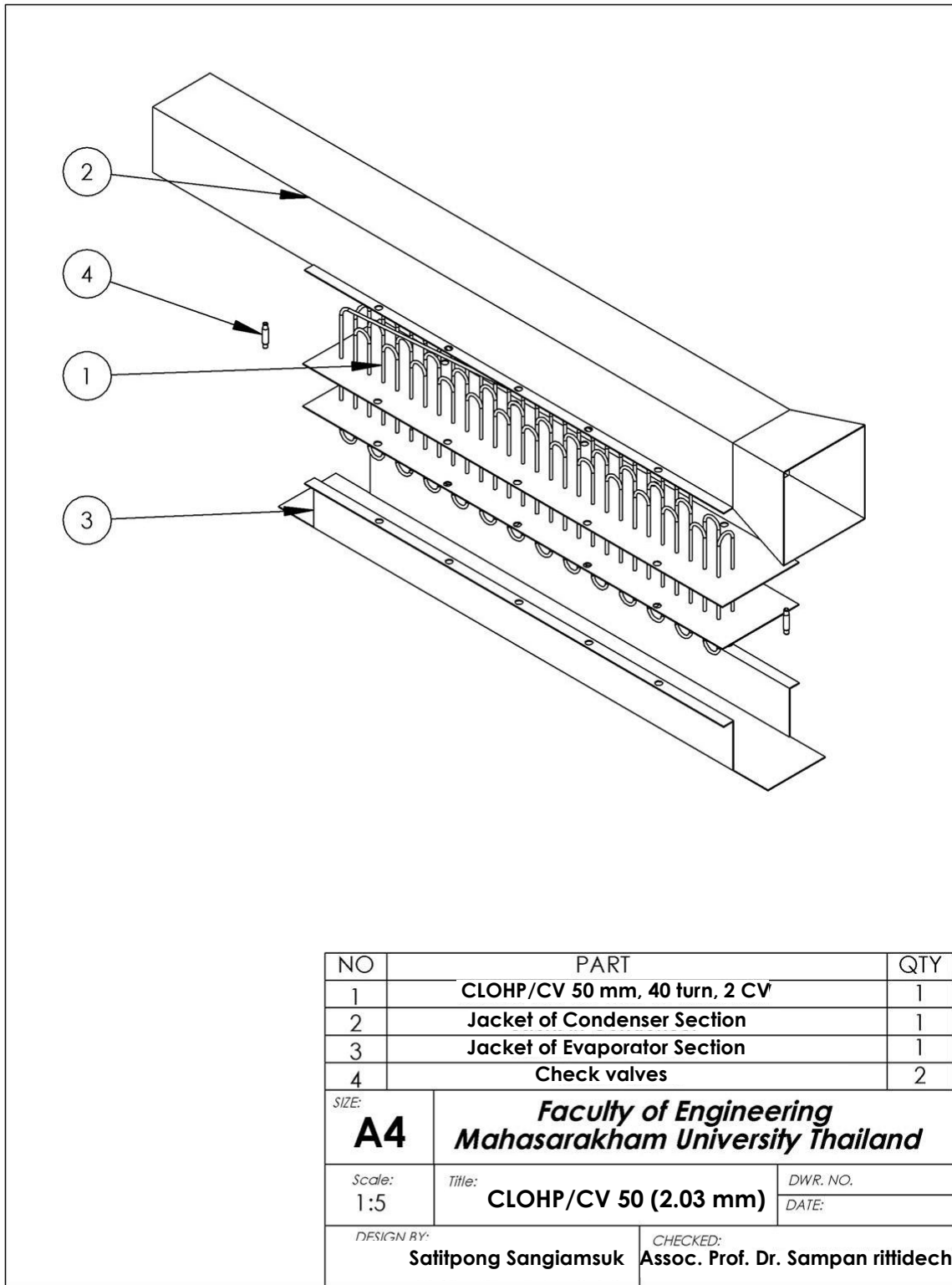
<b>SIZE:</b> <b>A4</b>	<b>Faculty of Engineering</b> <b>Maharakham University Thailand</b>	
	DWG. NO.	DATE:
<b>Scale :</b> 1:10	<b>Title:</b> <b>Jacket of Condenser Section</b>	
<b>DESIGN BY:</b> Saifitpong Sangiamsuk	<b>CHECKED:</b> Assoc. Prof. Dr. Sampan Rittidech	



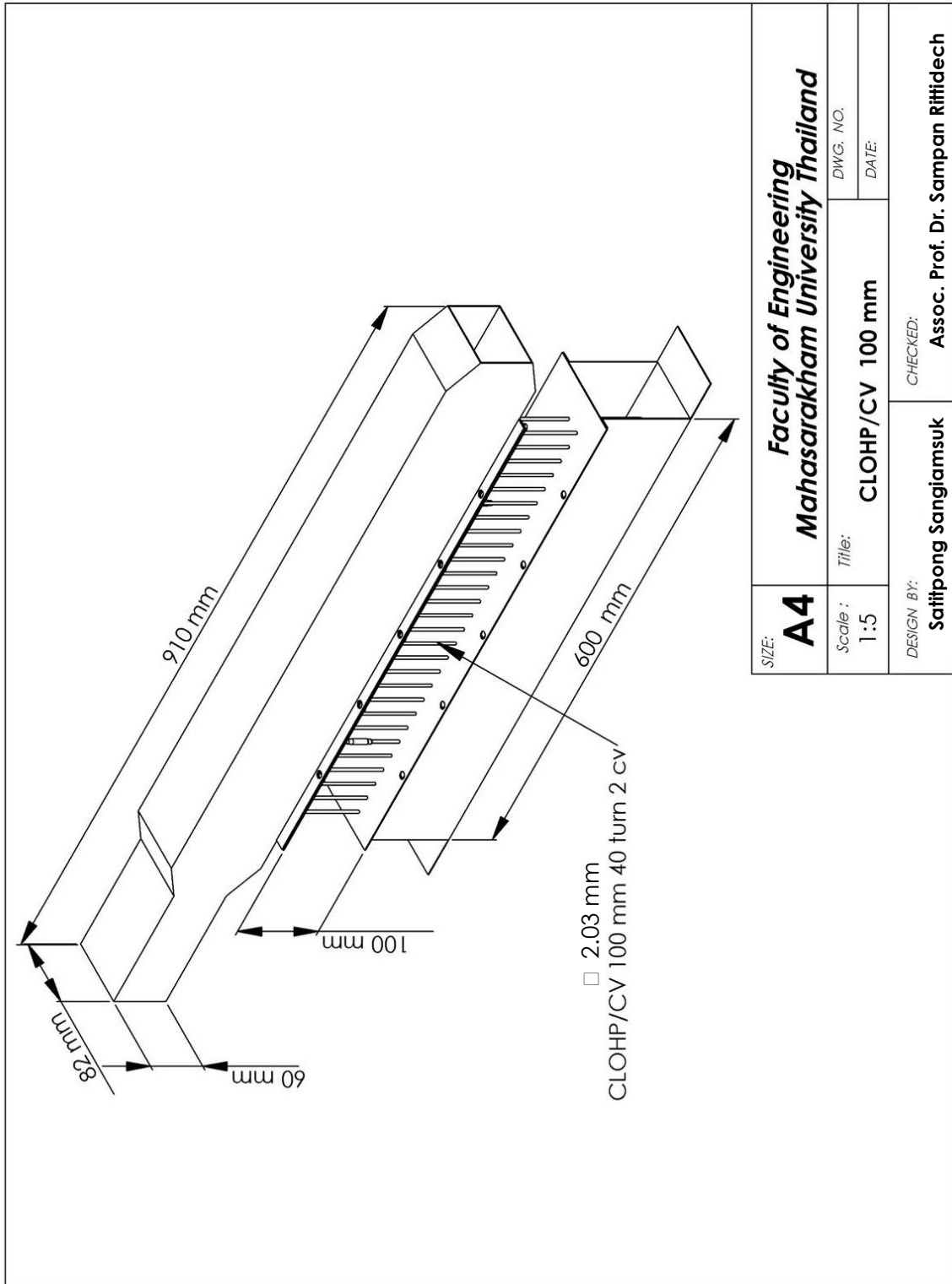
<b>SIZE:</b> <b>A4</b>	<b>Faculty of Engineering</b> <b>Maharakham University Thailand</b>	
	DWG. NO.	DATE
<b>Scale :</b> 1:10	<b>Title:</b> <b>Jacket of Evaporator Section</b>	
<b>DESIGN BY:</b> Saifpong Sangiamsuk	<b>CHECKED:</b> Assoc. Prof. Dr. Sampan Ritthidech	

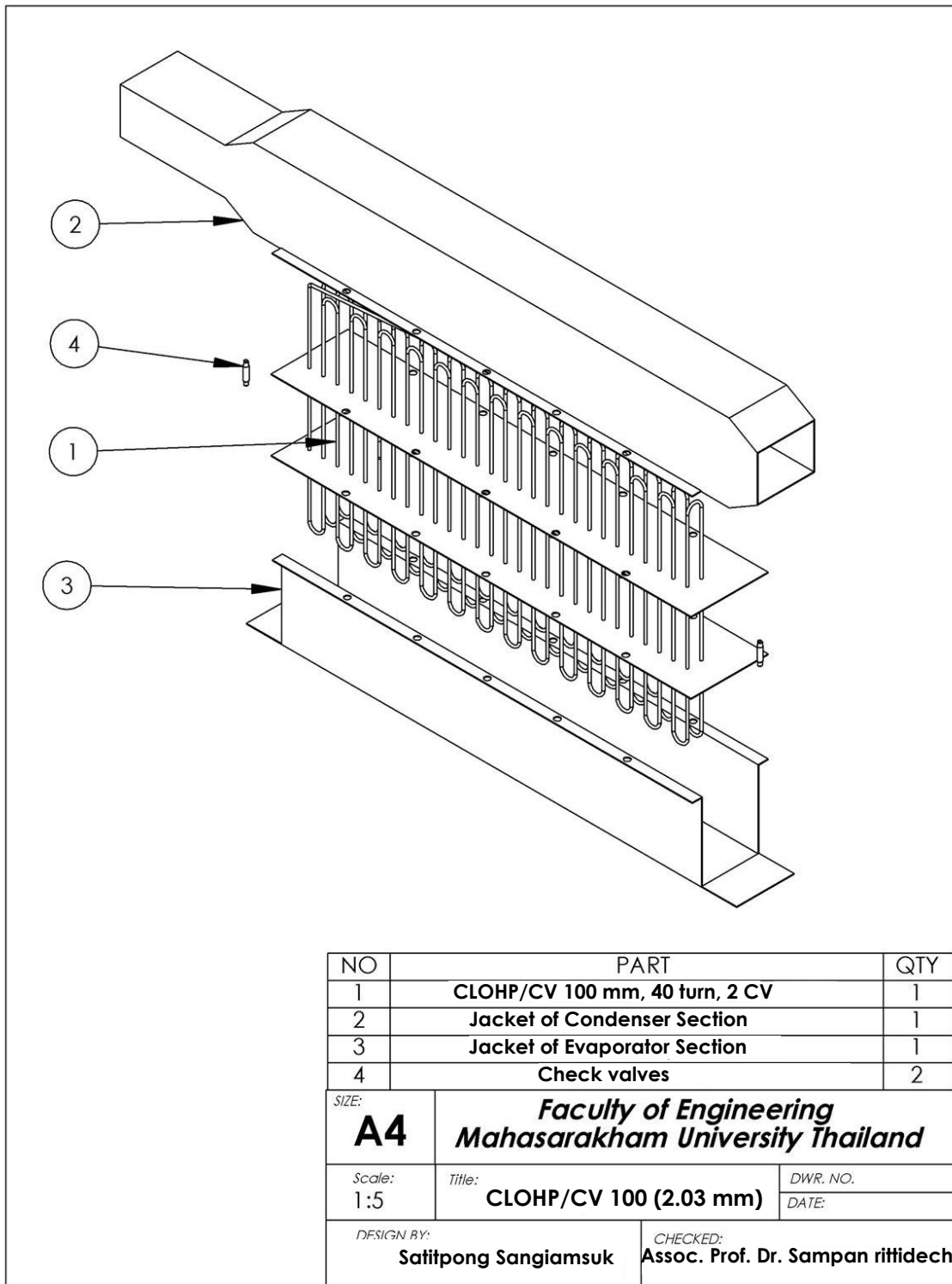


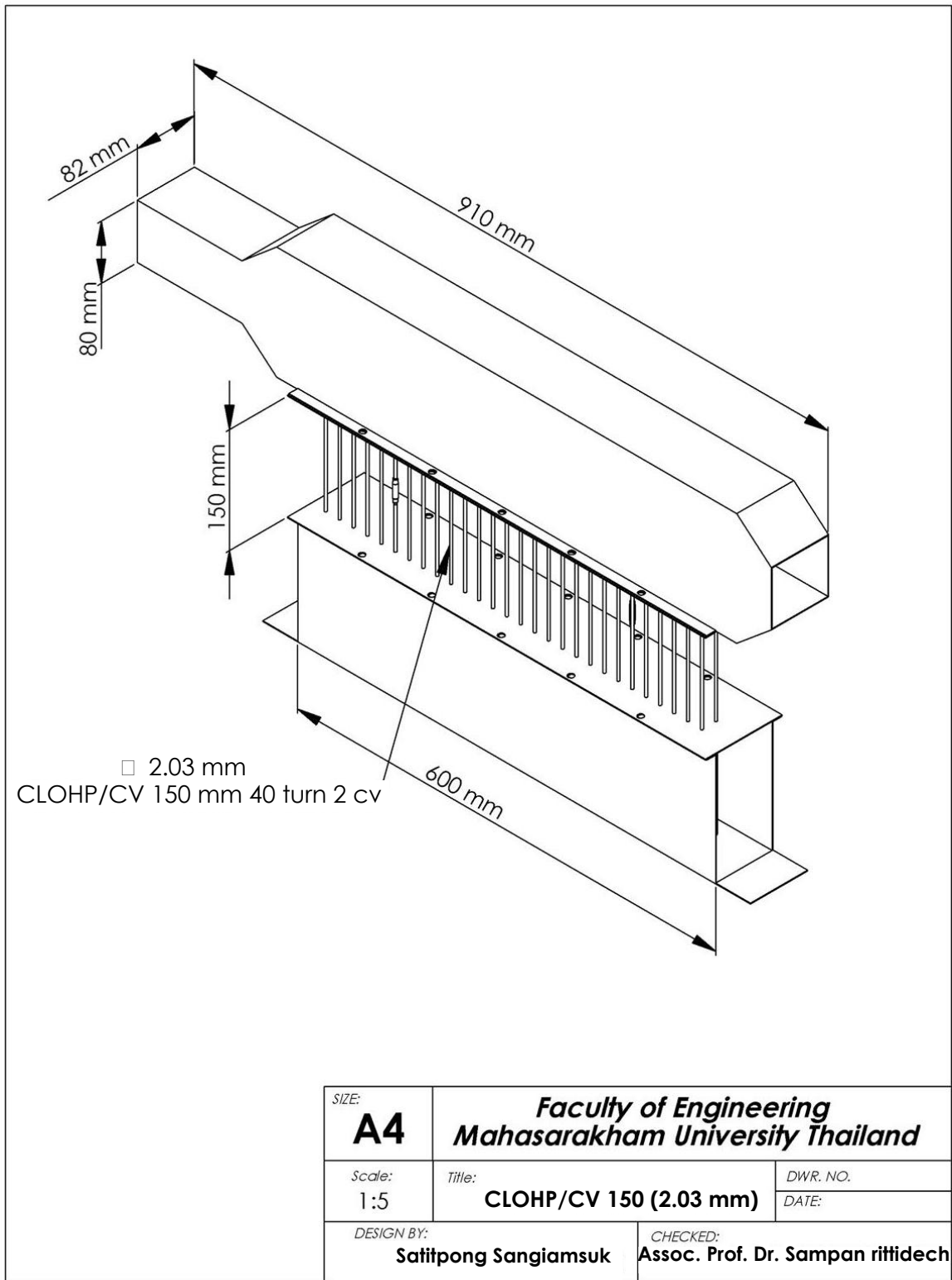


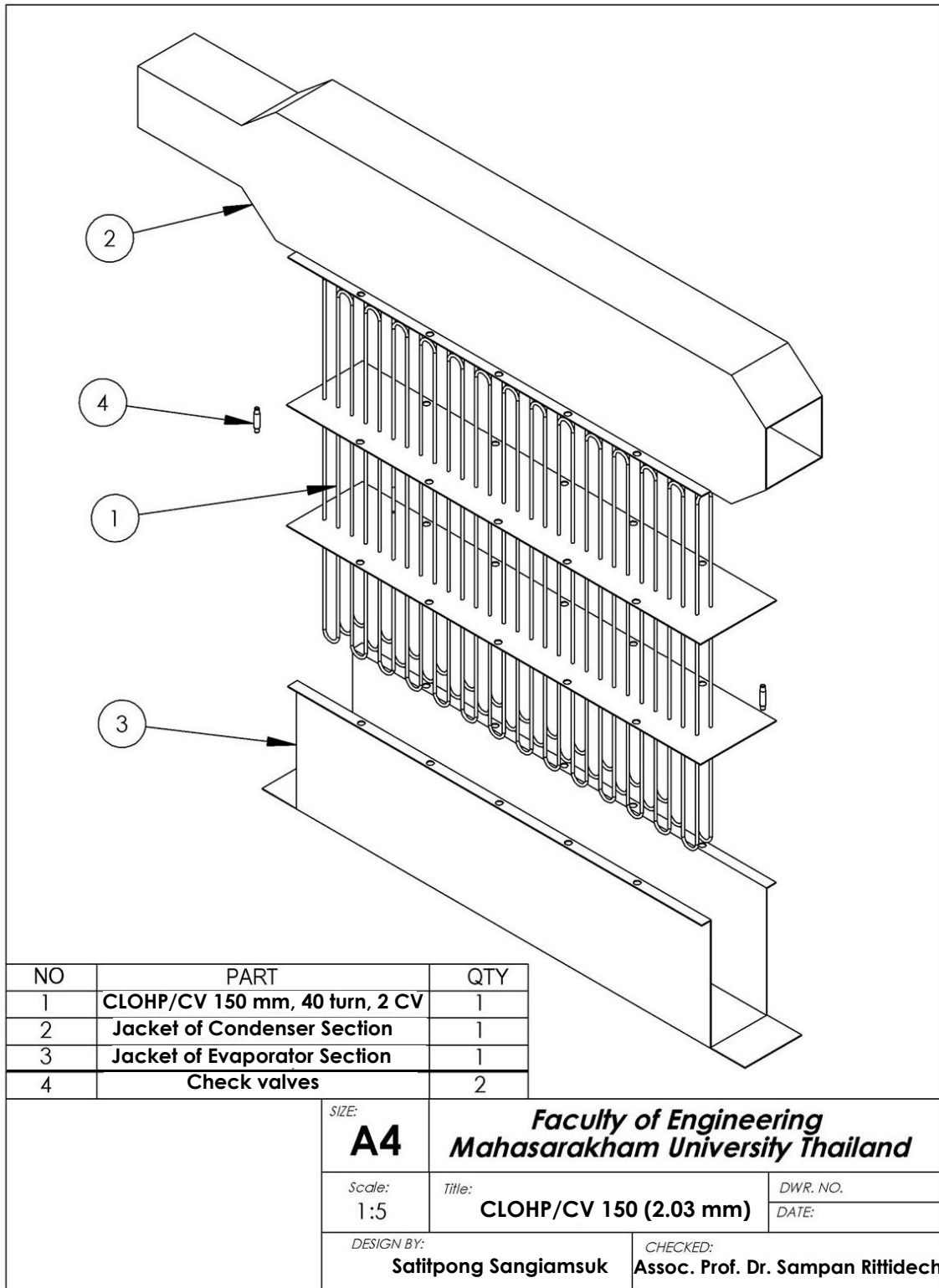


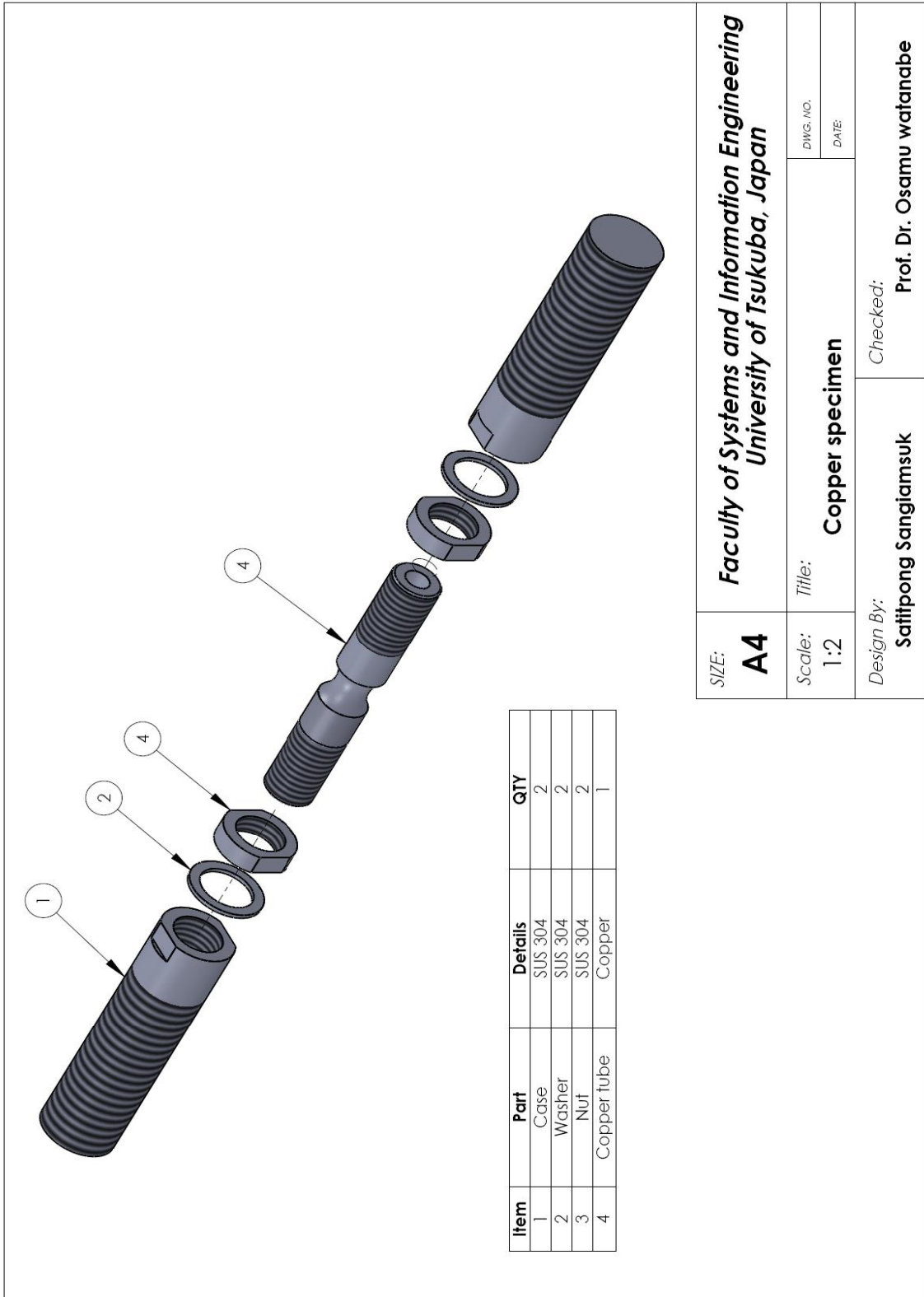
NO	PART	QTY
1	CLOHP/CV 50 mm, 40 turn, 2 CV	1
2	Jacket of Condenser Section	1
3	Jacket of Evaporator Section	1
4	Check valves	2
SIZE: <b>A4</b>		Faculty of Engineering Maharakham University Thailand
Scale: 1:5	Title: CLOHP/CV 50 (2.03 mm)	
DESIGN BY: Satitpong Sangiamsuk		CHECKED: Assoc. Prof. Dr. Sampan rittidech



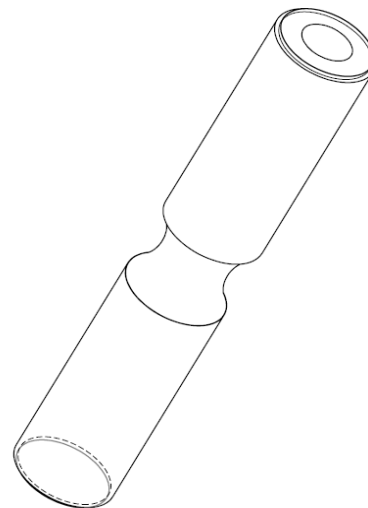
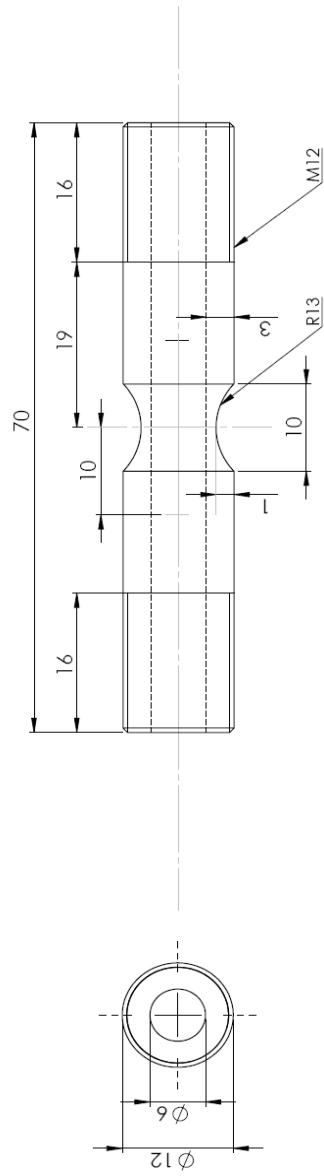




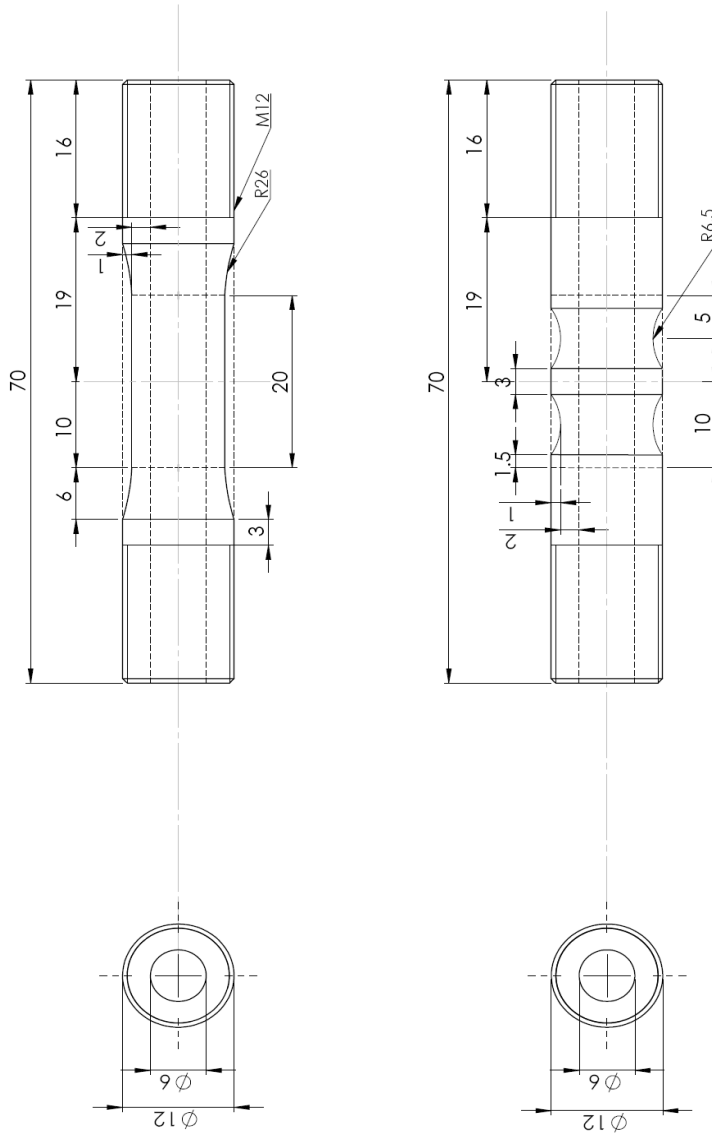




SIZE: <b>A4</b>	<b>Faculty of Systems and Information Engineering University of Tsukuba, Japan</b>	
Scale: 1:2	Title: <b>Copper specimen</b>	DWG. NO. DATE:
Design By: <b>Satitpong Sangiamsuk</b>	Checked: <b>Prof. Dr. Osamu watanabe</b>	

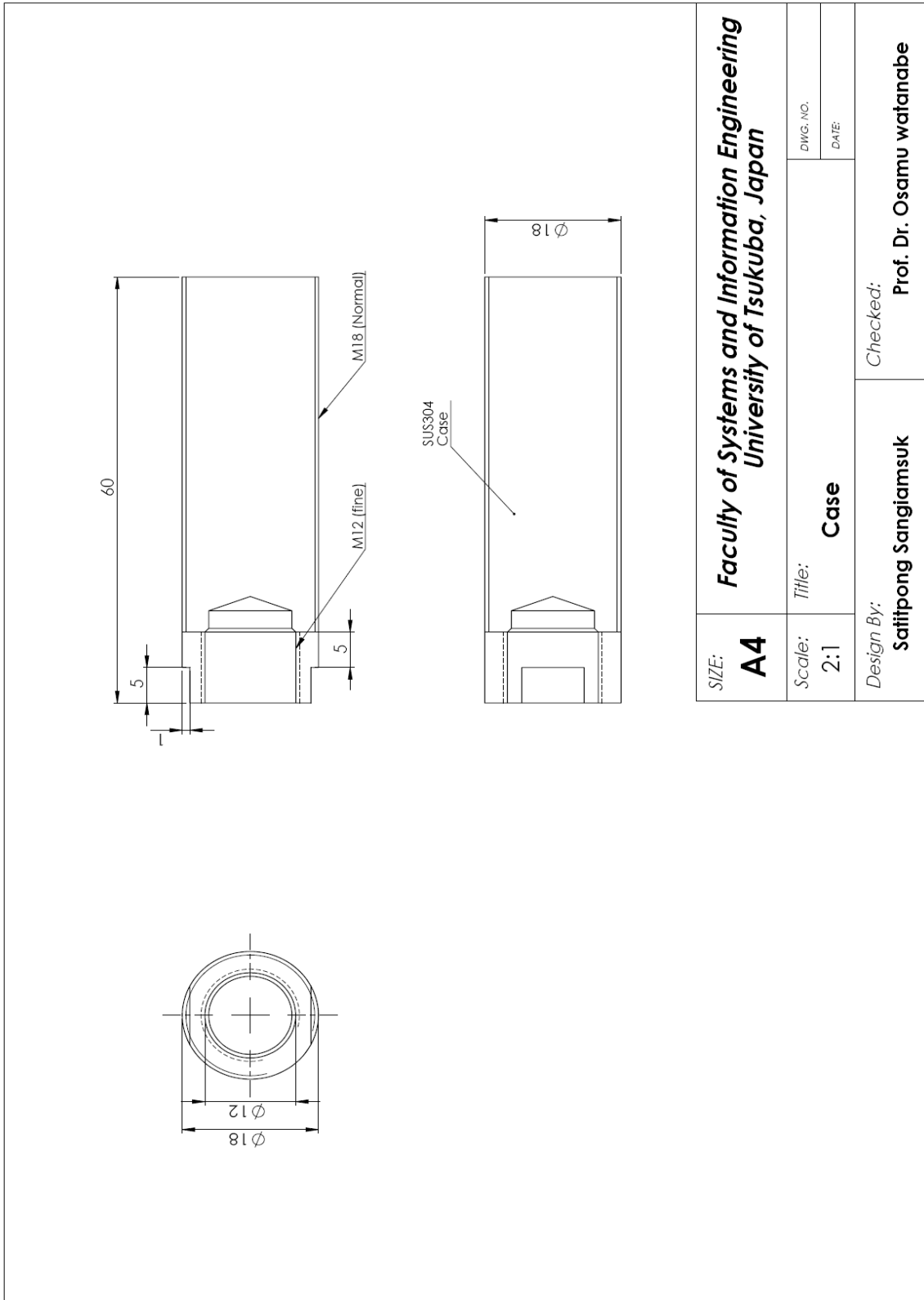


SIZE: <b>A4</b>	<b>Faculty of Systems and Information Engineering</b> <b>University of Tsukuba, Japan</b>	
	Title: <b>Copper tube</b>	DWG. NO.  DATE:
Scale: <b>2:1</b>	Design By: <b>Satitpong Sangiamsuk</b>	
Checked: <b>Prof. Dr. Osamu watanabe</b>		

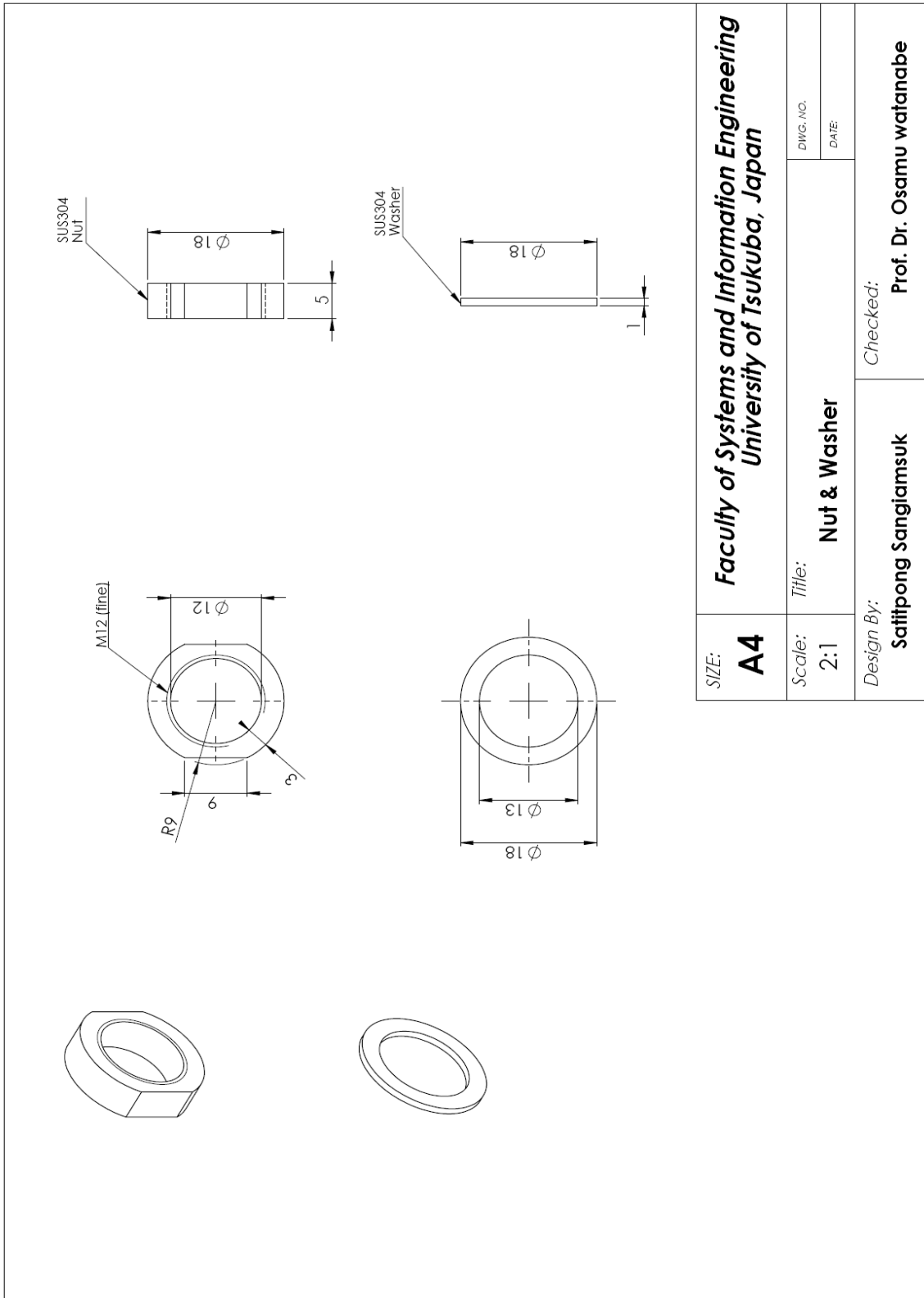


SIZE: <b>A4</b>	<b>Faculty of Systems and Information Engineering</b> <b>University of Tsukuba, Japan</b>		DWG. NO.
	Scale: 2:1	Title: <b>Copper tube</b>	DATE:
Design By: <b>Satitpong Sangiamsuk</b>		Checked: <b>Prof. Dr. Osamu watanabe</b>	





SIZE: <b>A4</b>	Faculty of Systems and Information Engineering University of Tsukuba, Japan	
	Scale: <b>2:1</b>	Title: <b>Case</b>
Design By: <b>Satitpong Sangiamsuk</b>	Checked: <b>Prof. Dr. Osamu watanabe</b>	DWG. NO.  DATE



**APPENDIX D**  
**Physical Properties of Working Fluids**



Table D.1 Thermo physical properties of water

Temp. °C	Pressure MPa	Density	Volume	Enthalpy		Viscosity		Specific Heat		Thermal C.		Surface Tension mN/m
		Kg/m <sup>3</sup>	m <sup>3</sup> /kg	kJ/kg		μ Pa.s		kJ/(kg.K)		mW/(m.K)		
		Liquid	Vapor	Liquid	Vapor	Liquid	Vapor	Liquid	Vapor	Liquid	Vapor	
0.01a	0.00061	999.8	205.98	0.0	2500.5	1792.4	9.22	4.229	1.868	561.0	17.07	75.65
5.00	0.00087	999.9	147.02	21.0	2509.7	1519.1	9.34	4.200	1.871	570.5	17.34	74.95
10.00	0.00123	999.7	106.32	42.0	2518.9	1306.6	9.46	4.188	1.874	580.0	17.62	74.22
15.00	0.00171	999.1	77.900	62.9	2528.0	1138.2	9.59	4.184	1.878	589.3	17.92	73.49
20.00	0.00234	998.2	57.777	83.8	2537.2	1002.1	9.73	4.183	1.882	598.4	18.23	72.74
25.00	0.00317	997.0	43.356	104.8	2546.3	890.5	9.87	4.183	1.887	607.1	18.55	71.98
30.00	0.00425	995.6	32.896	125.7	2555.3	797.7	10.01	4.183	1.892	615.4	18.88	71.20
35.00	0.00563	994.0	25.221	146.6	2564.4	719.6	10.16	4.183	1.898	623.2	19.23	70.41
40.00	0.00738	992.2	19.528	167.5	2573.4	653.2	10.31	4.182	1.905	630.5	19.60	69.60
45.00	0.00959	990.2	15.263	188.4	2582.3	596.3	10.46	4.182	1.912	637.3	19.97	68.78
50.00	0.01234	998.0	12.037	209.3	2591.2	547.0	10.62	4.182	1.919	643.5	20.36	67.95
55.00	0.01575	985.6	9.5730	230.2	2600.0	504.1	10.77	4.182	1.928	649.2	20.77	67.10
60.00	0.01993	983.2	7.6746	251.2	2608.8	466.5	10.93	4.183	1.937	654.3	21.18	66.24
65.00	0.02502	980.5	6.1996	272.1	2617.5	433.4	11.10	4.184	1.947	658.9	21.62	65.37
70.00	0.03118	977.8	5.0447	293.0	2626.1	404.0	11.26	4.187	1.958	663.1	22.07	64.49
75.00	0.03856	974.8	4.1333	314.0	2634.6	377.8	11.42	4.190	1.970	666.7	22.53	63.59
80.00	0.04737	971.8	3.4088	334.9	2643.1	354.5	11.59	4.194	1.983	670.0	23.01	62.68
85.00	0.05781	968.6	2.8289	355.9	2651.4	333.4	11.76	4.199	1.996	672.8	23.50	61.76
90.00	0.07012	965.3	2.3617	376.9	2659.6	314.5	11.93	4.204	2.011	675.3	24.02	60.82
95.00	0.08453	961.9	1.9828	398.0	2667.7	297.4	12.10	4.210	2.027	677.4	24.55	59.88
100.00	0.10132	958.4	1.6736	419.1	2675.7	281.8	12.27	4.217	2.044	679.1	25.09	58.92
105.00	0.12079	954.8	1.4200	440.2	2683.6	267.7	12.44	4.224	2.062	680.6	25.66	57.95
110.00	0.14324	951.0	1.2106	461.3	2691.3	254.8	12.61	4.232	2.082	681.7	26.24	56.97
115.00	0.16902	947.1	1.0370	482.5	2698.8	243.0	12.78	4.240	2.103	682.6	26.84	55.98
120.00	0.19848	943.2	0.89222	503.8	2706.2	232.1	12.96	4.249	2.126	683.2	27.46	54.97
125.00	0.23201	939.1	0.77089	525.1	2713.4	222.2	13.13	4.258	2.150	683.6	28.10	53.96
130.00	0.27002	934.9	0.66872	546.4	2720.4	213.0	13.30	4.268	2.176	683.7	28.76	52.94
135.00	0.31293	930.6	0.58234	567.8	2727.2	204.5	13.47	4.278	2.203	683.6	29.44	51.91
140.00	0.36119	926.2	0.50898	589.2	2733.8	196.6	13.65	4.288	2.233	683.3	30.13	50.86
145.00	0.41529	921.7	0.44643	610.8	2740.2	189.3	13.82	4.300	2.265	682.8	30.85	49.81
150.00	0.47572	917.1	0.39287	632.3	2746.4	182.5	13.99	4.312	2.299	682.1	31.59	48.75
155.00	0.54299	912.3	0.34681	654.0	2752.3	176.2	14.16	4.325	2.335	681.1	32.35	47.68
160.00	0.61766	907.5	0.30709	675.6	2758.0	170.3	14.34	4.338	2.374	680.0	33.12	46.60
165.00	0.70029	902.6	0.27270	697.4	2763.3	164.8	14.51	4.353	2.415	678.6	33.92	45.51
170.00	0.79147	897.5	0.24283	719.3	2768.5	159.6	14.68	4.369	2.460	677.1	34.74	44.41
175.00	0.89180	892.3	0.21679	741.2	2773.3	154.7	14.85	4.386	2.507	675.3	35.58	43.31



Table D.1 (Continue)

Temp. °C	Pressure MPa	Density	Volume	Enthalpy		Viscosity		Specific Heat		Thermal C.		Surface Tension mN/m
		Kg/m <sup>3</sup>	m <sup>3</sup> /kg	kJ/kg		μ Pa.s		kJ/(kg.K)		mW/(m.K)		
		Liquid	Vapor	Liquid	Vapor	Liquid	Vapor	Liquid	Vapor	Liquid	Vapor	
180.00	1.0019	887.1	0.19403	763.2	2777.8	150.2	15.02	4.403	2.558	673.4	36.44	42.20
185.00	1.1225	881.7	0.17406	785.4	2782.0	145.9	15.20	4.423	2.612	671.2	37.32	41.08
190.00	1.2542	876.1	0.15650	807.6	2785.8	141.8	15.37	4.443	2.670	668.8	38.23	39.95
195.00	1.3976	870.5	0.14102	829.9	2789.4	138.0	25.54	4.465	2.731	666.2	39.15	38.82
200.00	1.5536	864.7	0.12732	852.4	2792.5	134.4	15.71	4.489	2.797	663.4	40.10	37.68
205.00	1.7229	858.9	0.11517	875.0	2795.3	130.9	15.89	4.515	2.867	660.3	41.08	36.54
210.00	1.9062	852.8	0.10438	897.7	2797.7	127.6	16.06	4.542	2.943	657.1	42.07	35.39
215.00	2.1042	846.6	0.09475	920.5	2799.7	124.5	16.23	4.572	3.023	653.5	43.10	34.24
220.00	2.3178	840.3	0.08615	943.5	2801.3	121.6	16.41	4.604	3.109	649.8	44.15	33.08
225.00	2.5479	833.9	0.07846	966.7	2802.4	118.7	16.59	4.638	3.201	645.7	45.24	31.91
230.00	2.7951	827.2	0.07155	990.0	2803.1	116.0	16.76	4.675	3.300	641.4	46.35	30.75
235.00	3.0604	820.5	0.06534	1013.5	2803.3	113.4	16.94	4.715	3.405	636.9	47.51	29.58
240.00	3.3447	813.5	0.05974	1037.2	2803.0	110.9	17.12	4.759	3.519	632.0	48.70	28.40
245.00	3.6488	806.4	0.05469	1061.2	2802.1	108.5	17.31	4.806	3.641	626.8	49.94	27.23
250.00	3.9736	799.1	0.05011	1085.3	2800.7	106.2	17.49	4.857	3.772	621.4	51.22	26.05
255.00	4.3202	791.5	0.04596	1109.7	2798.8	103.9	17.68	4.912	3.914	615.6	52.57	24.88
260.00	4.6894	783.8	0.04219	1134.4	2796.2	101.7	17.88	4.973	4.069	609.4	53.98	23.70
265.00	5.0823	775.9	0.03876	1159.3	2793.0	99.6	18.07	5.039	4.236	603.0	55.47	22.52
270.00	5.4999	767.7	0.03564	1184.6	2789.1	97.5	18.28	5.111	4.418	596.1	57.04	21.35
275.00	5.9431	759.2	0.03278	1210.1	2784.5	95.5	18.48	5.191	4.617	588.9	58.72	20.17
280.00	6.4132	750.5	0.03016	1236.1	2779.2	93.6	18.70	5.279	4.835	581.4	60.52	19.00
285.00	6.9111	741.5	0.02777	1262.4	2773.0	91.6	18.92	5.377	5.077	573.5	62.47	17.84
290.00	7.4380	732.2	0.02556	1289.1	2765.9	89.7	19.15	5.485	5.345	565.2	64.59	16.68
295.00	7.9952	722.5	0.02354	1316.3	2757.8	87.8	19.39	5.607	5.644	556.6	66.91	15.52
300.00	8.5838	712.4	0.02167	1344.1	2748.7	85.9	19.65	5.746	5.981	547.7	69.49	14.37
310.00	9.8605	691.0	0.01834	1401.2	2727.0	82.2	20.21	6.084	6.799	529.0	75.61	12.10
320.00	11.279	667.4	0.01548	1461.3	2699.7	78.4	20.84	6.542	7.898	509.4	83.59	9.88
330.00	12.852	641.0	0.01298	1525.0	2665.3	74.6	21.60	7.201	9.458	489.2	94.48	7.71
340.00	14.594	610.8	0.01079	1593.8	2621.3	70.4	22.55	8.238	11.865	468.6	110.20	5.64
350.00	16.521	574.7	0.00881	1670.4	2563.5	65.9	23.81	10.126	16.110	447.6	134.65	3.68
360.00	18.655	528.1	0.00696	1761.0	2482.0	60.4	25.71	14.690	25.795	427.2	178.01	1.89
370.00	21.030	453.1	0.00499	1889.7	2340.2	52.3	29.57	41.955	78.751	428.0	299.38	0.39
373.99c	22.064	322.0	0.00311	2085.9	2085.9	43.1	43.13	∞	∞	∞	∞	0

ASHRAE HANDBOOK, 1993



Table D.2 Thermo physical properties of ethanol

Temp. °C	Pressure MPa	$h_{fg}$ Latent kJ/kg	$\rho_l$ Liquid $10^3$ kg/m <sup>3</sup>	$\rho_v$ Vapor kg/m <sup>3</sup>	$\mu_l$ Liquid $10^{-3}$ N.s/m <sup>2</sup>	$\mu_v$ Vapor $10^{-5}$ N.s/m <sup>2</sup>	$K_l$ Liquid W/m.K	$K_v$ Vapor W/m.K	$\sigma$ Liquid $10^{-3}$ N/m	$C_{p,l}$ Liquid kJ/kg.K	$C_{p,v}$ Vapor kJ/kg.K
0	0.012	1048.4	0.901	0.036	1.7990	0.774	0.183	0.0117	24.4	0.541	1.34
20	0.058	1030.0	0.800	0.085	1.1980	0.835	0.179	0.0139	22.8	0.574	1.40
40	0.180	1011.9	0.789	0.316	0.8190	0.900	0.175	0.160	21.0	0.615	1.48
60	0.472	988.9	0.770	0.748	0.5880	0.959	0.171	0.0179	19.2	0.665	1.54
80	1.086	960.0	0.757	1.430	0.4320	1.030	0.169	0.0199	17.3	0.723	1.61
100	2.260	927.0	0.730	3.410	0.3180	1.092	0.167	0.0219	15.5	0.789	1.68
120	4.290	885.5	0.710	6.010	0.2430	1.157	0.165	0.0238	13.4	0.863	1.75
140	7.530	834.0	0.680	10.670	0.1900	1.219	0.163	0.0256	11.2	0.945	-
160	12.756	772.9	0.650	17.450	0.1500	1.293	0.161	0.0272	9.0	-	-
180	19.600	698.8	0.610	27.650	0.1200	1.369	0.159	0.0288	6.7	-	-
200	29.400	598.3	0.564	44.480	0.0950	1.464	0.157	0.0395	4.3	-	-
220	42.800	468.5	0.510	74.350	0.0725	1.618	0.155	0.0321	2.2	-	-
240	60.200	280.5	0.415	135.500	0.0488	1.948	0.153	-	0.1	-	-

Dunn P. and Reay D.A., 1982



Table D.3 Thermo physical properties of R123

Temp. °C	Pressure MPa	Density Kg/m <sup>3</sup>	Volume m <sup>3</sup> /kg	Enthalpy kJ/kg		Viscosity μ Pa.s		Specific Heat kJ/(kg.K)		Thermal C. mW/(m.K)		Surface Tension mN/m
		Liquid	Vapor	Liquid	Vapor	Liquid	Vapor	Liquid	Vapor	Liquid	Vapor	
-40.00	0.00378	1613.2	3.3365	167.23	356.3	1048.8	-	-	0.594	-	-	23.49
-30.00	0.00698	1591.5	1.8798	175.47	362.04	884.0	-	-	0.611	-	-	22.20
-20.00	0.01221	1569.5	1.1145	183.38	367.87	755.0	-	-	0.629	89.7	-	20.93
-10.00	0.02041	1546.9	0.6904	191.48	373.77	652.4	-	-	0.648	86.8	-	19.68
0.00	0.03273	1523.8	0.4445	200.00	379.75	569.6	-	0.875	0.667	83.9	-	18.43
2.00	0.03581	1519.1	0.4088	201.76	380.95	555.0	-	0.885	0.670	83.3	-	18.19
4.00	0.03912	1514.3	0.37644	203.54	382.16	541.0	-	0.895	0.674	82.7	-	17.94
6.00	0.04267	1509.6	0.34709	205.34	383.37	527.5	-	0.905	0.678	82.1	-	17.70
8.00	0.04648	1504.8	0.32045	207.16	384.58	514.5	-	0.915	0.682	81.6	-	17.45
10.00	0.05057	1500.0	0.29622	209.00	385.79	502.0	-	0.924	0.636	81.0	-	17.21
12.00	0.05494	1495.2	0.27416	210.86	387.00	489.9	-	0.934	0.689	80.4	-	16.96
14.00	0.05961	1490.3	0.25405	212.74	388.22	478.3	-	0.943	0.693	79.8	-	16.72
16.00	0.06459	1485.5	0.23569	214.64	389.43	467.1	-	0.952	0.697	79.2	-	16.48
18.00	0.06990	1480.5	0.21890	216.55	390.65	456.3	-	0.961	0.701	78.7	-	16.24
20.00	0.07555	1475.6	0.20354	218.49	391.87	445.8	-	0.970	0.704	78.1	9.81	16.00
22.00	0.08157	1470.6	0.18946	220.44	393.09	435.7	-	0.978	0.708	77.5	9.95	15.76
24.00	0.08796	1465.7	0.17654	222.40	394.31	426.0	-	0.986	0.712	76.9	10.08	15.52
26.00	0.09473	1460.6	0.16467	224.39	395.54	416.5	-	0.994	0.716	76.3	10.22	15.28
27.84b	0.10133	1456.0	0.15460	226.22	396.66	408.1	-	1.001	0.719	75.8	10.35	15.06
28.00	0.10192	1455.6	0.15376	226.38	396.76	407.4	-	1.002	0.719	75.8	10.36	15.04
30.00	0.10952	1450.5	0.14371	228.40	397.98	398.5	-	1.009	0.723	75.2	10.49	14.80
32.00	0.11757	1445.4	0.13445	230.42	399.21	389.9	-	1.016	0.727	74.6	10.63	14.57
34.00	0.12607	1440.2	0.12590	232.46	400.43	381.6	-	1.023	0.731	74.0	10.77	14.33
36.00	0.13504	1435.1	0.11800	234.52	401.65	373.6	-	1.029	0.734	73.4	10.90	14.10
38.00	0.14451	1429.9	0.11070	236.59	402.88	365.7	-	1.035	0.738	72.9	11.04	13.86
40.00	0.15448	1424.6	0.10394	238.67	404.1	358.1	-	1.041	0.742	72.3	11.18	13.63
42.00	0.16498	1419.4	0.09768	240.76	405.32	350.7	-	1.047	0.745	71.7	11.32	13.39
44.00	0.17603	1414.0	0.09186	242.86	406.54	343.5	-	1.052	0.749	71.1	11.45	13.16
46.00	0.18764	1408.7	0.08647	244.97	407.76	336.5	-	1.058	0.753	70.5	11.59	12.93
48.00	0.19983	1403.3	0.08145	247.10	408.97	329.7	-	1.063	0.757	69.9	11.73	12.70
50.00	0.21261	1397.9	0.07678	249.23	410.19	323.0	11.72	1.067	0.760	69.4	11.56	12.47
52.00	0.22602	1392.4	0.07244	251.37	411.4	316.6	11.79	1.072	0.764	68.8	12.00	12.24
54.00	0.24007	1386.9	0.06839	253.53	412.61	310.2	11.86	1.076	0.768	68.2	12.14	12.01
56.00	0.25478	1381.4	0.06461	255.69	413.82	304.1	11.92	1.081	0.772	67.6	12.27	11.78



Table D.3 (Continue)

Temp. °C	Pressure MPa	Density	Volume	Enthalpy		Viscosity		Specific Heat		Thermal C.		Surface Tension mN/m
		Kg/m <sup>3</sup>	m <sup>3</sup> /kg	kJ/kg		μ Pa.s		kJ/(kg.K)		mW/(m.K)		
		Liquid	Vapor	Liquid	Vapor	Liquid	Vapor	Liquid	Vapor	Liquid	Vapor	
58.00	0.27016	1375.8	0.06108	257.85	415.02	298.0	11.99	1.084	0.775	67.0	12.41	11.55
60.00	0.28624	1370.2	0.05778	260.03	416.22	292.1	12.06	1.088	0.779	66.5	12.55	11.32
62.00	0.30304	1364.5	0.05469	262.21	417.41	286.4	12.12	1.092	0.783	65.9	12.68	11.10
64.00	0.32057	1358.8	0.05180	264.41	418.61	280.7	12.19	1.095	0.787	65.3	12.82	10.87
66.00	0.33887	1353.1	0.04910	266.60	419.79	275.2	12.26	1.099	0.791	64.7	12.96	10.65
68.00	0.35794	1347.3	0.04656	268.81	420.67	269.8	12.32	1.102	0.795	64.1	13.10	10.42
70.00	0.37782	1341.4	0.04418	271.02	422.15	264.5	12.39	1.105	0.798	63.6	13.23	10.20
72.00	0.39851	1335.5	0.04194	273.24	423.32	259.3	12.46	1.108	0.802	63.0	13.37	9.98
74.00	0.42005	1329.6	0.03983	275.46	424.49	254.2	12.52	1.111	0.807	62.4	13.51	9.76
76.00	0.44246	1323.6	0.03786	277.69	425.64	249.2	12.59	1.114	0.811	61.8	13.64	9.54
78.00	0.46575	1317.5	0.03599	279.92	426.8	244.3	12.66	1.117	0.815	61.2	13.78	9.32
80.00	0.48995	1311.4	0.03424	282.16	427.94	239.5	12.72	1.119	0.819	60.7	13.92	9.10
82.00	0.51508	1305.2	0.03259	284.40	429.08	-	12.79	1.122	0.823	60.1	14.05	8.88
84.00	0.54116	1299	0.03103	286.65	430.2	-	12.85	1.125	0.828	59.5	14.19	8.67
86.00	0.56822	1292.7	0.02955	288.91	431.32	-	12.92	1.127	0.832	58.9	14.33	8.45
88.00	0.59628	1286.4	0.02816	291.17	432.43	-	12.99	1.13	0.837	58.3	14.46	8.24
90.00	0.62537	1280	0.02685	293.43	433.54	-	13.05	1.133	0.842	57.8	14.60	8.02
92.00	0.65550	1273.5	0.02560	295.70	434.63	-	13.12	1.136	0.847	57.2	14.74	7.81
94.00	0.68670	1266.9	0.02443	297.97	435.71	-	13.18	1.138	0.852	56.6	-	7.6
96.00	0.71899	1260.3	0.02331	300.25	436.78	-	13.25	1.141	0.857	56.0	-	7.39
98.00	0.75240	1253.6	0.02225	302.54	437.84	-	13.31	1.144	0.862	55.4	-	7.18
100.00	0.78696	1246.8	0.02125	304.83	438.88	-	13.38	1.147	0.868	54.8	-	6.97
105.00	0.87851	1229.5	0.01896	310.58	441.44	-	13.54	1.156	0.883	-	-	6.45
110.00	0.97776	1211.6	0.01695	316.37	443.92	-	13.70	1.156	0.900	-	-	5.94
115.00	1.0851	1193.1	0.01517	322.20	446.29	-	13.87	1.177	0.918	-	-	5.44
120.00	1.2010	1173.9	0.01359	328.08	448.56	-	14.03	1.19	0.940	-	-	4.95
125.00	1.3258	1153.9	0.01219	334.02	450.71	-	14.19	1.207	0.965	-	-	4.47
130.00	1.4600	1133.0	0.01093	340.03	452.72	-	-	1.227	0.994	-	-	3.99
135.00	1.6042	1111.0	0.00980	346.13	454.58	-	-	1.252	1.029	-	-	3.53
140.00	1.7587	1087.7	0.00879	352.32	456.26	-	-	1.283	1.073	-	-	3.08
145.00	1.9241	1062.8	0.00787	358.64	457.72	-	-	1.323	1.129	-	-	2.64
150.00	2.1010	1036.0	0.00703	365.12	458.94	-	-	1.375	1.202	-	-	2.22
160.00	2.4921	974.2	0.00554	378.70	460.32	-	-	1.544	1.452	-	-	1.42
170.00	2.9390	893.3	0.00421	393.70	459.28	-	-	1.965	2.147	-	-	0.70





Table D.3 (Continue)

Temp. °C	Pressure MPa	Density	Volume	Enthalpy		Viscosity		Specific Heat		Thermal C.		Surface Tension mN/m
		Kg/m <sup>3</sup>	m <sup>3</sup> /kg	kJ/kg		μ Pa.s		kJ/(kg.K)		mW/(m.K)		
		Liquid	Vapor	Liquid	Vapor	Liquid	Vapor	Liquid	Vapor	Liquid	Vapor	
180.00	3.4545	756.2	0.00284	412.57	451.03	-	-	-	-	-	-	0.13
183.68c	3.6680	550.0	0.00182	431.77	431.77	-	-	∞	∞	∞	∞	0.00

ASHRAE HANDBOOK, 1993

Table D.4 Thermo physical properties of dry air

Temp $T, ^\circ\text{C}$	Density $\rho, \text{Kg/m}^3$	Specific Heat $C_p, \text{J/kg.K}$	Thermal Conductivity $k, \text{W/m.K}$	Thermal Diffusivity $\alpha, \text{m}^2/\text{s} (\times 10^{-5})$	Dynamic Viscosity $\mu, \text{kg/m.s} (\times 10^{-5})$	Kinematic Viscosity $\nu, \text{m}^2/\text{s} (\times 10^{-5})$	Prandtl Number Pr
-150	2.866	983	0.01171	0.4158	0.8636	0.3013	0.7246
-100	2.038	966	0.01582	0.8036	1.189	0.5837	0.7263
-50	1.582	999	0.01979	1.252	1.474	0.9319	0.7440
-40	1.514	1002	0.02057	1.356	1.527	1.008	0.7436
-30	1.451	1004	0.02134	1.465	1.579	1.087	0.7425
-20	1.394	1005	0.02211	1.578	1.630	1.169	0.7408
-10	1.341	1006	0.02288	1.696	1.680	1.252	0.7387
0	1.292	1006	0.02364	1.818	1.729	1.338	0.7362
5	1.269	1006	0.02401	1.880	1.754	1.382	0.7350
10	1.246	1006	0.02439	1.944	1.778	1.426	0.7336
15	1.225	1007	0.02476	2.009	1.802	1.470	0.7323
20	1.204	1007	0.02514	2.074	1.825	1.516	0.7309
25	1.184	1007	0.02551	2.141	1.849	1.562	0.7296
30	1.164	1007	0.02588	2.208	1.872	1.608	0.7282
35	1.145	1007	0.02625	2.277	1.895	1.655	0.7268
40	1.127	1007	0.02662	2.346	1.918	1.702	0.7255
45	1.109	1007	0.02699	2.416	1.941	1.750	0.7241
50	1.092	1007	0.02735	2.487	1.963	1.798	0.7228
60	1.059	1007	0.02808	2.632	2.008	1.896	0.7202
70	1.028	1007	0.02881	2.780	2.052	1.995	0.7177
80	0.9994	1008	0.02953	2.931	2.096	2.097	0.7154
90	0.9718	1008	0.03024	3.086	2.139	2.201	0.7132
100	0.9458	1009	0.03095	3.243	2.181	2.306	0.7111
120	0.8977	1011	0.03235	3.565	2.264	2.522	0.7073
140	0.8542	1013	0.03374	3.898	2.345	2.745	0.7041



Table D.4 (Continue)

Temp $T, ^\circ\text{C}$	Density $\rho, \text{Kg/m}^3$	Specific Heat $C_p, \text{J/kg.K}$	Thermal Conductivity $k, \text{W/m.K}$	Thermal Diffusivity $\alpha, \text{m}^2/\text{s} (\times 10^{-5})$	Dynamic Viscosity $\mu, \text{kg/m.s} (\times 10^{-5})$	Kinematic Viscosity $\nu, \text{m}^2/\text{s} (\times 10^{-5})$	Prandtl Number Pr
160	0.8148	1016	0.03511	4.241	2.420	2.975	0.7014
180	0.7788	1019	0.03646	4.593	2.504	3.212	0.6992
200	0.7459	1023	0.03779	4.954	2.577	3.455	0.6974
250	0.6746	1033	0.04104	5.890	2.760	4.091	0.6946
300	0.6158	1044	0.04418	6.871	2.934	4.765	0.6935
350	0.5664	1056	0.04721	7.892	3.101	5.475	0.6937
400	0.5243	1069	0.05015	8.951	3.261	6.219	0.6948
450	0.4880	1081	0.05298	10.04	3.415	6.997	0.6965
500	0.4565	1093	0.05572	11.17	3.563	7.806	0.6986
600	0.4042	1115	0.06093	13.52	3.846	9.515	0.7037
700	0.3627	1135	0.06581	15.98	4.111	1.133	0.7092
800	0.3289	1153	0.07037	18.55	4.362	1.326	0.7149
900	0.3008	1169	0.07465	21.22	4.600	1.529	0.7206
1000	0.2772	1184	0.07868	23.98	4.826	1.741	0.7260
1500	0.1990	1234	0.09599	39.08	5.817	2.922	0.7478
2000	0.1553	1264	0.11113	56.64	6.630	4.270	0.7539

Highered.mcgraw-hill.com//App 1.pdf



**APPENDIX E**  
**Nomenclature**



**Nomenclature**

$A$	Area	$m^2$
$C_p$	Specific heat capacity of dry air	$J/kg\ ^\circ C$
$CV$	Check valve	
$D$	Diameter	$m$
$Fr$	Filling ratio	$\%$
$g$	Gravitational constant	$m/s^2$
$k$	Thermal conductivity	$W/m^\circ C$
$L$	Length	$m$
$\dot{m}$	Mass flow rate of dry air	$kg/s$
$N$	Number	
$P$	Pressure	$Pa$
$Q$	Heat transfer rate	$W$
$q$	Heat flux	$W/m^2$
$R$	Thermal resistance	$^\circ C/W$
$T$	Temperature	$^\circ C$ or $K$
$\Delta T$	Temperature difference	$^\circ C$
$t$	Time	hour
$V$	Volume	$m^3$
$v$	Velocity of dry air	$m/s$

**Greek symbols**

$\rho$	Density	$kg/m^3$
$\sigma$	Surface tension	$N/m$
$\varepsilon$	Thermal efficiency	

**Subscripts**

$a$	Adiabatic
$c$	Condenser
$Cu$	Copper metal



e	Evaporator
E	Ethanol
f	Failure
g	Gravity
in	Inlet, inner
l	Liquid
max	Maximum
min	Minimum
out	Outlet
v	Vapor
w	Wall
W	Water



## **Biography**



## Biography

<b>Name</b>	Mr. Satitpong Sangiamsuk
<b>Date of birth</b>	June 19, 1985
<b>Place of birth</b>	Surin, Thailand
<b>Address</b>	156 M 7 Radbumrung Road, Prakhon Chai Sub-District, Prakhon Chai District, Buriram, Thailand, 31140
<b>Institution attended</b>	
2008	Bachelor of Mechanical Engineering (Energy) (B.Eng.) Mahasarakham University, Thailand
2010	Master of Mechanical Engineering (M.Eng.) Mahasarakham University, Thailand
2013	Doctor of Philosophy (Mechanical Engineering) Mahasarakham University, Thailand
<b>Collaborative internship</b>	2012 Engineering Mechanics and Energy, Systems and Information Engineering, University of Tsukuba, Tsukuba, Japan, 3058573
<b>Scholarship</b>	Royal Golden Jubilee Ph.D. Program (RGJ-Grant No. PHD/0002/2553)
<b>Contact address</b>	156 M 7 Radbumrung Road, Prakhon Chai Sub-District, Prakhon Chai District, Buriram, Thailand, 31140

